

©Copyright 2015

Regina C. Carns

Measured and modeled albedos of sea-ice surfaces with implications for Snowball Earth

Regina C. Carns

A dissertation submitted in partial fulfillment of the requirements for the degree of Doctor of

Philosophy

University of Washington

2015

Reading Committee:

Stephen G. Warren, Chair

Edwin D. Waddington, Chair

Bonnie Light

Program Authorized to Offer Degree:

Department of Earth and Space Sciences

Department of Astrobiology

Abstract

Measured and modeled albedos of sea ice surfaces with implications for Snowball Earth

Regina C. Carns

Supervisory Committee Co-Chairs:

Stephen G. Warren

Earth and Space Sciences, Astrobiology Program

Edwin D. Waddington

Earth and Space Sciences

The Snowball Earth episodes were extensive glaciations that occurred during the Neoproterozoic, between 600 and 800 million years ago, during which ice covered much or all of the oceans. These glaciations were a result of ice-albedo feedback, a process likely to occur on any Earthlike planet with oceans covering most of its surface. Modeling shows that sublimation would exceed precipitation over large regions of the ice-covered ocean on a Snowball planet; during the initial stages of the Snowball episode, these areas would be entirely covered by sea ice containing inclusions of brine, and sea ice could remain in smaller regions through the whole episode. At temperatures likely to prevail in the Snowball climate, sodium chloride precipitates within brine inclusions as the hydrated salt hydrohalite ($\text{NaCl} \cdot 2\text{H}_2\text{O}$, also known as sodium chloride dehydrate). This work used field measurements, laboratory experiments and modeling to constrain the albedo of sea ice surfaces relevant to Snowball Earth. Field measurements of cold sea ice in McMurdo Sound show an increase in the albedo of natural sea ice with decreasing temperatures. Laboratory experiments on natural sea ice show that brine pockets can become supersaturated with respect to sodium chloride at low temperatures, creating a hysteresis in hydrohalite precipitation and dissolution. Experiments show this effect in laboratory-grown ice of several different compositions: grown from an NaCl

solution, grown from artificial seawater, and grown from artificial seawater with added extracellular polysaccharides.

Sufficiently cold sea ice in a region of net sublimation will eventually develop a lag deposit of salt as the ice sublimates away from precipitated hydrohalite in brine pockets. No sea ice on modern Earth stays cold and dry long enough for such a deposit to form, so we developed a method for measuring the albedo of ice surfaces in a cold-room laboratory. The method uses a dome with a diffusely reflecting interior surface to emulate the light from an overcast sky. We created a crust of hydrohalite and used this “albedo dome” method to measure albedo of the crust as it developed and dissolved. Using these measurements along with a radiative transfer code, we inferred the complex refractive index for hydrohalite and developed a parameterization for the albedo of hydrohalite crusts of any thickness.

These results have implications for Earthlike exoplanets with sizable oceans, which would also be susceptible to ice-albedo feedback. The formation of hydrohalite in sub-eutectic sea ice and the development of a lag deposit in cold, dry conditions could intensify the positive feedback that leads to Snowball conditions. This work shows that the albedo of hydrohalite is much higher than that of snow in the near-infrared, which could make the formation of hydrohalite crusts particularly important to the climates of planets that orbit M-dwarf stars, which output a large fraction of their energy in the near-infrared.

Table of Contents

Introduction: “Follow the Water” and Find Ice	6
Chapter I: Salt precipitation in sea ice and its effect on albedo, with application to Snowball Earth.	15
Chapter II: Measuring the albedo of a lab-created hydrohalite crust with the “Albedo Dome” ...	44
Chapter III: An optical model of high-albedo salt crusts on Snowball Earth	78
Discussion	101
References	107

Acknowledgements

First off I want to acknowledge the glaciology and astrobiology communities for being full of kind and curious people and inspiring me to join their fields.

Thanks to Steve Warren for keeping me on track, always having a reference to hand when interesting questions arise, and bringing me along on great adventures. Thanks to Ed Waddington for patience, humor, Gilbert and Sullivan, cats, and snow physics. Thanks to Bonnie Light for lots of excellent advice on life as a scientist and lots of opportunities to build cool stuff in the lab. Thanks to Jody Deming for taking time to introduce me to the wonders of biology. Thanks to Seelye Martin for acting as my GSR.

The graduate students of Earth and Space Sciences and Astrobiology have made my time here both intellectually stimulating and fun. If I try to list names I will inevitably leave out someone important, so if you're reading this please assume that your friendship has brightened my days here. You're awesome.

Thanks to Northwest Seaport and the Chantey Sing regulars for sanity maintenance and to my non-grad-student friends for keeping me connected to The World Outside.

Thanks to my clone-sibling and my pseudo-sister for lots of sisterly hugs and support.

Thanks to my wonderful partner Deke for providing me with both emotional and physical sustenance and getting me out of the house.

Thanks to my parents, who instilled in me a love of learning and a thirst for adventure (also thanks Mom for helping with dissertation edits).

Thanks to the University of Washington and the National Science Foundation for financial support.

Dedication

For Jessie Withrow, inspirer of awesomeness.

Introduction

1. “Follow the Water” and Find Ice

“Follow the water” is a fundamental principle in the search for extraterrestrial life. All known Earth life requires liquid water, and almost every Earth environment with liquid water also contains life. Knowing this, we hypothesize that life elsewhere in the Universe would similarly take advantage of water’s abundance and its excellent solvent properties. In addition to its benefits as a biological solvent, water in the form of surface oceans can help to stabilize planetary climates by buffering changes in temperature.

Water’s property of expanding when frozen is also generally counted in the “beneficial to life” column, since it helps prevent lakes and oceans from freezing solid. On planets with extensive oceans, however, this surface layer of ice can act to destabilize the climate by rapidly increasing surface albedo. Just a few centimeters of ice can double the albedo of the ocean surface, and even a thin layer of snow can increase albedo by thirty percentage points [*Brandt et al.*, 2005]. This effect can act to enhance a cooling trend. In the most extreme case, it can lead to a runaway positive feedback, shifting the climate into a new, much colder equilibrium with its oceans nearly or entirely ice-covered [*Budyko*, 1969].

1.1 Snowball Earth

1.1.1 Evidence for an Earth Snowball

The Earth itself appears to have experienced global glaciation at least twice between 850 and 635 million years ago. These episodes, often called “Snowball Earth” events, left behind evidence in the form of glacial deposits and ice-rafted dropstones on continental shelves that were, at the time, near the equator [*Hoffman et al.*, 1998; *Hoffman and Schrag*, 2002]. Above these deposits are thick layers of carbonate, which point to an escape mechanism from the seemingly stable Snowball state. With little liquid water at the planet’s surface and the oceans largely cut off from the atmosphere, the silicate weathering that removes CO₂ from the

atmosphere shuts down. Volcanic activity, however, continues, and eventually the greenhouse effect from the buildup of CO₂ overcomes the extreme albedo of the Snowball [Kirschvink, 1992]. The climate would shift from snowball to hothouse, re-starting silicate weathering processes at a rapid pace and transferring carbon from the atmosphere to the thick layers of carbonate seen in the geologic record.

1.1.2. Models of the Earth Snowball

Some debate exists over whether ice completely covered the Earth's oceans (a "Hard Snowball") or whether some areas of open ocean were left at the equator [Hyde *et al.*, 2000; Peltier *et al.*, 2007; Micheels and Montenari, 2008; Abbot *et al.*, 2011; Yang *et al.*, 2012a, 2012b]. A mostly glaciated planet with a band of open water has often been called a "Soft Snowball" or "Slushball", but Pierrehumbert *et al.* [2011] argue that it is more accurately called a "Waterbelt" state.

A "Hard Snowball", with CO₂ weathering processes shut down entirely, seems to better explain geochemical evidence such as cap dolostone [Hoffman *et al.*, 2007] and oxygen isotopic evidence of high CO₂ levels [Bao *et al.*, 2009]. However, explaining the survival of photosynthetic eukaryotes through a Hard Snowball is more difficult, leading some to prefer the Waterbelt hypothesis [e.g. Moczydlowska, 2008]. Finding refugia that would provide both liquid water and sunlight for photosynthetic eukaryotes is an ongoing question of study [Campbell *et al.*, 2011; Tziperman *et al.*, 2012].

2. Ice Surfaces on Snowball Earth

An Earth covered in ice is very cold and very dry compared to modern Earth [Pierrehumbert *et al.*, 2011]; the ice that forms under such conditions can have different properties than the ice typical of the warmer, wetter modern Earth, so we cannot assume that our assumptions about albedo will hold true. This issue is doubly true for Snowball exoplanets, which may diverge even further from familiar Earth conditions.

Relatively small differences in the albedo of ice used in climate models can make the difference between ice a few meters thick and ice hundreds of meters thick [Warren and Brandt, 2006], between a stable open ocean and thick ice at the equator [Yang et al., 2012a, 2012b], or between stable ice and deglaciation [Le Hir et al., 2010]. The albedo of ice surfaces impacts not only the overall energy balance of the planet, but also the viability of refugia for photosynthetic life on a hard Snowball planet. The existence of the inland-sea refugia proposed by Campbell et al., [2011] depends on the sublimation rates of sea glaciers, a property heavily influenced by the glaciers' surface albedo. To maintain a refugium, the sea glacier must sublimate quickly enough to preclude overriding the inland sea and to maintain a nutrient-importing connection to the open ocean beneath the floating ice; moreover, any ice that forms on the open inland sea must transmit enough light to support photosynthesis beneath it.

2.1. Surface Types

A large proportion of a Snowball planet would be covered by the snow that gives the phenomenon its name. The optical properties of snow are well understood, although the physical processes influencing snow grain size in a Snowball climate are not known with certainty. Regions of very low accumulation in Antarctica are known to develop large grain sizes through metamorphism [Albert et al., 2004], but wind patterns and snowfall frequency may alter effective grain size on the surface.

In an oceanic region spanning the equator, sublimation would dominate over precipitation [Abbot and Pierrehumbert, 2010; Le Hir et al., 2010; Pierrehumbert et al., 2011]. In these regions of net sublimation, several types of ice would develop, as enumerated below.

2.1.1. Salt Ice Surfaces

During a period of uncertain length during the transition to a Snowball state, all floating ice near the equator would originate from the freezing of the oceans during runaway ice-albedo feedback. When ocean water freezes, pockets of brine become trapped within the growing ice matrix. Some brine is expelled during the freezing process, so newly formed sea ice may have

salinity anywhere from a few parts per thousand to more than 20‰ [Untersteiner, 1968]. This snow-free sea ice, we will call ice type (1). The albedo of thick snow-free sea ice has been measured at the coast of Antarctica at a temperature of -5°C [Figure 1 in Brandt *et al.*, 2005; Figure 8 in Warren *et al.*, 2002].

As sea ice cools, water freezes onto the walls of the brine pockets, concentrating the brine. At sufficiently low temperatures (nominally -23°C for the salt composition of the modern ocean, but sometimes lower, as we will see in Chapter I of this work), the sodium chloride in the brine pockets begins to precipitate as $\text{NaCl} \cdot 2\text{H}_2\text{O}$, or hydrohalite. This cold, “subeutectic” sea ice is our ice type (2). If the cold sea ice is in the region of net sublimation, the ice at the surface will sublimate away over time, leaving behind a crust of salt. Cold sea ice with a crust of hydrated salt is ice type (3). Chapter I of this work concerns ice type (2), and chapters II and III concern ice type (3).

2.1.2. Meteoric Ice Surfaces

Outside the regions of net sublimation, snow would gradually accumulate on top of floating sea ice and begin to compress into glacial ice. The thickness of the glacial ice would be small in comparison to the thickness of marine ice below it, accreted by freezing from ocean water [Goodman, 2006]; equilibrium thickness for ice on Snowball Earth, where geothermal heat from below is balanced with the loss of heat to the atmosphere above, would be several hundred meters. The thickness would vary with mean surface temperature, creating a thickness gradient that would cause ice to flow from the poles to the equator, similar to the flow of an ice shelf but self-sustaining rather than fed from a continental ice sheet. The flow of these “sea glaciers” would bring meteoric ice from regions of net accumulation to the region of net sublimation around the equator.

As snow sublimated away from the surface, old snow that had undergone extensive metamorphism and densification would be exposed. This sublimation-exposed snow and firn is ice type (4) (where “firn” in this context refers to snow that has passed the first stage of densification and reached a density of 550 kg m^{-3}). Exposure to sunlight and the high

temperature gradients near the surface would further alter the appearance of the snow and firn. As the firn sublimated away in turn, the next surface to appear would be ice type (5), sublimation-exposed glacier ice. These two types of ice are found in the “blue ice” regions of the Antarctic ice sheet, and their albedo has been measured and modeled [*Dadic et al.*, 2013].

3. Measuring Albedo

Albedo is defined as the ratio of reflected irradiance to incident irradiance with reference to some surface or boundary. Knowing the value of this ratio is an important factor in determining the energy balance of the system defined by that boundary.

3.1. Methods of Measurement

The easiest way to measure the albedo of a surface is to use a radiometer designed to collect light from all directions, such as a pyranometer, to measure downwelling and upwelling radiation. The radiometer must be close enough that the target surface fills most of its field of view, yet far enough away that it does not shadow the surface during measurement of upwelling irradiance; for ground-based measurements this distance is typically on the order of half a meter. This method is useful for most diffusely reflecting surfaces of reasonably large horizontal extent [*Levinson et al.*, 2010].

3.1.1. Measuring difficult-to-find surfaces

Surfaces like cold subeutectic sea ice are more difficult to measure, because the regions of modern Earth where they can even exist are quite limited. The vast majority of sea-ice surfaces are covered with snow unless they are newly formed or actively melting. Bare, non-melting sea ice can sometimes be found in areas of high wind; finding bare sea ice that is also below -23°C requires careful timing, especially since such low temperatures rarely coexist with the sunlight required for albedo measurements. In Chapter I of this thesis I describe measurements of cold sea ice made at the Delbridge Islands near the end of the Antarctic winter. In this case the ice

was kept relatively free from snow by wind, rather than primarily by sublimation as would happen on Snowball Earth.

Lag deposits of hydrohalite on sea ice are entirely absent from modern Earth. Hydrohalite anywhere on the surface is rare, although it has been observed at a saline spring in the high Arctic [Bishop *et al.*, 2014]. Crusts of mirabilite, another hydrated salt ($\text{Na}_2\text{SO}_4 \cdot 10\text{H}_2\text{O}$) are known to develop on frozen, high-salinity lakes in the Dry Valleys of Antarctica, but sodium sulfate is likely to be less relevant to the formation of a salt crust since it would have been less abundant than sodium chloride in the Snowball ocean.

3.1.2. Measuring surfaces created in the laboratory

To measure the albedo of a lag deposit of hydrohalite, it was necessary to create one in the laboratory, where temperatures could be controlled. A laboratory setting introduces a number of difficulties in the measurement of albedo; in particular, the surface being measured is generally too small to fill more than a fraction of the field of view of a field-style radiometer unless the radiometer is placed so close that it will shadow the surface. The challenges of measuring albedo in the laboratory, and the ways in which we addressed those challenges with the use of a novel apparatus and technique, are addressed in Chapter II.

Not every possible configuration of hydrohalite and ice together could be measured in the laboratory. To better understand the results of the measurements made with the dome, and to extend them to other possible scenarios, we used a model of Mie scattering and a discrete-ordinates radiative transfer model to determine the optical properties of hydrohalite and the albedo of hydrohalite crusts of varying thickness. This modeling is discussed in Chapter III.

4. Goals

The exact ways in which Snowball Earth influenced the evolutionary trajectory of life on Earth are still not well understood; microfossils and biomarkers can be difficult to interpret, and the record is old and fragmentary. Could populations undergoing divergent evolution in isolated refugia during the Snowball Earth have contributed to later biodiversity, or did Snowball

episodes represent a step backwards for life? The only point on which there is general agreement is that such a massive event must have made its mark on the planet's ecosystems as they existed at the time. Isotopic excursions in the rock record make it clear that the biogeochemical systems of the Earth underwent enormous perturbations [*Hoffman et al.*, 1998; *Halverson et al.*, 2010].

The ice-albedo feedback that caused Snowball Earth could occur on any planet with extensive surface oceans (although the ease with which the runaway change in state can be triggered differs with the spectrum of the planet's star [*Shields et al.*, 2013].) The distance from its star at which a planet enters an irreversible Snowball state marks the outer edge of the habitable zone [*Kasting et al.*, 1993]. Understanding how Snowball events are triggered, what the climate is like during the event, and how they can be terminated will improve our guesses of where to look for life and what the course of its evolution might be on other Earthlike planets.

Since the processes that make Earth's ocean salty are likely to occur on any Earthlike planet, salt is an intrinsic part of the formation and development of ice on a Snowball planet. Current Snowball Earth models use values appropriate for relatively warm modern Earth sea ice, and therefore do not take into account the effects of hydrohalite precipitation. Developing albedo parameterizations for subeutectic sea ice and hydrohalite lag deposits will bring Snowball models closer to an accurate representation of their subject.

Chapter I: Salt precipitation in sea ice and its effect on albedo, with application to Snowball Earth.

A version of this chapter has been submitted to Journal of Geophysical Research – Oceans, with coauthors Rich Brandt and Steve Warren. This chapter describes fieldwork undertaken in McMurdo Sound, measuring the albedo of cold, bare sea ice. We made the field measurements in September and October of 2009, when the weather was still cold enough that the ice surface dropped below the precipitation temperature of hydrohalite but the sun was up for long enough to get measurements.

I worked with Steve Warren and Rich Brandt to take albedo measurements and ice cores. I did some sample processing in the lab, including a lot of melting and filtering to measure amount of extracellular polysaccharide substances (EPS) in the ice cores. The EPS work was done with the idea that EPS might influence the albedo properties, but measured EPS showed no clear relationship to albedo, so the results are not discussed in this paper.

The peculiarities of the hydrohalite precipitation led me to do the laboratory experiments discussed in the paper, using data analysis techniques and scripts developed by Rich Brandt and with advice from Bonnie Light and Steve Warren.

Chapter I: Salt precipitation in sea ice and its effect on albedo,
with application to Snowball Earth

Regina C. Carns^{1,2}, Richard E. Brandt³, and Stephen G. Warren^{1,2}

¹Department of Earth and Space Sciences,
University of Washington, Seattle, Washington, USA

²Astrobiology Program, University of Washington, Seattle, Washington, USA

³Atmospheric Sciences Research Center, University at Albany - State University of
New York, Whiteface Mountain Field Station, Wilmington, NY 12997, USA.

Abstract

During the initial freezing of the tropical ocean on Snowball Earth, the first ice to form would be sea ice, which contains salt within inclusions of liquid brine. At temperatures below -23°C , significant amounts of the salt begin to crystallize, with most abundant salt being hydrohalite ($\text{NaCl}\cdot 2\text{H}_2\text{O}$.) These crystals scatter light, increasing the ice albedo. In this paper we present field measurements of the albedo of cold sea ice and laboratory measurements of hydrohalite precipitation.

Precipitation of salt within brine inclusions was observed on windswept bare ice of McMurdo Sound at the coast of Antarctica (78°S) in early austral spring. Salinity and temperature were measured in ice cores. Spectral albedo was measured on several occasions during September and October. The albedo showed a gradual increase with decreasing temperature, consistent with salt precipitation.

Laboratory examination of thin sections from the ice cores showed that the precipitation process exhibits hysteresis, with hydrohalite precipitating over a range of temperatures between -28°C and -35°C but dissolving at about -23°C . The causes of the hysteresis were investigated in experiments on laboratory-grown sea ice with different solute mixtures. All mixtures showed hysteresis, suggesting that it may be an inherent property of hydrohalite precipitation within brine inclusions rather than being due to biological macromolecules or interactions between various salts in seawater.

1. Introduction

As new sea ice grows, inclusions of seawater become trapped in the thickening ice. These brine inclusions have typical diameters 10-200 mm, and can have average number-densities as high as 20 per mm³ [Weeks and Ackley, 1982; Perovich and Gow, 1991, 1996; Light *et al.*, 2003].

Consequently, the salinity of young ice is 12-20 parts per thousand (‰) by mass when growing from seawater of normal salinity (32-35‰). With further cooling during winter, some of the water in the brine inclusions freezes; the increase in pressure causes cracks to form, and some of the brine is expelled, reducing the bulk salinity. The surface salinity of first-year sea ice can vary between 8 and 16‰ [Cox and Weeks, 1988].

As the upper layers of the ice cool, water in a brine inclusion freezes to the walls of the inclusion, so that the salinity of the remaining liquid adjusts to that required for phase equilibrium at the lower temperature. As the concentration of ions increases, salts precipitate out of solution, including ikaite ($\text{CaCO}_3 \cdot 6\text{H}_2\text{O}$) near the freezing point of seawater [Hu *et al.*, 2014], and mirabilite ($\text{Na}_2\text{SO}_4 \cdot 10\text{H}_2\text{O}$) around -8°C [Marion *et al.*, 1999]. The major salt in seawater is NaCl. For a binary mixture of NaCl and H_2O in equilibrium, the NaCl precipitates as the dihydrate $\text{NaCl} \cdot 2\text{H}_2\text{O}$ (“hydrohalite”) at the eutectic temperature of -21.1°C . When accompanied by the mixture of salts present in natural seawater, hydrohalite begins to precipitate at -22.9°C [Spencer *et al.*, 1990; Wettlaufer, 1998]. For brevity, in this paper we will use the term “subeutectic” to refer to natural sea ice colder than -22.9°C .

1.1 Hydrohalite Occurrence and Influence on Snowball Earth

The precipitated salt crystals can scatter sunlight, but only if sunlight is available. On the modern Earth, temperatures low enough to cause salt precipitation occur only during winter on the polar oceans, when there is little sunlight and when the ice is usually hidden beneath a layer of snow. The increase in albedo caused by salt precipitation in sea ice therefore is not significant for climate on the modern Earth, but it could have been important at times in the

distant past. In particular, the "Snowball Earth" events of the Neoproterozoic (600 – 800 million years ago) [*Hoffman and Schrag, 2002*] may have been characterized by a frozen ocean with tropical surface temperatures below -30°C in all months (Figure 7 of *Pollard and Kasting [2004]*; Figure 2 of *Pierrehumbert [2005]*).

In some oceanic regions of Snowball Earth the ice surface would have been mostly free of snow. On the modern Earth, evaporation exceeds precipitation on the subtropical oceans, $\sim 20\text{-}30^{\circ}$ latitude. On the Snowball planet, by contrast, the Hadley-cell circulation is altered so that the zone of net sublimation would instead be centered at the equator [*Pierrehumbert et al., 2011*], but would encompass large areas of the tropical ocean [*Pollard and Kasting, 2004*; *Pierrehumbert et al., 2011*].

In Snowball Earth scenarios ice extends to low latitudes where it is exposed to intense sunlight, so small changes in surface albedo can have significant consequences in climate models. For example, *Pierrehumbert et al. [2011]* showed that a change of ice albedo from 0.55 to 0.65 means that a factor-of-10 increase in the mixing ratio of atmospheric CO_2 is required to end the snowball state. [*Abbot et al., 2011*] found that a narrow belt of open water could persist along the equator if the sea-ice albedo was 0.45 but not if it was ≥ 0.55 . *Yang et al. [2012b]* found that a change of prescribed albedo from 0.55 to 0.58 had large effects on the speed of snowball initiation and on the eventual fraction of the ocean covered by sea ice in equilibrium. To improve the realism of these models, we are working to determine accurate albedos for the variety of ice types that might have existed on the snowball ocean.

1.2 Ice Types on Snowball Earth and Modern Analogues

In zones of net sublimation, the ocean surface would have exhibited a sequence of four ice types with different albedos. Newly formed sea ice without salt precipitation, ice type (1), would resemble the rapidly growing new sea ice found in polar winters today. Later, as the interior ice temperatures dropped below the temperature of initial precipitation, salt would crystallize in brine inclusions, forming ice type (2): cold "subeutectic" sea ice. A salt crust would develop as a "lag deposit" after significant loss of ice to sublimation; cold ice with a salt

crust constitutes ice type (3). Finally, the ice cover on the midlatitude and polar oceans, built up from above by snowfall and from below by freezing of seawater, would be expected to reach thicknesses of several hundred meters. This thickness is sufficient to permit flow as “sea glaciers”, like modern ice shelves but not dependent on continental glaciation for their existence [Goodman and Pierrehumbert, 2003; Goodman, 2006]. The sea glaciers flowing toward the equator (and sublimating) would likely displace the sea ice, but in some models the sea ice persists [Pollard and Kasting, 2005, 2006; Warren and Brandt, 2006]. The sublimating sea-glacier surface would be freshwater ice: ice type (4). Its albedo would be determined by its bubble content.

The albedo of ice type (1) has been measured at the coast of Antarctica at a temperature of -5°C [Figure 1 of Brandt *et al.*, 2005; Figure 8 of Warren *et al.*, 2002]. Ice type (4), the ice of sublimating sea glaciers, has been measured in the blue-ice regions of the Transantarctic Mountains [Dadic *et al.*, 2013]. Ice type (3), the salt crust, apparently does not occur on the modern Earth, because the atmospheric conditions favoring ablation by sublimation do not persist long enough before the springtime warming. Therefore, to investigate that surface type we are sublimating artificial sea ice in our freezer-laboratory (see Chapter II of this work.) Ice type (2), the subeutectic sea ice, is the topic of this paper.

Sea ice that formed during the rapid freezing phase of a snowball event would probably not experience surface melting, so it would not experience the annual flushing events that purge salt from the upper ice layers on the modern Earth. Instead, salt would remain within brine inclusions, precipitating at low temperatures and increasing the albedo of the ice. Our measurements of the albedo of subeutectic sea ice in nature, reported in this paper, were motivated by the dramatic result of a laboratory experiment reported by Perovich and Grenfell, [1981]. In that experiment, laboratory-grown sea ice, containing NaCl as its only salt, was illuminated by a broad-spectrum light. At an ambient temperature of -37°C , the spectral albedo was extremely high; as the temperature was raised to -22°C , just above the eutectic temperature of -22.9°C , the albedo dropped dramatically (Figure 1).

Light et al., [2003, 2004] also investigated the precipitation of hydrohalite in first-year sea ice and its effects on the optical properties of the ice. They measured transmittance instead of albedo, but their results also showed a change with salt precipitation. They found that the transmittance of natural ice in the laboratory dropped slightly during initial cooling to -20°C , above the precipitation temperature of hydrohalite, and then dropped dramatically when the ice was cooled to -25°C (Figure 2).

To examine hydrohalite precipitation (and its effect on albedo) in nature, the ice must satisfy four criteria: it should be first-year ice (i.e., has not experienced summer drainage of brine), snow-free, colder than -23°C , and exposed to adequate sunlight or twilight for visible and near-infrared radiation measurements. These criteria are satisfied by shorefast sea ice in many places along the coast of Antarctica during late winter and early spring, at locations where the snow is blown away by wind [*Purdie et al.*, 2006]. Ice that has survived a summer melt season (multi-year ice) has become largely desalinated by flushing of meltwater [*Untersteiner*, 1968], so salt precipitation will be most readily apparent only in first-year ice.

2. Field measurements

We drove about 100 km of reconnaissance on the landfast sea ice of McMurdo Sound between McMurdo Station and Cape Royds; the best site for snow-free first-year ice was identified on the west side of Tent Island, one of the Delbridge Islands. Figure 3 is a photograph of our principal site at 77.68°S , 166.35°E . Ice temperatures at the surface and at 10-cm depth were measured using thermistors embedded in the ice and logged at 1-minute intervals using a Campbell CR10X data logger. The difference between the surface and 10-cm depth varied from 0 to 3 K, with periods of gradual cooling and rapid warming. The measurements taken on 22, 23 and 26 Sept. were taken during a several-day period of cooling, during which the ice temperature decreased steadily with only small diurnal changes, and never increased above -23°C after falling below it. The 5 Oct. measurement was taken at the peak of a two-day warming period, during which the surface temperature increased from -24°C to -18°C .

Several ice cores were extracted to examine temperature and salinity profiles and ice

microstructure, using a manually operated ice-coring drill which cut cores with diameter 10 cm. Some of these ice cores were 1m long; others included only what we considered to be the portion of the ice relevant to albedo, approximately the upper 30 cm.

The ice salinity (Figure 4) was 10‰ at the surface, decreasing to 6‰ at 25 cm, and then nearly constant at 5-7‰ down to 90 cm. A 3-mm surface crust of higher salinity (about 18‰) was often present. A research group of the New Zealand Antarctic Programme (NZAP), who had monitored the sea ice in McMurdo Sound throughout that winter, had observed this crust to form during the early stages of freezing in autumn as a result of metamorphism of “frost flowers” [Perovich and Richter-Menge, 1994; Rankin *et al.*, 2002; Style and Worster, 2009]. However, the crust re-formed later after we removed it from the surface, suggesting that it could also (or instead) be windblown snow which stuck to a thin film of brine seeping from the top of the ice (Hajo Eicken, personal communication.)

Ice temperatures at the study site varied with time and depth, crossing the threshold for hydrohalite precipitation. On one occasion the surface brightening was visible by eye as the ice cooled in late afternoon and salt crystallization occurred in patches, then spread throughout the area.

We measured spectral albedo on seven occasions, both for the intact ice and after removal of the snow-like surface crust; both types may be relevant for Snowball Earth. Spectral albedo measurements are most accurate under diffuse illumination, so we favored measurements made under overcast sky or in the shadow of the adjacent islands. The albedo was measured using a portable scanning spectroradiometer manufactured by Analytical Spectral Devices (ASD; Kindel *et al.*, [2001]). The instrument employs three separate grating spectrometers that simultaneously measure radiance across three wavelength regions covering 350-2500 nm, with spectral resolution 3-10 nm, and can average 100 scans in 10 seconds. It is designed specifically to cover the solar spectrum, and has order-blocking and cutoff filters to ensure uncontaminated spectra.

The ASD radiometer and its computer were both battery-powered and housed in separate

insulated boxes. At ambient temperatures of -20 to -35°C the electronics were kept warm by self-heating supplemented by battery-powered heaters. For albedo measurements a Spectralon diffuser-plate receptor was mounted on a rod suspended 0.7 m above the ice, supported at one end by a tripod resting on the ice (Figure 3). The light is carried by a fiber-optic guide to the radiometer.

2.1. Results of field measurements

As the temperature drops below the initial precipitation point of hydrohalite, the albedo of bare sea ice in McMurdo Sound increases. Figure 5 shows spectral albedos of the bare sea ice (after removal of the snow-like surface crust) in McMurdo Sound for four ice temperatures. As expected, the colder ice does exhibit higher albedo. However, the apparent dramatic jump in albedo for subeutectic ice seen in the laboratory experiments on artificial NaCl-ice [Perovich and Grenfell, 1981] does not appear in our McMurdo albedos. The albedos are also lower than expected from the results of Perovich and Grenfell, [1981], who found visible albedo >0.9 for sub-eutectic ice. In their case the ice surface temperature was -32°C , colder than any of our profiles, although its temperature at 10 cm below the surface was -20°C [Perovich, 1979:p86]. Their ice was also grown at a constant -37°C , while average air temperatures in McMurdo Sound during the period of initial ice formation were closer to -20°C . Lower temperatures at the time of ice formation lead to faster ice growth, which in turn leads to higher salinity ice and to higher albedos at a given temperature [Perovich and Grenfell, 1981] so this may also contribute to the higher albedo of the laboratory ice.

The spectral albedos are integrated over three broad wavelength-bands, using an incident solar spectrum obtained from an atmospheric radiation model. Two solar spectra are used, one for clear sky and one for cloudy sky; they are similar to solar spectra shown in Figure 1 of Brandt and Warren [1993]. These broadband albedos are plotted versus ice surface temperature in Figure 6, showing the gradual slight decrease of albedo as the temperature rose from -29°C to 18°C . Even at the lowest temperature, the broadband albedos are close to the value 0.49 measured for bare sea ice near Davis Station at -5°C , well above the temperature where

significant salt precipitation would be expected (Figure 1 of *Brandt et al.*, [2005]). Our laboratory measurements indicate that precipitation continues well below -28°C , so lower temperatures would likely result in higher albedos.

3. Laboratory Measurements

Our laboratory experiments were motivated by our observations of sea ice in the field, which showed a gradual increase in albedo, rather than the discontinuous jump we had been led to expect by laboratory observations. We hypothesized that the difference between our results and those of Perovich and Grenfell could be due to the natural ice undergoing supersaturation, with sodium chloride in some brine inclusions resisting precipitation. The results of Perovich and Grenfell do not exclude this possibility, since their albedos were taken during warming rather than during cooling. Supersaturation of solutions containing sodium chloride has been previously reported in sea ice [*Light et al.*, 2003; *Pringle et al.*, 2009] as well as in biological contexts [*Han and Bischof*, 2004]. We therefore initiated laboratory experiments to investigate this possibility.

3.1. Temperature Cycling of Natural Sea Ice

We extracted cores of the ice near our measurement site as described in the previous section. The cores were transported from the field at ambient temperatures (generally between -30°C and -20°C) and stored in freezers at McMurdo Station (-20°C). We used a bandsaw in a -20°C cold room to cut sections of ice $<1\text{cm}$ in thickness from the cores, cutting along the vertical axis of the core with respect to its original orientation *in situ*. The sections were taken from the top or near the top of the core, since we were most interested in the brine inclusions at or near the surface where their influence on the ice albedo would be greatest.

Sections were mounted on glass slides and a microtome was used to shave each face, giving the sections optically smooth surfaces and reducing their thickness to a few millimeters. After preliminary imaging at McMurdo Station, the sections were transported at -60°C back to the laboratory at the University of Washington, where they were stored at -20°C .

Thin-sections were prepared for observation under a microscope in our cold-room laboratory by first freezing a temperature probe to the thin section surface. Temperature-cycling of the ice was achieved by setting the laboratory temperature to either -15°C or -40°C and allowing it to come to equilibrium at that temperature, generally over a period of 5 to 7 hours of rapid temperature change ($3\text{-}4^{\circ}\text{C}$ per hour) followed by 12-24 hours of stable temperature (excursions of up to 3 K above the set temperature occurred during defrost cycles). A Nikon D40 DSLR camera attached to the microscope was used to take pictures of the ice at 5-minute intervals as the temperature of the cold room changed (Figure 7). Sample temperatures were monitored at 10-second intervals.

The highly scattering nature of hydrohalite crystals makes it easy to detect their presence. A pocket full of clear liquid brine transmits approximately the same amount of light as the ice around it, but after hydrohalite precipitates within the pocket, the small crystals block most of the light coming from below. This property allowed us to use image-analysis software ["ImageJ"; *Abràmoff et al.*, 2004] to detect how much of the image area had changed in brightness as a proxy for the amount of hydrohalite precipitation. A Matlab script matched photos to the temperature at the time they were taken.

The images showed that hydrohalite did not begin to precipitate within brine inclusions until temperatures well below the expected -23°C , with the first precipitation occurring around -28°C . The precipitation occurred unevenly; within each individual brine pocket it was rapid and complete, but individual brine inclusions precipitated at different temperatures. Even at -38°C some brine inclusions remained completely transparent, likely indicative of a lack of salt precipitation. However, on warming the crystals dissolve at about -23 to -24°C , close to the expected temperature.

We hypothesized that precipitation in some brine inclusions may be retarded by the presence of other constituents within certain brine inclusions. Since the presence of other sea salts is known to depress the precipitation point of hydrohalite from -21.2°C to -22.9°C , perhaps it might also lead to supersaturation of some brine inclusions. Alternatively, since the sea ice we

measured was natural rather than laboratory-grown, it undoubtedly contained microbial life forms. Sea-ice algae and bacteria are known to produce large quantities of mucus-like extracellular polysaccharides (EPS) [Krembs *et al.*, 2011] that may interfere with hydrohalite crystallization. Krembs *et al.* [2011] did show that the EPS influences the structure of brine inclusions and channels, tending to make them more tortuous and interconnected.

3.2. Temperature Cycling of Artificial Sea Ice

To investigate these possible reasons for the uneven crystallization, we grew artificial sea ice in the laboratory with three different compositions. The first sample was frozen from an initial solution of water and pure NaCl, as used by Perovich and Grenfell [1981]. The salinity of the solution, approximately half that of seawater at 18‰, was chosen because rejection of salt by the freezing ice concentrates the remaining solution, so starting at a lower concentration than seawater allows the middle portion of the sample to freeze from solution with concentration close to that of seawater. The results in Perovich and Grenfell [1981] used ice frozen from a solution of 31.1‰ [Perovich, 1979:p.49].

The second sample was frozen from an initial solution consisting of artificial seawater made from *Sigma Artificial Sea Salts* at a concentration of 18‰. These salts replicate the ionic composition of seawater but are free from biological material. The third was frozen from an artificial seawater solution to which 1000 mg/L of xanthan gum, a form of EPS, had been added. This concentration was chosen to be several times that found in natural sea ice, where the bulk concentration of EPS can be up to 200 mg/L [Krembs *et al.*, 2002]. We hoped that the high concentration would increase the magnitude of any effects EPS might have on the precipitation of hydrohalite, making them easier to observe.

The artificial sea ice was frozen at approximately -25°C in cylindrical containers with an inner diameter of 10 cm and a depth of 25 cm, constructed from expanded polystyrene foam lined with thin plastic. The foam containers insulated the bottom and sides of the artificial seawater samples, encouraging them to freeze only from the top down, so that the structure of ice crystals and brine inclusions would resemble that of natural sea ice. The samples were allowed

to remain at -25°C for several days to ensure that they froze completely. After freezing, the laboratory-grown samples were processed in the same way as the samples of natural sea ice: sectioned, frozen to glass plates and subjected to temperature cycling in a freezer laboratory. Figure 9 shows the hysteresis in precipitation and dissolution of brine inclusions within sections taken from lab-grown salty ice. The results suggest that supersaturation of the solutions cannot be attributed to interactions of NaCl with other salts or with polysaccharide material, since all three solutions show precipitation occurring at a temperature approximately 5 K below the temperature of dissolution.

The hydrohalite in the ice containing xanthan gum precipitated at a slightly higher temperature than the ice containing only artificial sea salt, suggesting that the xanthan gum acted to promote precipitation rather than inhibit it, perhaps by nucleating hydrohalite crystals. Extracellular polysaccharides can differ in their chemical properties, so it is possible that EPS made by microbes native to sea ice could be adapted specifically to interact with hydrohalite, whereas xanthan gum (which is made by a soil microbe) would be less likely to have such an adaptation.

Each graph in Figures 8 and 9 represents analysis of a representative 30 mm² area of a single section, so these results should be considered somewhat qualitative. Given the stochastic nature of sea ice structure at the scale being considered, and the unpredictable pattern of brine pocket crystallization, each repetition of the experiment was expected to give slightly different results. Determining the exact effect of brine pocket size and shape on the timing of hydrohalite precipitation would require many more experimental runs and more complex image analysis. Such an experiment could be a promising candidate for future study.

3.3. Effects of Freezing Rate and Brine Volume

An additional experiment was carried out to investigate the effects of the rate of change in temperature. A sample containing artificial sea salts and xanthan gum was placed in the cold room using the same setup as before, but this time the temperature was lowered in 2-degree steps and allowed to remain steady for approximately 48 hours at each step. We expected that

the hydrohalite precipitation might occur at a higher temperature when given time to equilibrate. Contrary to our expectations, we found that the precipitation pattern of the hydrohalite within brine inclusions in this ice section was substantially similar to that of more rapidly-cooled sections. The first precipitation occurred around -26°C , and small brine inclusions continued to precipitate even at -35°C and below, after spending more than 10 days below -23°C .

As described in section 3.1, we noted that precipitation in any individual brine pocket was always rapid and complete; the brine pocket would be filled with hydrohalite crystals within one time step (5 to 15 minutes) and change very little afterward. This observation suggests that precipitation within supersaturated brine is initiated by the chance formation of a single crystal and then propagate rapidly through the whole pocket. In this case a larger volume of brine should show less supersaturation, since it would be more likely to contain a crystallization nucleus. If larger volumes of brine promote crystallization, this phenomenon would represent another mechanism by which the presence of EPS could enhance crystallization in some cases, as EPS is known to increase the interconnectivity (and therefore the effective size) of brine inclusions [Krembs *et al.*, 2011].

To test this idea, we put solutions of brine at 233‰ salinity, similar to what would be found in the brine inclusions near the precipitation temperature, into 40mL polyethylene bottles and placed them in a cold room at -37°C . In this experiment we used a temperature probe (inserted through a hole in the top of the bottle) to detect crystallization, by observing the rate of cooling over time and identifying plateaus where phase transitions were taking place. The solutions were of the same types as the ones used in creating artificial sea ice (NaCl, sea salts, and sea salts with 1000mg/L xanthan gum). In these containers, with a volume about 10^7 times the size of a brine pocket, no supersaturation occurred; precipitation took place near the nominal precipitation temperature of the solutions (Table 1). However, similar experiments conducted by Toner *et al.*, [2014] found significant supersaturation. In these experiments the supersaturation persisted even when the salt solution was mixed with soil to provide nucleation

points for hydrohalite.

4. Discussion

4.1. Fieldwork

The fieldwork results show small systematic increases in albedo with decreasing temperatures. Interpretation of these data is complicated by the fact that these measurements at different temperatures were also made on different days. Most notably, blowing snow could stick to the ice and increase its albedo; this possibility was strikingly demonstrated by the re-formation of the snow crust several days after it was originally removed. Frost might also have formed on the surface. We did visually inspect the ice before each measurement, and brushed away any apparent deposits of snow. It is conceivable, however, that frost or blown snow could have accumulated enough to influence the measurements without being visually apparent. Over the period during which we regularly visited the study site, however, the general trend was toward thinning or disappearance of snow crusts. In many areas the snow crust, which had appeared optically thick when first observed, became thin and patchy over the subsequent weeks.

The spectral albedos in Figure 5 show a relatively even increase in albedo across the measured wavelengths for the three measurements made when the ice was below the expected precipitation temperature for hydrohalite. All of the measurements show a slight peak around 500nm. This peak suggests contamination by absorbing particles, since the absorption coefficient of ice and water increase monotonically in this wavelength region. The wind that blew fallen snow away from (and sometimes onto) the ice at this location also transported volcanic dust from Tent Island, so the ice surface contained some dust which would have lowered the albedo at visible wavelengths (Figure 5 of *Warren and Wiscombe*, [1980]; Figure 7 of *Warren*, [1982]). The crossover of the albedo curves for 5 Oct. and 22 Sept. in Figure 5 could occur if the ice measured on 22 Sept. contained more dust. The influence of the dust would be highest at short wavelengths, decreasing at longer wavelengths where the absorption from ice and water becomes significant.

During all measurements, the ice was warmer at a depth of 10 cm than at the surface. This temperature gradient almost certainly led to a gradient in the amount of hydrohalite precipitation, with more precipitation, and therefore more scattering of light, occurring in colder ice.

4.2. Laboratory work

Our technique for measuring the amount of hydrohalite precipitation relies on analyzing two-dimensional images of thin sections photographed in transmitted light. This technique has some limitations that compromise its accuracy. It captures only the cross-sectional area of the brine inclusion, not its volume, so it does not necessarily represent the total amount of hydrohalite in the brine inclusions. In order to quantitatively determine the amount of brightening expected based on a given amount of hydrohalite precipitation, we would need to know the volume and number of brine inclusions that had crystallized. The shape of the inclusions would also influence the albedo of the ice. Determining brine pocket shape and volume from two-dimensional images, however, is non-unique, and it would be necessary to analyze a large population of brine inclusions to understand the distribution of shape and size. Moreover, our cold room was evidently unable to achieve a sufficiently low temperature to cause all brine inclusions to precipitate. Some brine pockets in the thin sections we imaged did not show hydrohalite crystallization, perhaps because the temperature was not low enough. In light of these limitations, we draw no quantitative conclusions from these precipitation experiments. They simply demonstrate qualitatively that precipitation can occur gradually over time, and that it exhibits hysteresis.

In some ways the results of our laboratory experiments complicate the interpretation of the field albedos, since field albedos show an increase even at -23°C , whereas brine inclusions in the laboratory did not precipitate until -26°C or below. However, the laboratory experiments were necessarily conducted on just a few brine inclusions, whose size was somewhat limited by the experimental technique itself, since large brine inclusions would intersect the surface of the thin ice section and drain, or even cause the section to break during microtoming and be

discarded. Among the hundreds of millions of brine inclusions near the surface of a square meter of natural sea ice [Light *et al.*, 2003], it seems likely that some possess the right properties—perhaps large size or the presence of material that can act as a nucleation site--to precipitate at -23°C . Future work could include radiative transfer modeling to show what percentage of pockets would need to precipitate to account for the observed increase in albedo, along with more laboratory analysis of what properties of a brine pocket influence its precipitation.

4.3. Implications for Snowball Earth

As temperature decreases, the precipitation of salt within brine inclusions causes the albedo to rise, leading to further cooling and thus a positive feedback on the progression to a frozen ocean. This bare subeutectic sea ice would be the surface type on the ocean in snow-free regions; i.e., regions of net sublimation.

The effect of hydrohalite precipitation on the climate of Snowball Earth would be enhanced by an additional positive feedback. As sublimation continues during the cold early part of a snowball event, precipitated hydrohalite is expected to accumulate on the surface of the ice as a lag deposit. In laboratory experiments this lag deposit, with its small crystals of hydrohalite, forms a brightly reflective white surface (Figure 5c of Light *et al.*, [2009]).

Acknowledgments. This research was supported by NSF grants ANT-07-39779 and ANT-11-42963. We thank the staff of McMurdo Station for their assistance in supporting our field campaign. We also thank Andrew Mahoney and Alex Gough (New Zealand Antarctic Programme) for their winter observations of McMurdo sea ice and assistance with preparing thin sections using their microtome at Scott Base. We acknowledge Hajo Eicken and Bonnie Light for helpful discussion. The data used to generate the figures in this paper may be found at <http://dx.doi.org/10.6084/m9.figshare.1258839> .

Figures

Solution	Precipitation temperature (°C)
233 ppt NaCl (this work)	-22.6
226 ppt NaCl (Toner et al. 2014)	-27.9
260 ppt NaCl (Toner et al. 2014)	-29.6
233 ppt artificial sea salt	-24.2
233 ppt artificial sea salt+1 ppt xanthan gum	-24

Table 1. Temperature at which salt and ice precipitated in 40-mL beakers. These volumes of solution, larger than brine inclusions by a factor of $\sim 10^7$, show very little supersaturation, precipitating at most 1.5 K below the expected temperature. The samples were cooled further to -30°C with no significant additional precipitation.

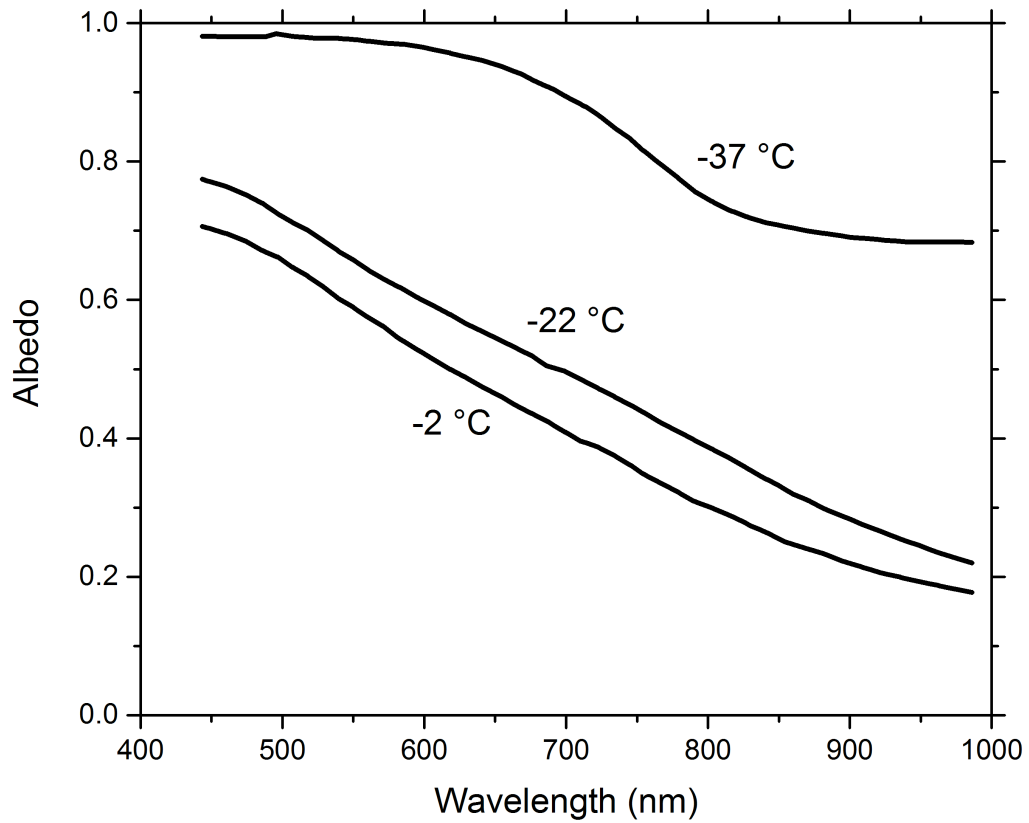


Figure 1. Spectral albedos of artificial salt-ice (containing NaCl as the only salt), measured in a freezer laboratory as the temperature was increasing from -37°C . The albedo curves are labeled with laboratory air temperatures at the time they were measured. Redrawn from *Perovich and Grenfell* [1981], with modifications.

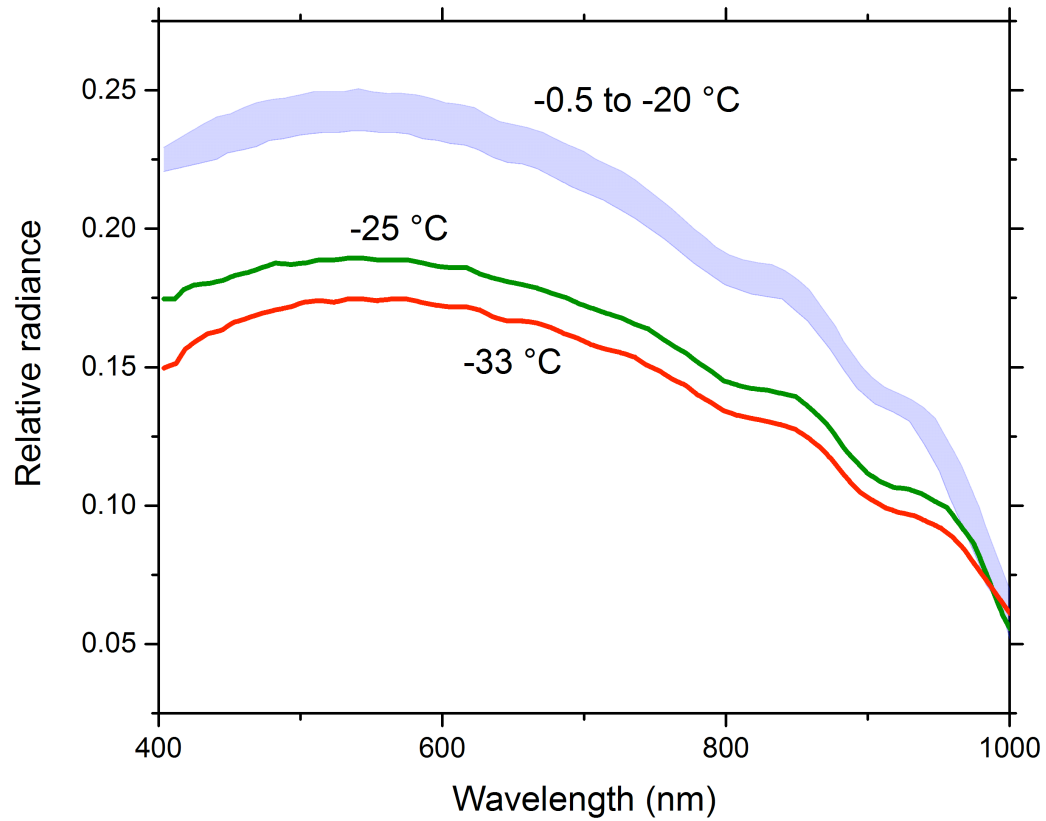


Figure 2. Temperature-dependent changes in the spectral radiance of transmitted light, normalized by the incident irradiance. At -25°C and -33°C , highly-scattering hydrohalite crystals block a significant fraction of the light. Redrawn from *Light et al.* [2004], with modifications.



Figure 3. ASD radiometer measuring spectral albedo of sea ice in McMurdo Sound. Note cleared area, from which the 3mm crust of salty snow has been removed. 78°S, September 2009.

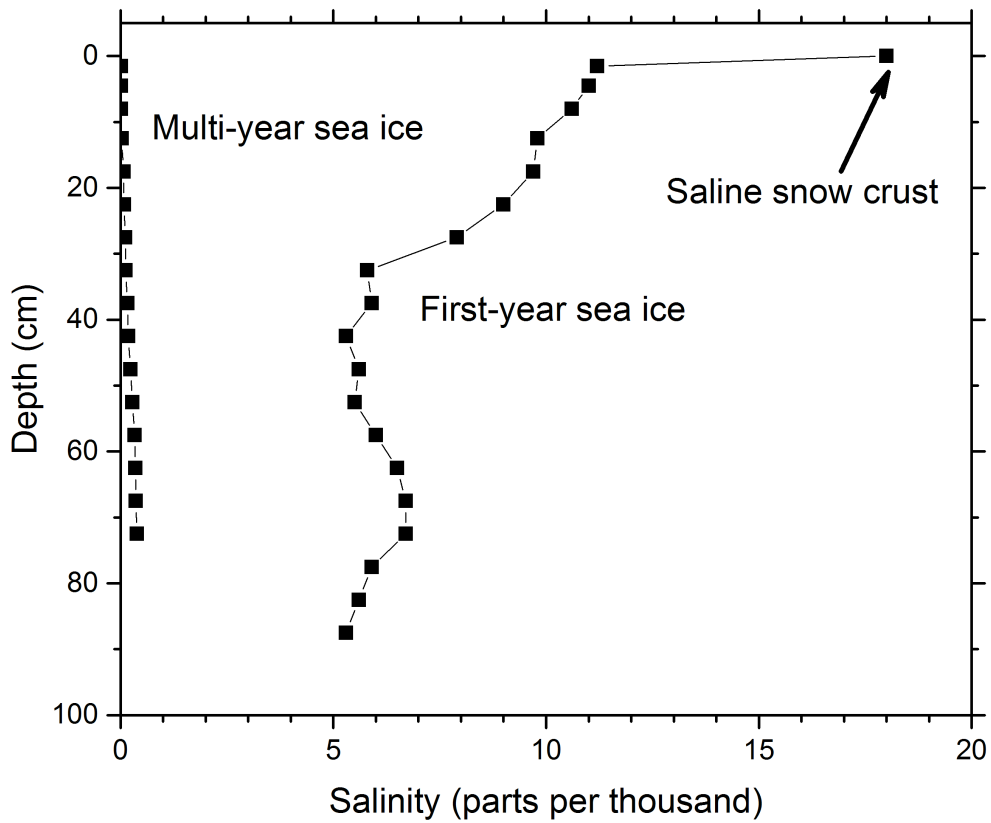


Figure 4. Salinity of ice in McMurdo Sound as a function of depth, measured in sections of 1-m cores. The core of first-year ice was taken from the site for albedo measurement; the core of multi-year ice (MYI) was taken near the shore of Ross Island, 12 km farther south. The very low salinity of the MYI is the result of brine drainage during summer. The salinity at the top of the MYI is 7 ppm.

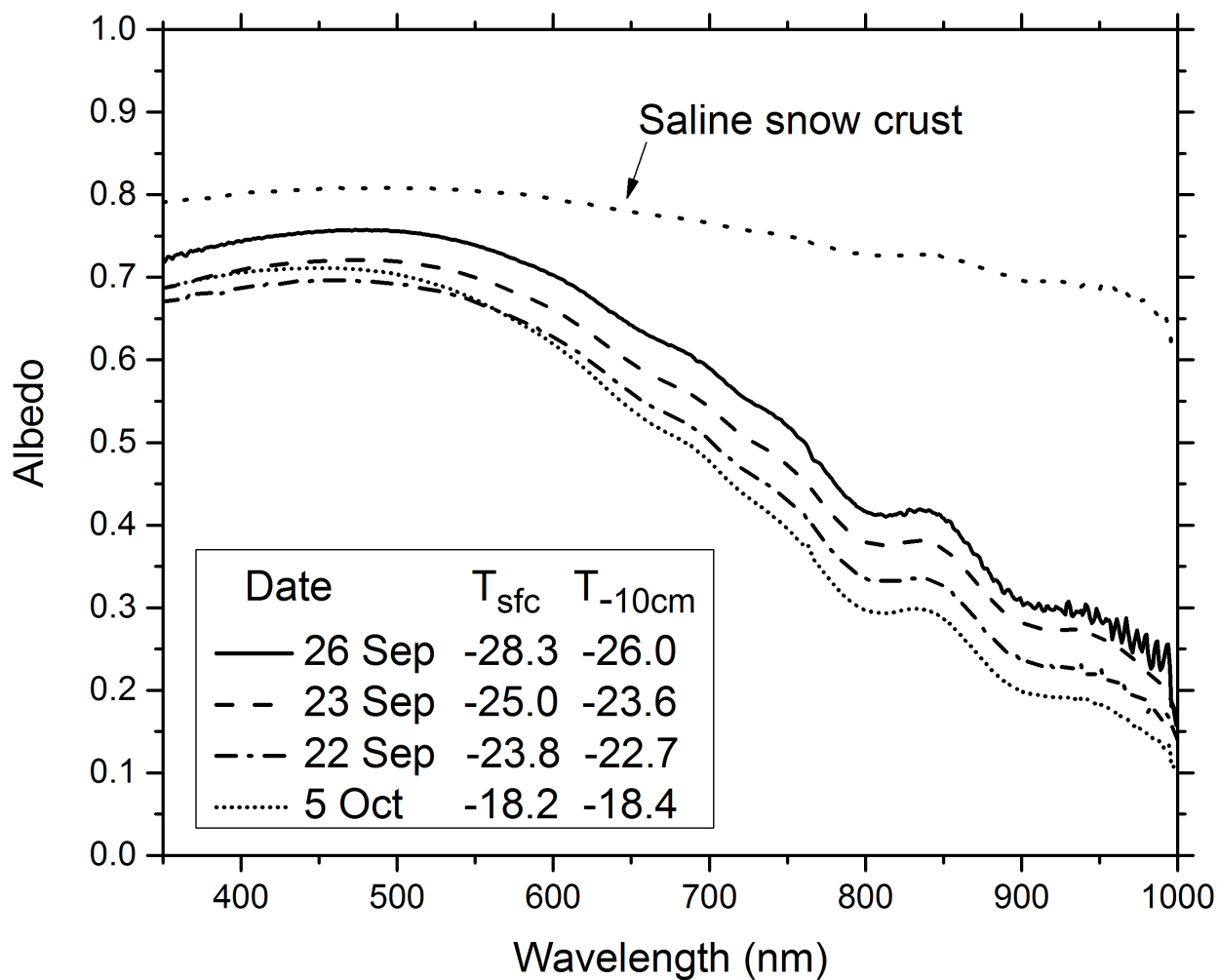


Figure 5. Spectral albedos of sea ice in McMurdo Sound during September and October of 2009. Except for the top curve, all measurements were of ice whose surface crust of salty snow had been scraped off. Legend shows date of measurement, surface temperature at time of measurement, and temperature at 10cm depth at time of measurement for each curve.

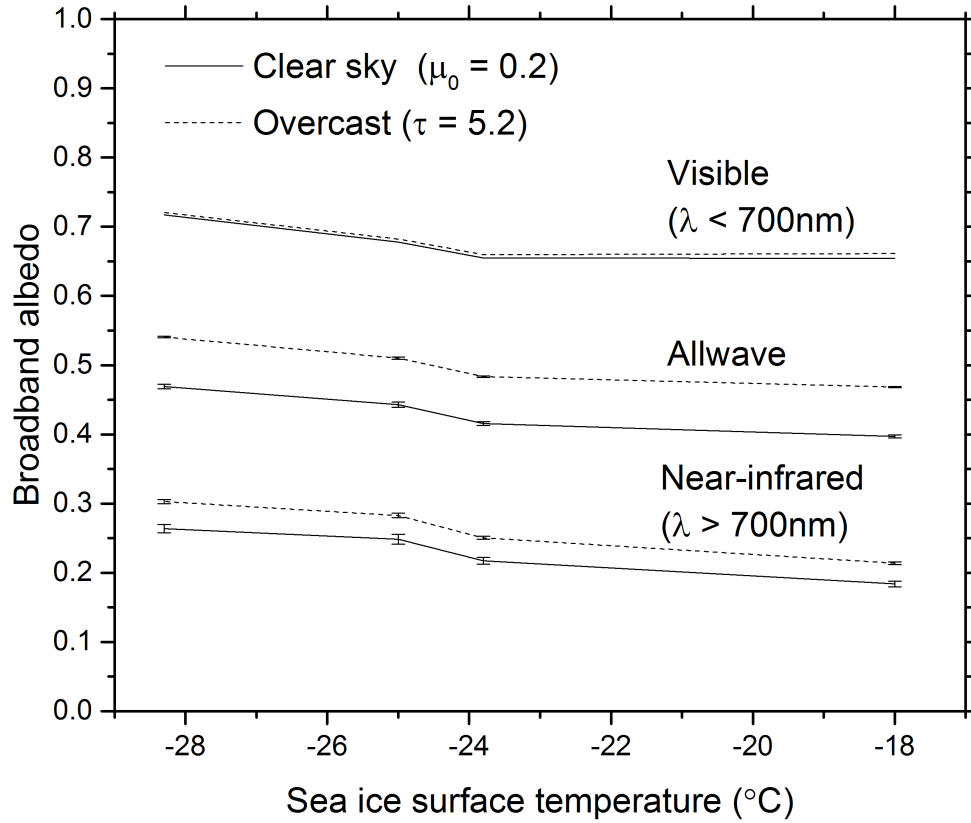


Figure 6. Broadband albedo as a function of temperature for three wavelength bands. To compute broadband albedo $\bar{\alpha}$, the spectral albedos $\alpha(\lambda)$ of Figure 5 are weighted by the incident solar spectra $F(\lambda)$ from an atmospheric radiation model [Wiscombe *et al.*, 1984]:

$$\bar{\alpha} = \frac{\int \alpha(\lambda) F(\lambda) d\lambda}{\int F(\lambda) d\lambda}$$

The limits of integration for the “allwave” band are 290 and 3000 nm. For the wavelengths not measured, albedos for $\lambda < 350$ nm were set to that of 350 nm; albedos for $\lambda > 1500$ nm were set to that of 1500 nm, as discussed by Brandt *et al.*, [2005].

Two atmospheric conditions are considered: clear sky at zenith-angle cosine $\mu_0=0.2$ (solar zenith angle 78.5°), and overcast cloud of optical thickness $\tau=5.2$, with a base at 1.27 km

above the surface (cloud thickness 1.46 km). Atmospheric temperature and humidity profiles are modified from the subarctic winter profile of *McClatchey et al.* [1972], as follows: All temperatures were multiplied by 0.9730 so that the surface temperature is 250 K; water vapor was scaled at each level to preserve the relative humidities of *McClatchey et al.* [1972].

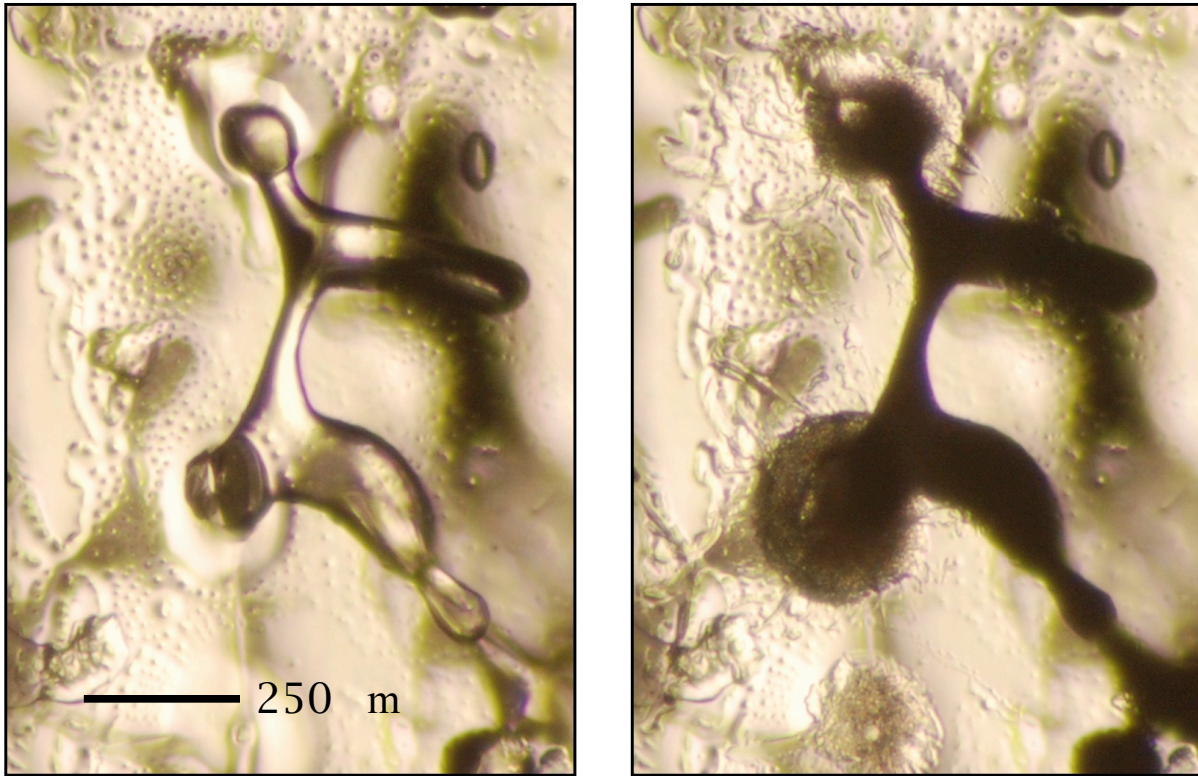


Figure 7. A brine pocket in lab-grown ice viewed under a microscope in transmitted light. In the lefthand image the brine pocket is filled with liquid; in the righthand image the sodium chloride has crystallized as hydrohalite, filling the pocket with small crystals that block the light. The images were taken 15 minutes apart at -28.7°C .

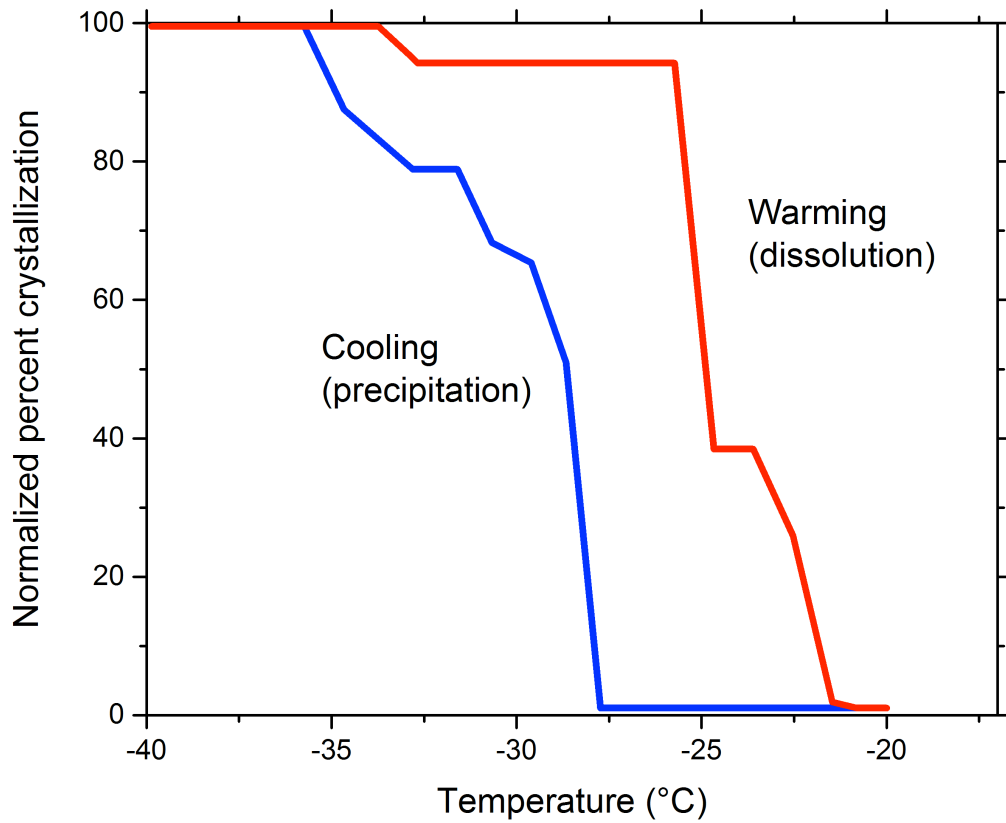


Figure 8. Hysteresis during a single temperature cycle of a thin section from an ice core taken in McMurdo Sound. The plot shows the amount of brine pocket area within the microscope's field of view that has crystallized, measured as a percentage of the total area of hydrohalite precipitation at the lowest temperature reached during the experiment.

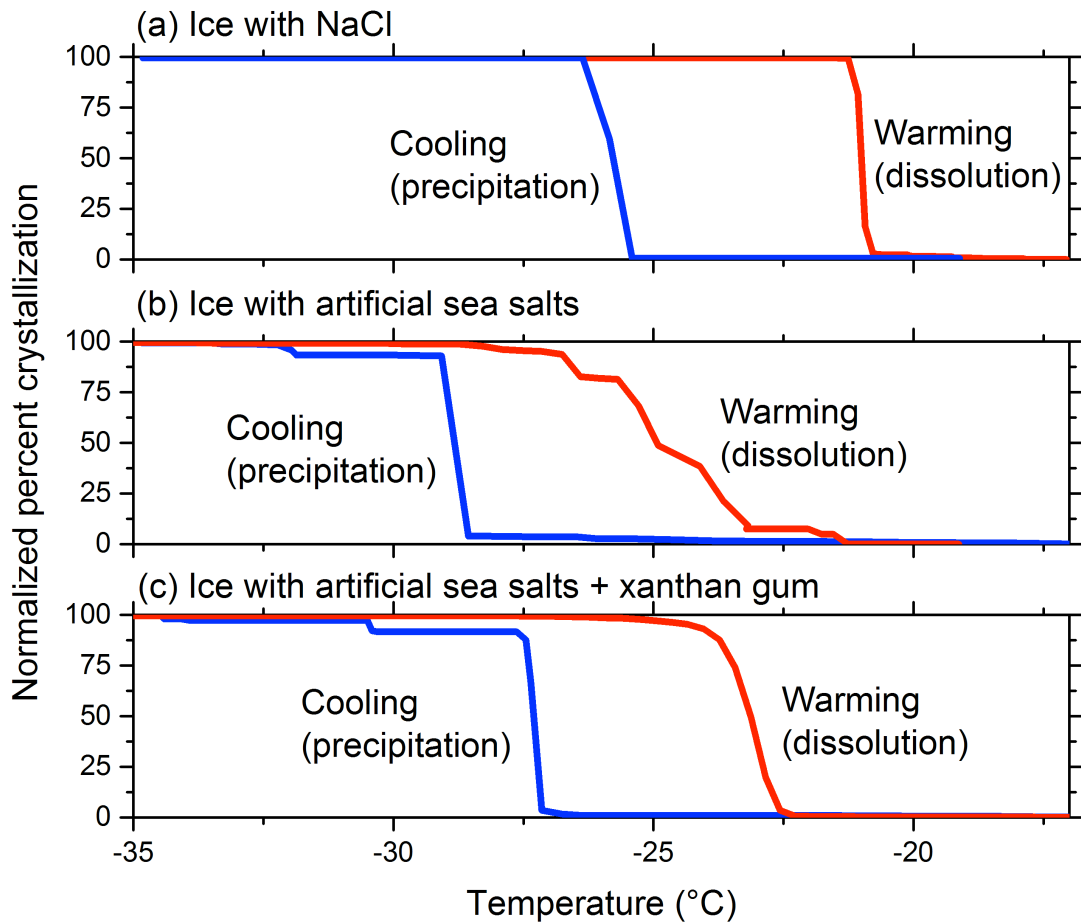


Figure 9. Selected experimental runs showing hysteresis of hydrohalite precipitation and dissolution during temperature cycling in three sections from different types of artificial sea ice. In all cases the brine inclusions do not crystallize until well below the expected precipitation temperature of -21.1°C for NaCl and -22.9°C for sea salt.

Chapter II: Measuring the albedo of a lab-created hydrohalite crust with the “Albedo Dome”

This chapter describes work performed with Bonnie Light. I am a coauthor with her on a manuscript about the “Albedo Dome” method and another manuscript about the hydrohalite crust measurements, both soon to be submitted. I have combined the two efforts here into one dissertation chapter. Since it is not a stand-alone paper, the Introduction to this dissertation also constitutes the introduction to Chapter II. (The written material in the dissertation chapter borrows a figure and some calculations from our “Albedo Dome” paper, but the rest has been written independently of that work, with advice from Bonnie.)

I joined the Albedo Dome project after the first experimental run had been completed, and helped to refine and validate the technique. Bonnie and I designed a number of changes and additions to the dome, including adding the “chimney” baffle, moving the Spectralon disk from a crossbeam to the ice surface, and guides to improve repeatability of ASD probe measurements; I worked with Allen Hart in the ATG machine shop to fabricate the new parts. We measured the albedo of a tarp outdoors and in the dome to test the accuracy of the dome procedure. I worked with Bonnie to develop the technique for making a hydrohalite crust that would be ready to measure before the cold room failed again. We both measured albedos during the experiment and worked on engineering problems as they arose. Bonnie developed the methods for calculating albedo from the dome measurements.

Chapter II:

Measuring the albedo of a lab-created hydrohalite crust with the “Albedo Dome”

Regina C. Carns^{1,2}, Bonnie Light³, and Stephen G. Warren^{1,2}

¹Department of Earth and Space Sciences,

University of Washington, Seattle, Washington, USA

²Astrobiology Program, University of Washington, Seattle, Washington, USA

³Polar Science Center, Applied Physics Laboratory, University of Washington, Seattle,
Washington, USA

1. Measuring albedo in the laboratory

Albedo is defined by the American Meteorological Society as “the ratio of reflected flux density to incident flux density, referenced to some surface.” Since flux density measures the rate at which radiant energy crosses a surface, albedo is a central component of most energy balance calculations, whether for an entire planet or for some smaller region. Accurately measuring albedo requires a full accounting of light energy crossing the reference surface (which may be the top of the atmosphere, a land or ocean surface, or an intermediate boundary) in all directions.

The amount of light reflected from a given area on a Lambertian surface is proportional to the cosine of the angle of incidence, so the easiest way to accurately integrate light from all directions is to use a radiometer whose response to light is proportional to the cosine of the angle of incidence (a cosine collector) to measure the upwelling and downwelling irradiance. This method is applicable to most outdoor surfaces [Levinson *et al.*, 2010]. The cosine collector must be raised high enough above the surface that its shadow does not interfere too much with the incident light, so the surface being measured must extend for several meters around the radiometer in order to fill its field of view. For example, if a radiometer is placed 70 cm above a surface, 90% of the light it samples will originate within a two-meter radius [Light *et al.*, 2015]. Translating this method of measurement to the laboratory without modifications introduces significant errors. A surface within a laboratory will necessarily be limited in size; the walls of the laboratory will constitute a significant fraction of the instrument’s field of view unless the laboratory is unusually large. The size of the laboratory may also restrict the distance between the surface, the radiometer, and the light source, causing the radiometer to shadow the surface. Laboratory light sources require a collimator to reproduce the approximately-parallel beams of light coming from an unobscured solar disk, or a diffuser to reproduce the omnidirectional light from an overcast sky.

Because some surfaces require a controlled environment to stay stable, efforts have been made to overcome these challenges and measure albedo in the laboratory. An early experiment

similar to the one described in this chapter was that of *Perovich and Grenfell* [1981], who illuminated a tank of artificial sea ice with a diffuser-equipped bank of incandescent light bulbs and measured the incident and reflected radiation with the fiber-optic probe of a spectrophotometer. However, this experiment did not correct for the shadowing from laboratory equipment or the uncertain angular distribution of the incident light source. Another laboratory measurement of albedo was that of *Hadley and Kirchstetter* [2012], who measured the albedo of black-carbon-infused artificial snow using a spectrophotometer equipped with a 15-cm integrating sphere. This technique worked well for snow, whose optical properties allow it to have effectively semi-infinite optical depth even with a small quantity of snow. Snow can also be packed into a sample holder without significantly changing its optical properties. Sea ice is more transparent than snow and more difficult to extract from the location where it was grown without disrupting the microstructure that determines its optical properties. We needed a solution that could measure the ice albedo in situ as it evolved over time.

2. Methods: the albedo dome

Our albedo measurement system had to fulfill several requirements. It had to produce an even, diffuse light field over the surface. It had to provide a platform from which to measure the incident and reflected irradiance without shadowing the surface unnecessarily. It had to be usable without disrupting the surface, since some of the surfaces we intended to measure would be delicate. And it had to be able to be removed and replaced to grant access to the sea ice tank.

To simulate the diffuse light from an overcast sky, we opted to use a half-sphere with a diffusely reflecting inner surface. By placing a light source at the center of the sphere, a uniform illumination would reach the surface below it. Our laboratory sea ice simulant was created in a tank 1.22 m by 1.12 m in area, so the simplest approach was to use a half-sphere similar in size to the tank and use the tank edge itself to support the structure. Using such a

large hemisphere also minimizes the area of the ports compared to the area of the hemisphere itself.

2.1. The albedo dome

The resulting apparatus, which we call the “albedo dome” due to its hemispherical shape, was designed to illuminate the surface with diffuse light while also allowing measurements of irradiance with a minimum of interference with the light field. Figure 1 shows a schematic of the dome.

The dome itself is a 1.22m acrylic half-sphere purchased from California Quality Plastics [<http://www.calplastics.com/>] with a 4-cm flange on its rim allowing it to be secured in place. The dome is sized to rest on top of the 1.12 mx1.22 m sea ice tank; in use, the ice surface being measured will form its “floor.” The interior of the dome was painted with six layers of white latex paint followed by eight layers of a 70/30 mixture of white latex paint and barium sulfate (BaSO_4) as a reflectance coating. The mixture used the maximum quantity of barium sulfate that still allowed the paint to coat the surface evenly without cracking. Opaque black landscaping plastic was attached to the outside of the dome to prevent any light from leaking into the dome.

Initially the light source for the dome was suspended in the center of the dome just above the ice surface, but the light output proved to be uneven and the proximity of the light to the ice surface threatened to cause melting. In the current design, a lamp mounted next to the dome houses a 750W tungsten-halogen bulb. The bulb is housed in an Oriel 66013 Lamp Housing. The light from the bulb is collimated by a parabolic reflector mounted within the lamp housing and by an F/0.7 fused silica condenser mounted in the exit aperture of the housing. This beam is directed at a mirror with broad spectral reflectivity, 50mm in diameter with a UV-enhanced aluminum coating, which reflects the light directly downwards through a hole cut into the top of the dome. The beam of light strikes a flat disk of Spectralon® material which rests on a three-legged aluminum stand which rests on the ice surface. Spectralon® is a manmade material engineered to be a near-perfect Lambertian reflector, and thus should direct the light equally

toward the entire inside surface of the dome, which diffusely reflects it back toward the surface.

To prevent stray light from entering through the hole in the top of the dome at oblique angles, and to reduce spreading of the beam, a short pipe made of black-painted aluminum is mounted in the hole at the top of the dome. The goal of this intervention was to ensure that all light entering the dome struck the Spectralon® disk before being redirected to the dome's interior surface, ensuring even illumination of the ice surface.

2.1.1. Dome coordinate system

To refer to specific points on the dome during its construction and when making measurements, we adopted a coordinate system using lines of constant zenith angle on the dome ("latitude lines"), measured from the surface to the top of the dome. Thus the rim of the dome is at latitude 0 degrees and the top of the dome is at 90 degrees. Because the dome sits atop the ice tank, with the surface of the ice some distance below the rim, we also define a line at -10 degrees, which sits on the wall of the tank.

2.1.2. Measurement ports

Holes were drilled into the dome along one side, all at the same azimuthal angle, to allow measurement of incident light on the dome interior and reflected light from the surface beneath. Since the Spectralon® reflecting plate occupied the center of the dome, an off-center area (hereafter referred to as the "footprint") was chosen for the reflected irradiance measurement. Three ports are located at latitude 60 degrees, 34.4 degrees, and 10.3 degrees on the dome, corresponding to zenith angles of 0, 30, and 70 degrees relative to the footprint. The holes at 60 degrees and 34.4 degrees are fitted with guides into which the fiber optic probe can be inserted, directing it at the center of the footprint. The hole at 10.3 degrees is used for measurement of incident irradiance, which is calculated from radiance measurements taken along the opposite wall of the dome.

See section 2.2 for more details on measurement procedure and 2.3 for calculation of albedo from measured radiances.

2.2. Measurement process

Radiance measurements were made using a fiber-optic probe attached to an Analytic Spectral Devices scanning spectroradiometer (ASD; *Kindel et al.*, [2001]). The instrument employs three separate grating spectrometers that simultaneously measure radiance across three wavelength regions covering 350-2500 nm, with spectral resolution 3-10 nm, and can average 100 scans in 10 seconds. It is designed specifically to cover the solar spectrum, and has order-blocking and cutoff filters to ensure uncontaminated spectra. The ASD radiometer was housed in an insulated box within the cold room laboratory, attached to a computer in the adjacent warm room.

The procedure uses radiance from 7-10 points on the interior wall of the dome to calculate incident light. Measurements of incident light target the 'latitude lines' of the dome at 80, 70, 60, 50, 40, 30, and 20 degrees. The fiber is attached to a rigid holder that allows it to be accurately and repeatably aligned with the measured points. Measurements of reflected light use the three ports described in section 2.1.

The procedure was repeated between 3 and 10 times, depending on the acceptable level of precision for the albedo measurement. Since the measurements were performed in the -30°C cold room, sets of measurements were sometimes broken up into parts or split between investigators to allow for re-warming.

2.3. Calculation of albedo from radiance measurements

The albedo is simply the ratio of upwelling over downwelling irradiance. The following sections describe how the incident and backscattered irradiances are computed from the radiance measurements.

2.3.1. Estimation of incident (downwelling) irradiance

If the dome were a perfect sphere with an isotropic point source of light in its center, the radiance on the interior surface would be completely uniform. The dome deviates from this ideal situation in a few ways: it is a half-sphere, truncated by the ice surface; the light from the Spectralon® disk is not perfectly isotropic; the disk has a finite extent; the dome's interior surface is not perfectly Lambertian; and there are interruptions in the dome surface created by ports which allow measurement and admit light. Except for the interference from ports, which is fairly small, all of these effects should be azimuthally symmetrical. Therefore we assume that the radiance leaving the dome's interior surface varies with latitude angle θ but not azimuthal angle ϕ .

Since the center of the dome is occupied by the light source (the Spectralon® disk), we must calculate the downwelling irradiance at the off-center "footprint" targeted by the measurements of reflected radiance. We introduce a coordinate system centered on the footprint, an "inner dome", with a subscript f . In this coordinate system, the incident irradiance on the footprint is

$$F_f = \int_0^{\frac{\pi}{2}} \int_0^{2\pi} I(\theta_f, \phi_f) d\phi_f \cos\theta_f \sin\theta_f d\theta_f \quad (1)$$

The red lines in Figure 3 are lines of constant θ_f on the inner dome. Each (θ_f, ϕ_f) coordinate pair on the inner dome over the footprint has a corresponding (θ, ϕ) , calculated by determining the intersection of a unit vector in the (θ_f, ϕ_f) direction with the outer dome; the projections of the lines of constant θ_f onto the outer dome are shown as circles of blue points. Most of these circles pass through several latitude bands on the outer dome.

To calculate the irradiance from a finite number (k) of radiance measurements I_k , we treat each I_k as representative of the value of radiance for a latitude band on the outer dome centered at θ_k and spanning width $d\theta$. The values of I_k are multiplied by weights m_k based on the solid angle of intersection between the projection of constant θ_f lines from the interior dome and the latitude bands of the exterior dome:

$$\int_0^{2\pi} I(\theta_f, \phi_f) d\phi_f = \sum_k m_k(\theta_f) I_k \quad (2)$$

Substituting equation (2) into equation (1) gives:

$$F_f = \int_0^{\pi/2} \frac{1}{2} \sin(2\theta_f) [\sum_k m_k(\theta_f) I_k] d\theta_f \quad (3)$$

Rewriting as a sum and moving I_k outside it:

$$F_f = I_k \sum_0^{\pi/2} \frac{1}{2} \sin(2\theta_f) [\sum_k m_k(\theta_f)] d\theta_f \quad (4)$$

This allows us to define constants C_k :

$$C_k = \sum_0^{\pi/2} \frac{1}{2} \sin(2\theta_f) \Delta\theta_f m_k(\theta_f) \quad (5)$$

such that:

$$F_f = \sum_k C_k I_k \quad (6)$$

The constants C_k used in calculating albedo are shown in Table 1.

Due to the design of the dome, the Spectralon® disk interferes with radiance measurements at the 20-degree latitude line or below, and the “chimney” in the top of the dome interferes with measurements near the top. Thus only the measurements from 30 degrees to 80 degrees are used to estimate the downwelling irradiance. Radiance measurements taken at other parts of the dome where the Spectralon® disk did not interfere suggest that the radiance at the unmeasured points can be estimated by linear extrapolation from the measured points.

The value for the point at the top of the dome (the 90-degree “line”) is extrapolated from the slope of a line passing through the values for 60, 70 and 80. Values for the 20-degree and 10-degree lines of latitude are extrapolated based on the slope of the line passing through the values for 30, 40 and 50. The value for the 0-degree line, where half of the field of view of the fiber is the tank wall, is 0.5 times the extrapolated value from the 30-40-50 line. The value for the -10-degree line, which is mostly the tank wall, is set to 0.

2.3.2 Estimation of reflected (upwelling) irradiance

The dome was designed with the intention of using measurements taken at the 10.3-degree port (70 degrees zenith angle relative to the footprint) and the 34.4-degree port (30 degrees zenith angle) to determine total reflected irradiance by integrating using Gaussian quadrature.

Unfortunately, at 70 degrees zenith angle, either the Spectralon® disk or ice shadowed by the disk was frequently within the field of view of the fiber, making the measurement inaccurate.

Measurements from the ports at 0 and 30 degrees generally supported an assumption of approximate isotropy in the upwelling radiance field. These measurements were slightly more different than could be accounted for by typical measurement error, but still generally within 10% of each other. Using the assumption of isotropy, we averaged these two measurements and multiplied by π to find the total upwelling irradiance:

$$F^{\uparrow} = \pi \frac{(I_0 + I_{30})}{2}$$

2.4. Validation of dome technique

To evaluate the accuracy of the dome technique, we needed to measure the same surface both using the dome and using a more traditional albedo-measuring technique. For the comparison surface we chose a white tarp, backed with opaque black landscaping plastic to avoid any interference from the surface underneath. The albedo technique we chose for our outdoor measurement uses a cosine collector mounted on a long arm, which is counterweighted and supported by a tripod (Figure 4.) The collector gathers light from the sky, then is rotated to collect light from the underlying surface.

We chose a cloudy day to make our outdoor measurement to be consistent with the diffuse illumination provided by the albedo dome. We used two tarps to cover an area of approximately 6 by 9 meters. We laid out the tarp in a large, mostly empty parking lot, at least several meters away from any cars or trees. We arranged the tripod so that the cosine collector was centered on the tarp, with the ASD itself located near the edge. The sky was completely overcast and no solar disk was visible, but we minimized possible shadows by placing the tripod, observer, and

electronics (anything that could shadow) to the north of the measurement area. In analyzing the data, we applied a small correction (1.7%) for the shadowing effect of the tripod and ASD on the albedo results. We took 10 measurements, alternating between up and down.

To measure the albedo of the tarp using the albedo dome, we cut a piece from the tarp that was of the correct size to cover the surface of the tank. We backed it with opaque black landscaping plastic as in the outdoor measurement. We placed the black plastic and the tarp on the flat ice surface and took measurements using the same procedure as described for the ordinary tank surface measurements.

Figure 5 shows the results of these measurements. The dome albedo is an average of ten sets of measurements; the error bars show one standard deviation.

2.5. Sources of error in dome measurements

2.5.1. Errors reduced by re-design of apparatus and procedure

The measurement procedure requires two observers, since the computer controlling the ASD is located outside of the cold room. To test reproducibility between observers and to prevent excessive exposure to cold for the observer taking measurements in the cold room, observers traded off between roles. Initially radiance measurements were made while holding the fiber by hand and estimating the correct angle, but these proved to be inconsistent between different observers. To improve consistency in the measurements of reflected light, guides were fabricated and attached to the dome, allowing the fiber to be placed in exactly the same position each time. To improve the incident measurements, all of which were made through the same opening in the dome but at many different angles, a holder for the fiber was constructed which could be aligned at reproducible angles using a marked plastic guide. Some measurements still showed a small systematic difference between observers, but for the most part this was within the normal variations seen from measurement to measurement in the experiment.

The “chimney”, an aluminum tube projecting down from the hole in the top of the dome, was installed to prevent light from straying outside the designated path. The interior of the chimney is painted flat black, but some light may still be reflected from the tube’s interior surface and fall outside the Spectralon® target in the center of the dome. In future versions of the dome, better collimation of the light beam using a lens, or a more absorptive surface for the interior of the aluminum light “chimney”, might reduce this stray light further; even without these enhancements, however, light leakage appears to be small.

The Spectralon® disk was initially mounted on a crossbar attached to the dome, approximately two inches above the ice surface due to the gap between the ice surface and the tank edge. Calculations and observations suggested that the disk was shading an unacceptably large area of the ice surface, so it was moved to a small platform placed on the surface itself. When attached to the dome, the Spectralon® disk was automatically centered beneath the aperture in the top of the dome regardless of the dome’s location; after the two were decoupled, the disk had to be carefully placed using a makeshift plumb bob. The disk remained in place on the ice except during the creation of the spray crust described in section 3.2 and the dome’s position above it was exactly replicated each time it was removed and replaced.

2.5.2. Other sources of error

Despite the brightness of the 750W bulb, considerable light is lost to the laboratory and the lamp interior, and light levels within the dome are low compared to the conditions for which the ASD spectroradiometer is designed. Measurements are noticeably noisy in regions of the spectrum where photon counts are low. We compensate by using multiple measurements to reduce noise in the final result. The tarp validation results suggest that the low counts do not introduce any wavelength-dependent bias. The exception is wavelengths below 500nm, where reported albedos are consistently too high; the effect (which is a result of low output at these wavelengths from the light source) is too unpredictable to fix using a correction, so we simply do not report albedos at shorter wavelengths.

Light leakage into the interior of the dome is another possible error source, since the calculation of downwelling irradiance depends on the assumption of azimuthally uniform illumination. The reflective coating on the interior of the dome and the opaque black landscaping plastic on the exterior create an effective barrier to light, and the laboratory is darkened during measurement, aside from the lamp illuminating the interior of the dome. Due to the mismatch between the circular shape of the dome and the square shape of the sea ice tank, however, there are gaps between the dome and the tank walls; it is possible that some light could enter these gaps after reflecting off of the floor or walls of the laboratory. Light leaks near the footprint would cause the incident light measurement, based only on the light reflected from the walls, to underestimate the amount of light actually falling on the surface and being backscattered. This would increase the apparent albedo. Light leaks on the opposite side of the dome, where incident radiance measurements are taken, would have the opposite effect.

Another possible source of error is the geometry of the ice surface itself, which is somewhat uneven and sits approximately two inches below the edge of the tank on which the dome rests. The tank wall is dark gray in color, contrasting with the ice and the dome. We compensate for this by adjusting the calculation of incident irradiation as discussed in section 2.3.1.

3. Methods: Creating and measuring a hydrohalite crust

3.1. The Ice

The artificial sea ice surface is created in an insulated tank 1.12 m wide by 1.22 m long, with a capacity of 988 liters, originally manufactured as a commercial container for liquids such as milk, juice or liquid soap (<http://www.bonarplastics.com/Products/BagintheBox.aspx>). A large plastic liner fitted with a drain spout sits inside the tank to improve leak resistance and allow easier cleanup. The tank walls are approximately 2" thick and filled with polyurethane foam to provide insulation for the contents.

The tank was filled using filtered tap water. (Local Seattle tap water generally has <50 ppm total dissolved solids, according to analyses by Seattle Public Utilities.) The tank could not be filled all the way to the rim without risking overflow, so the water level was brought to approximately five inches below the rim. We added reagent-grade sodium chloride, stirring and measuring salinity after each addition, until the salinity of the tank reached 24‰. The cold room was set to -20°C and the tank allowed to freeze. After freezing, approximately two inches of the gray tank wall were exposed between the ice surface and the tank rim on which the dome rested. Thermistors mounted in a length of PVC pipe at 5cm intervals monitored the temperature of the ice during experiments; temperature measurements were logged on a computer at a customizable interval.

3.2. The crust

Initial experiments attempted to replicate a “Snowball Earth” salt crust as closely as possible by allowing the NaCl ice to sublime naturally. The crust developed slowly over a period of months, and some preliminary measurements were acquired, but mechanical failures in the cold room refrigeration repeatedly destroyed the hydrohalite crust by allowing temperatures to rise above the eutectic.

3.2.1. HH-rich ice layer

The unpredictability of cold room failures necessitated a more proactive approach to the development of a lag deposit on the ice surface. The cold room laboratory was set to -30°C , resulting in a surface temperature of approximately -27°C . Containers of 233‰ NaCl solution were chilled to just above the eutectic temperature and sprayed onto the ice surface using trigger-type pump spray bottles. This near-eutectic mixture was sprayed onto the ice surface in thin, even layers. Each new application of solution was allowed to freeze for between 5 and 24 hours before the next was added. When the layer was thick enough to obscure dark-colored markers placed on the ice surface before the spraying (11 layers thick), it was judged to be optically thick.

The NaCl solution sprayed onto the tank was not observed to melt the ice beneath it, so we assumed that the layer of hydrohalite-rich ice contained the same relative amounts of sodium chloride and water molecules as the initial solution. The original 233‰ solution contained 193 grams, or 10.7 moles, of water per mole of sodium chloride [(58.5 g mol⁻¹ ÷ 233‰) – 58.5 g]. The solid mixture of ice and hydrohalite thus contained 8.7 moles of water (157 grams of water) per mole of hydrohalite (94.5 grams), making it 360‰ (36%) hydrohalite by weight. It was 25% hydrohalite by volume assuming a density of 1.6 grams per cubic centimeter for hydrohalite [Adams and Gibson, 1930]. Compare this to sea ice with a typical salinity of 10‰, which is only 16‰ hydrohalite by weight or 9‰ by volume. Over 30 times as much ice must sublimate from natural sea ice to leave the same thickness of hydrohalite crust.

Although the hydrohalite-rich ice layer was created in the laboratory for reasons of practicality, it is an analog to a situation that could arise naturally on a Snowball planet: the melting and re-freezing of an established hydrohalite lag deposit. This situation occurred in the laboratory tank when the freezers malfunctioned during an early run of the experiment. A hydrohalite crust had developed over a period of time below –21.9°C; when the temperature rose above –21.9, the crust dissolved. (Pure, dry hydrohalite is stable up to 0.1°C, but in contact with ice above the eutectic point it will melt the ice [Marion and Grant, 1994].) When the laboratory dropped back below the eutectic point, the brine refroze as a layer of hydrohalite-rich ice and the crust gradually re-formed. The same sequence of events—a crust forms below the eutectic temperature, melts when temperatures rise, then re-freezes when they decrease again—would almost certainly occur at some places and times on Snowball Earth.

3.2.2. Sublimation process

The ice in the crust sublimated over a period of 47 days. We made observations at regular intervals during this period—48 hours after applying the hydrohalite-rich ice layer, 5 days after, 7 days after, and once a week after that. Between measurements the dome was elevated by blocks placed between it and the edge of the tank, with a small electric fan pulling air through the gap to help speed the sublimation process.

Inspection of the crust during the sublimation process did not provide clear indication as to how the sublimation front progressed through the ice. The top layer of the ice did become less cohesive during this time; the newly-frozen HH-rich ice was hard and required firm scraping to sample, while the final hydrohalite crust was flaky and easy to remove from the surface. Figure 6a shows the initial crust; Figure 6b shows it at a later stage.

Figure 7 shows the progression of the hydrohalite crust albedo over time. Day 47 was similar to day 42 to within the uncertainty of the measurement, leading us to conclude at this point that the albedo had stopped increasing. This conclusion is supported by the albedo measured 60 days later (on Day 107) just before the melting phase of the experiment, which falls between the Day 42 and Day 47 albedos.

We assume that albedo stopped increasing because the crust had become optically thick. Another possible interpretation is that the sublimation front hit the bottom of the HH-rich layer, e.g the interface with the lower-salinity ice surface. Hitting the bottom would cause the increase in albedo to slow down considerably even if the hydrohalite layer was not yet optically thick. However, given that the albedo had not measurably increased after 60 additional days had passed, it seems likely that the hydrohalite crust was effectively semi-infinite.

3.2.3. Melting process

After the crust reached its maximum albedo, we prepared to increase the temperature of the cold room above the eutectic point and observe the albedo of the crust during melt. We hoped to see a puddle of standing water—a “melt pond” —form, but we were concerned that the meltwater from the warming surface would run off of the surface of the tank, since its center was slightly domed from the pressure of the ice during freezing. We constructed barriers on the edge of the tank by placing strips of foam on the tank surface and slowly saturating them with water, creating an ice barrier while disrupting the surface as little as possible.

We prepared for the melt by slowly (over several days) increasing the temperature of the cold room to near the eutectic temperature. Somewhat contrary to our expectations, the temperature readings from the under-ice thermistors showed that the tank was almost isothermal during

the period of warming, with the thermistors near the bottom of the tank differing by only a degree or two from the thermistors at the surface.

On the day set for the melt, we raised the temperature of the room from approximately -22°C to slightly below 0°C . Figure 9 shows the thermistor readings from just above and just below the surface, as well as one reading from deeper in the ice and one from the highest thermistor (about 30 cm above the ice.) The readings are not an exact indication of the temperature of the “footprint” area whose albedo is being measured, because the thermistors were several tens of centimeters away from the footprint in a different corner of the tank. However, the changes in the tank surface during melt appeared to be the same in all areas of the tank (Figure 8), so it is likely that the error introduced by any horizontal inhomogeneity is small.

Albedo was measured approximately every 20 minutes during the first two hours of the melting process, and at 1-2 hour intervals thereafter. We made 4 separate measurements of albedo at each interval; each set of 4 albedo measurements took 7-12 minutes. The albedo began to drop rapidly around 30 minutes after the beginning of the experiment. Dark patches were visible on the surface of the crust where liquid brine was beginning to saturate the hydrohalite crystals (see Figure 8b.) By 120 minutes after the beginning of warming, specular reflections showed that a film of liquid brine covered the hydrohalite crystals, and the albedo was only marginally higher than the albedo of the original bare sub-eutectic ice. By hour 5 the albedo had dropped below that of sub-eutectic ice; over the next three hours it continued to drop slightly.

4. Results

Figure 7 shows the sequence of albedos during crust growth. The albedo increases dramatically in the infrared as the hydrohalite crust begins to form, especially between 1500 and 1900 nm. The albedo in the visible range starts relatively high, so it increases more slowly. Between day 21 and day 35, the albedo stops increasing, and even appears to decrease slightly. Given the uncertainty in the measurements it is not possible to tell whether this is a real effect. If it is real, it could be due to moisture fluctuations in the air of the cold room laboratory; higher humidity would slow the sublimation of the ice and could even condense on the surface as

frost. Day 42 is clearly higher. On day 47, as previously discussed, we stopped our measurements. When we measured the crust again on day 107 in preparation for the melting phase, the albedo had not measurably increased.

Figure 10 shows the reduction of albedo during melting. Note that the spectral peaks in the infrared are slightly different than those of the HH-rich ice layer (overlaid on Figure 10); the measurement of melting crust albedo at 52 minutes is lower in albedo than the HH-rich ice layer at most wavelengths, but it shows a prominent peak near 1700 that is higher than that in the HH-rich ice layer and also shifted somewhat toward shorter wavelengths.

The albedo decreased below that of the bare sub-eutectic ice because the ice below the surface was no longer sub-eutectic. At this point ice in the tank was nearly isothermal, so it is difficult to say how deep within the ice the dissolution front progressed, but it is clear that most of the ice near the surface was significantly above the eutectic. The continuing decrease in albedo probably represents a decrease in scattering surfaces as crystals of ice and hydrohalite dissolve into the brine. At this point the ice surface most closely resembles ordinary sea ice during the melt season.

The integrated broadband albedos for the two phases of the experiment are shown in Figure 11 and Figure 12. For ease of comparison with other measurements they are calculated from 300-700nm and from 700-2500nm. The laboratory measurements are noisy below 500nm and above 2200nm, so the calculation assigns the 300-500nm region the mean albedo value from 495-505nm, and assigns the 2200-2500nm region the mean albedo value from 2150-2200nm.

5. Discussion

We expected the hydrohalite crust to have high albedo, based on previous experiments [*Light et al.*, 2009]. However, we were somewhat surprised by the magnitude of the effect. The broadband albedo of the hydrohalite crust itself is above 0.9 at its highest point. This is higher even than sea ice with thick dry snow, which has an albedo of ~ 0.83 [*Grenfell et al.*, 1994]. Sea ice that is snow-free due to melt, rather than due to wind or sublimation, has an albedo of 0.6-0.7 if melt ponds are absent [*Perovich et al.*, 2002].

Bare sea ice whose temperature falls below the eutectic point is known to increase in albedo by a modest amount [Chapter 1]. However, sublimation sufficient to remove snow from the sea ice will quickly begin to sublimate the ice itself and create a hydrohalite crust if the ice remains below the eutectic point. The rapid increase of albedo during the first few days of the growth phase of the experiment shows that even a small amount of sublimation can have a noticeable effect on albedo.

5.1. Implications for Snowball Earth

The presence of salt in the ice introduces new positive feedbacks. Snow-free ice that cools below the precipitation temperature of hydrohalite will increase in albedo [Chapter 1], introducing one modest positive feedback.

If the ice remains below this temperature for an extended period of time in a net-sublimation environment, it is likely to develop a lag deposit of hydrohalite. The nature of the deposit will depend on both the composition of the ocean and the ambient temperature. If temperatures are between the precipitation point of hydrohalite and the eutectic point of the brine with its full complement of salts, a deposit of brine-wetted hydrohalite crystals may form. The current experiment can say little about such a deposit, but it is a potential candidate for further study. If temperatures remain lower than the eutectic temperature of the ocean's mixture of salts, a dry deposit with very high albedo will form, cooling the climate further. While this deposit was slow to develop in the laboratory, net-evaporation environments on Snowball Earth would be exposed to strong sunlight and wind that could accelerate the process.

If a dry deposit forms and later warms above the eutectic, the deposit will rapidly dissolve and reduce the albedo of the surface. The low-albedo surface will absorb sunlight and warm further, introducing yet another positive feedback. The dissolution phase of the dome experiment shows how quickly this effect can take hold. The cycle of cooling, formation of a lag deposit, and subsequent melting could even occur many times over. The results of such a cycle are difficult to predict.

The high albedo of hydrohalite compared to that of snow in the near-infrared also has implications for the dynamics of Snowball Earth states on planets orbiting lower-temperature stars, where more of the incident radiation is in the near-infrared. Such planets have a more difficult time reaching ice-albedo runaway feedback due to absorption by ice in the near-infrared [*Shields et al., 2013*] but once in a Snowball state, the development of salt crusts might inhibit melting to a comparatively greater degree than it would for a planet around a hotter star.

Figures

Latitude	Weight
90	0.0179
80	0.1074
70	0.2120
60	0.3107
50	0.3992
40	0.4711
30	0.5141
20	0.5050
10	0.4058
0	0.1731
-10	0.0249

Table 1. Weights used for calculation of incident irradiance.

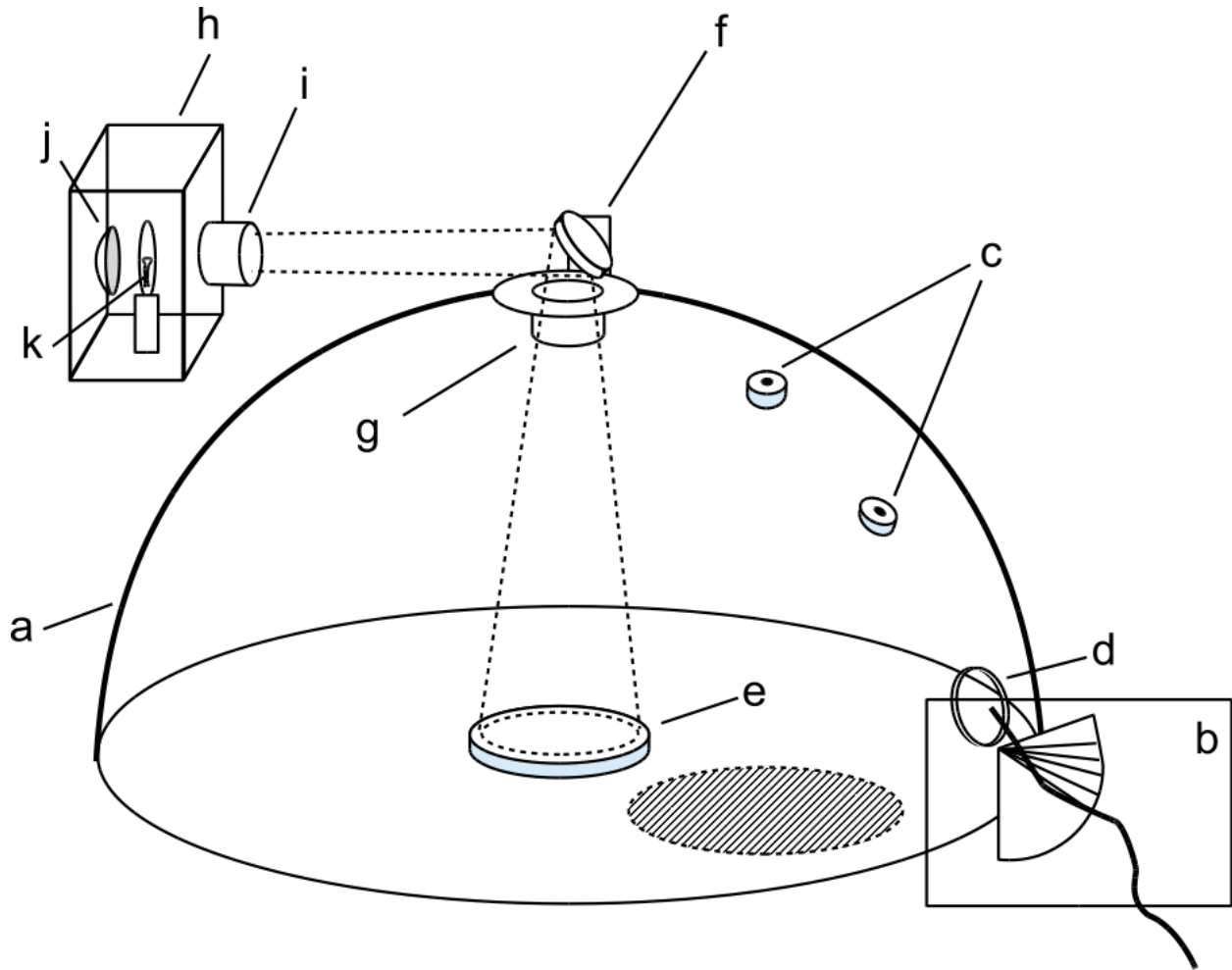


Figure 1: A schematic of the albedo dome. Shown are a) the dome itself, b) the optical fiber of the ASD and protractor (see Fig 1b), c) the 0 degree and 30 degree viewing ports with attached guides for the optical fiber, d) the 70 degree viewing port, e) the Spectralon disk which reflects the light beam onto the interior of the dome walls, f) the mirror which redirects the beam into the dome, g) the “chimney” which reduces stray light from the beam, h) the lamp housing, i) the lamp aperture with lens, j) the collimating parabolic mirror, k) the light bulb.

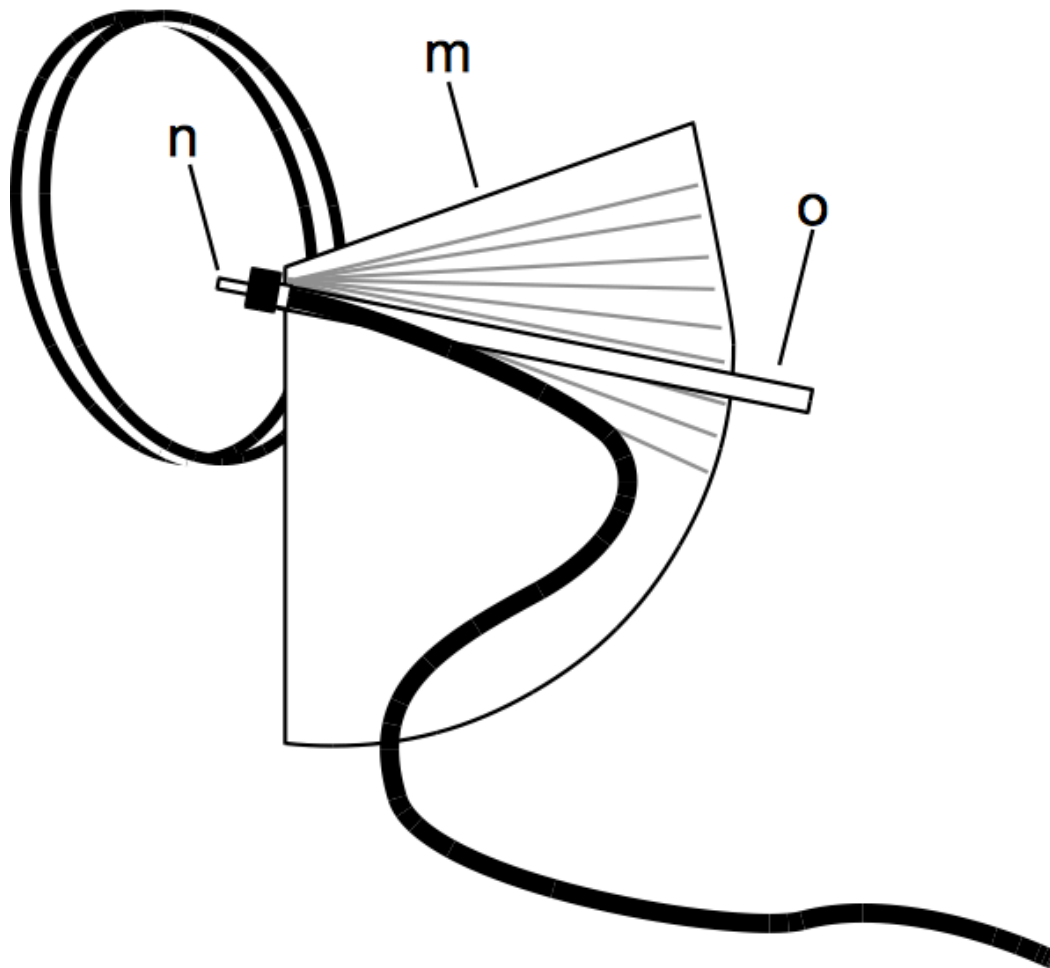


Figure 2. Close-up of apparatus for measuring the incident light on the wall of the dome interior: n) the fiber, o) the fiber holder which allows it to be accurately directed, and c) the protractor used to align the fiber with specific points on the far wall of the dome.

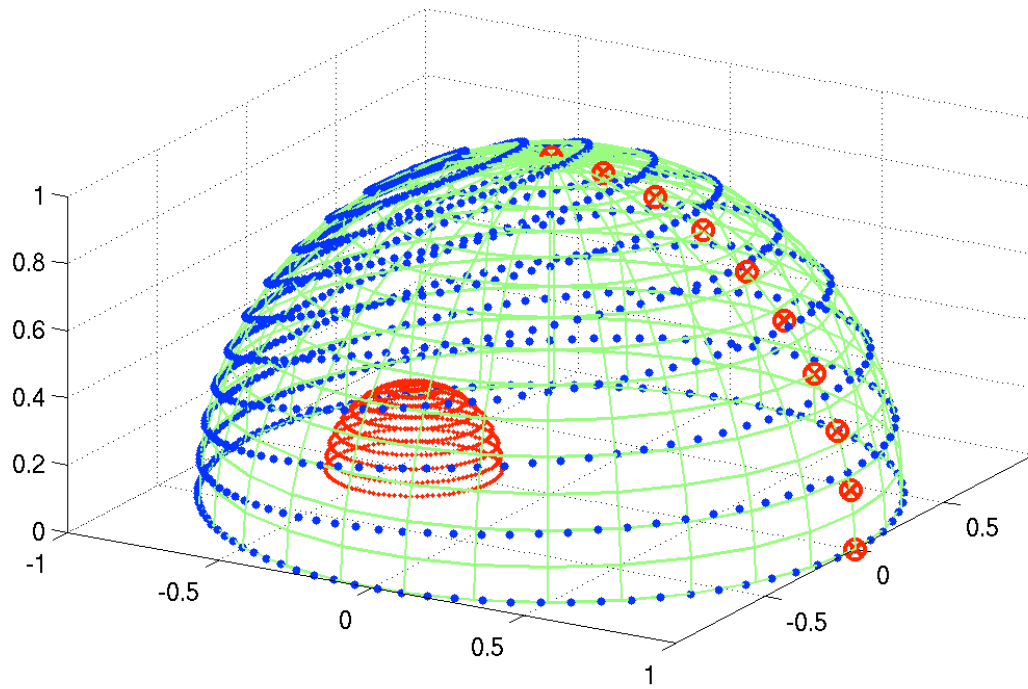
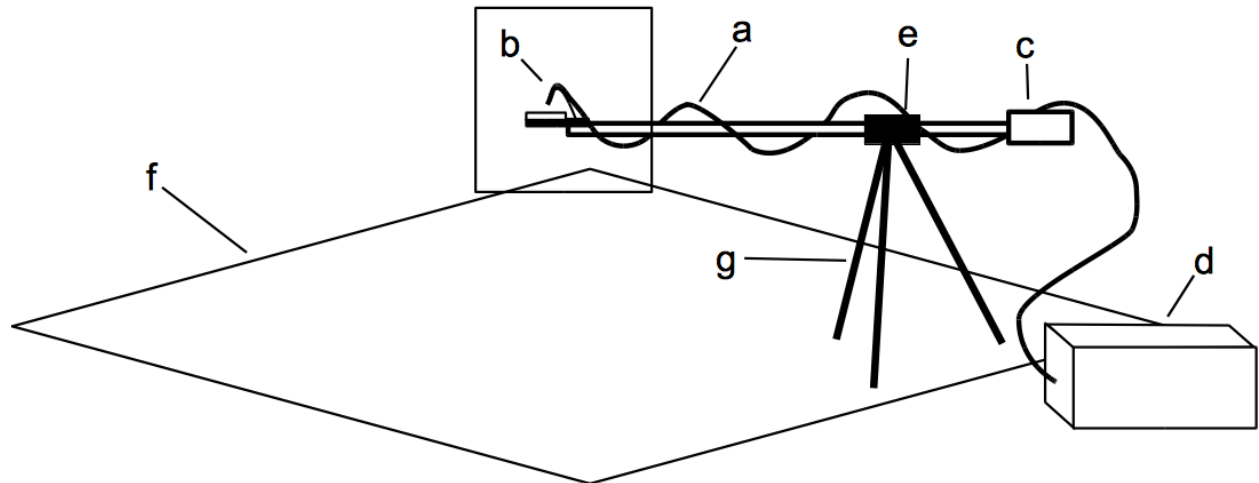
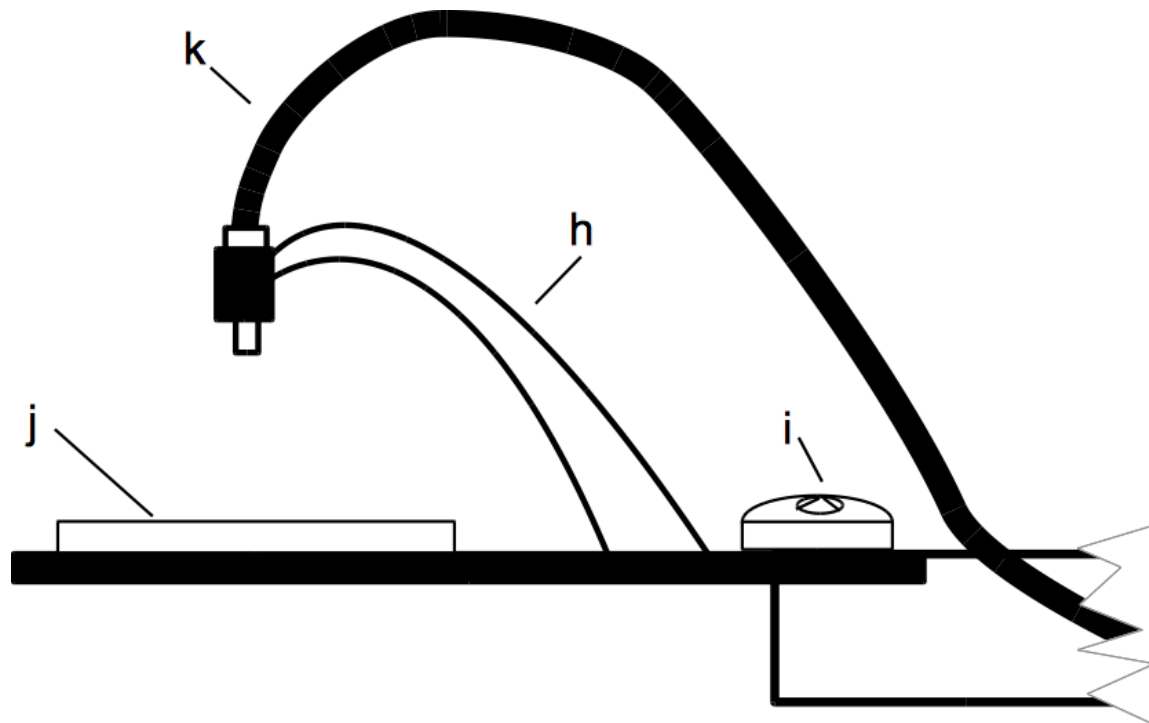


Figure 3. Derivation of the weighting factors for the measurements of incident light. The red lines show the inner dome centered over the footprint; the blue points represent projections of the red lines onto the outer dome. The red marks show the points where radiance measurements are taken.

a)



b)



a)

Figure 4a, outdoor measurement apparatus. a) the optical fiber, b) the fiber holder and cosine collector, c) the counterweight, d) the ASD spectrophotometer, e) holder allowing

pole to be rotated freely, f) the tarp, g) the supporting tripod. Inset b) shows h) the fiber holder, i) removeable bubble level, j) Spectralon plate, k) the optical fiber.

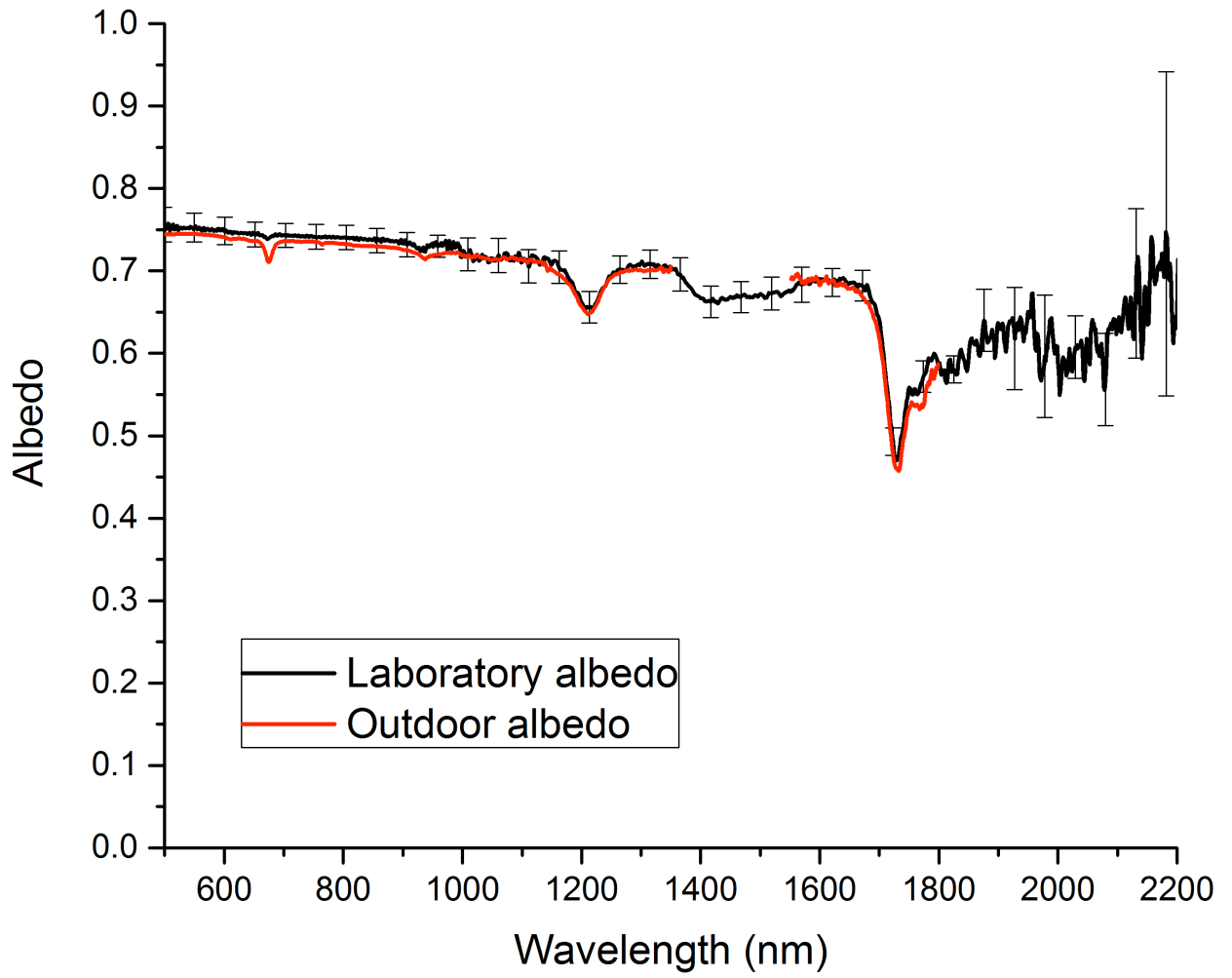
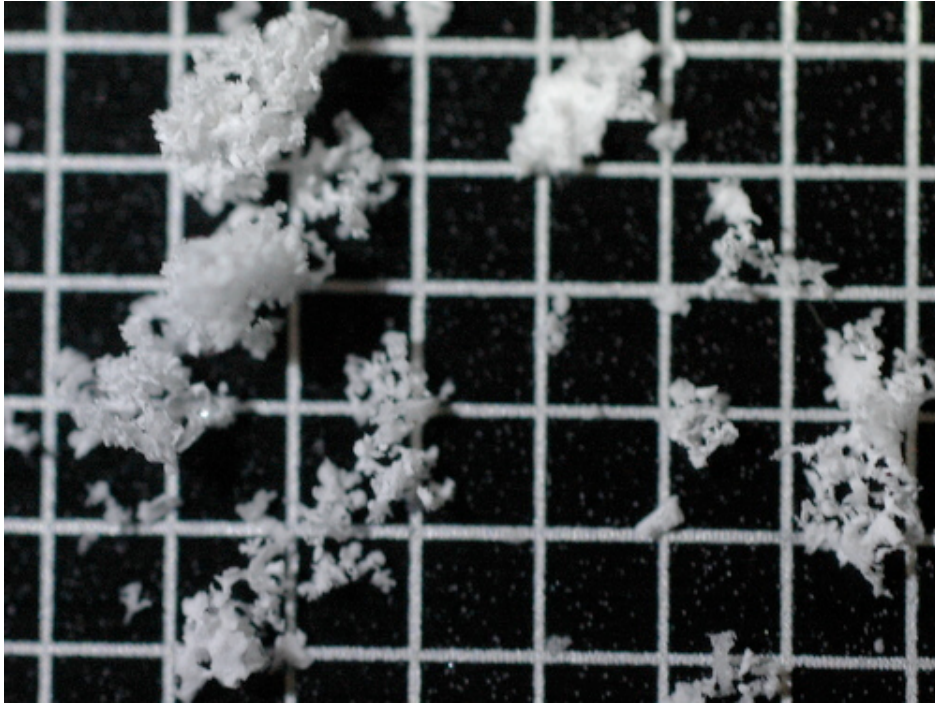


Figure 5. Results of the test versus more established methods.

a)



b)

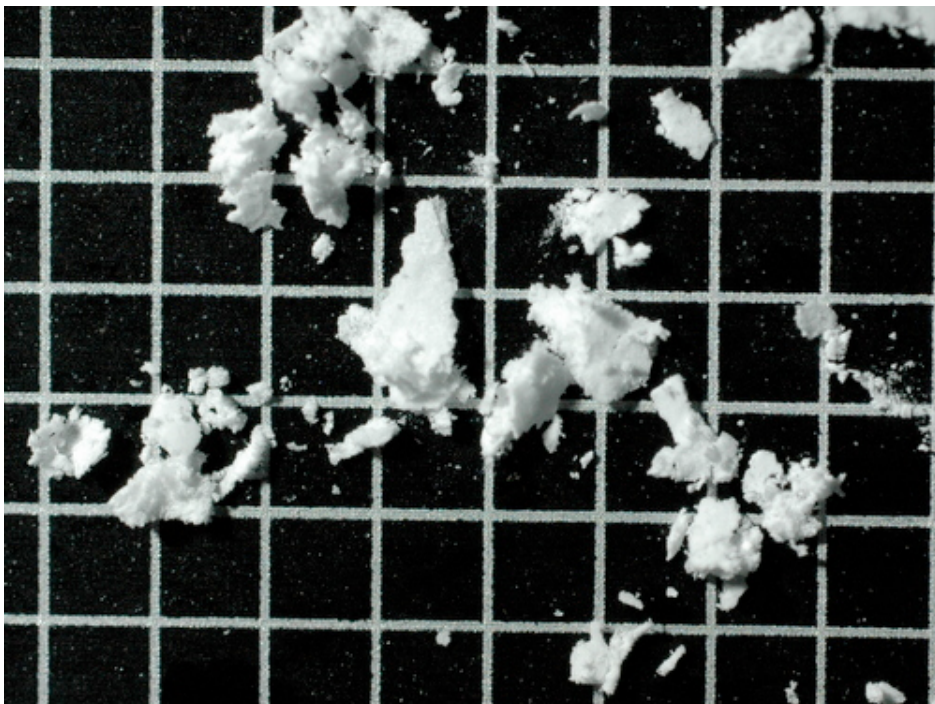


Figure 6. Hydrohalite from the crust. The sample in image a) was taken immediately after the crust was sprayed. The sample in image b) is from Day 35.

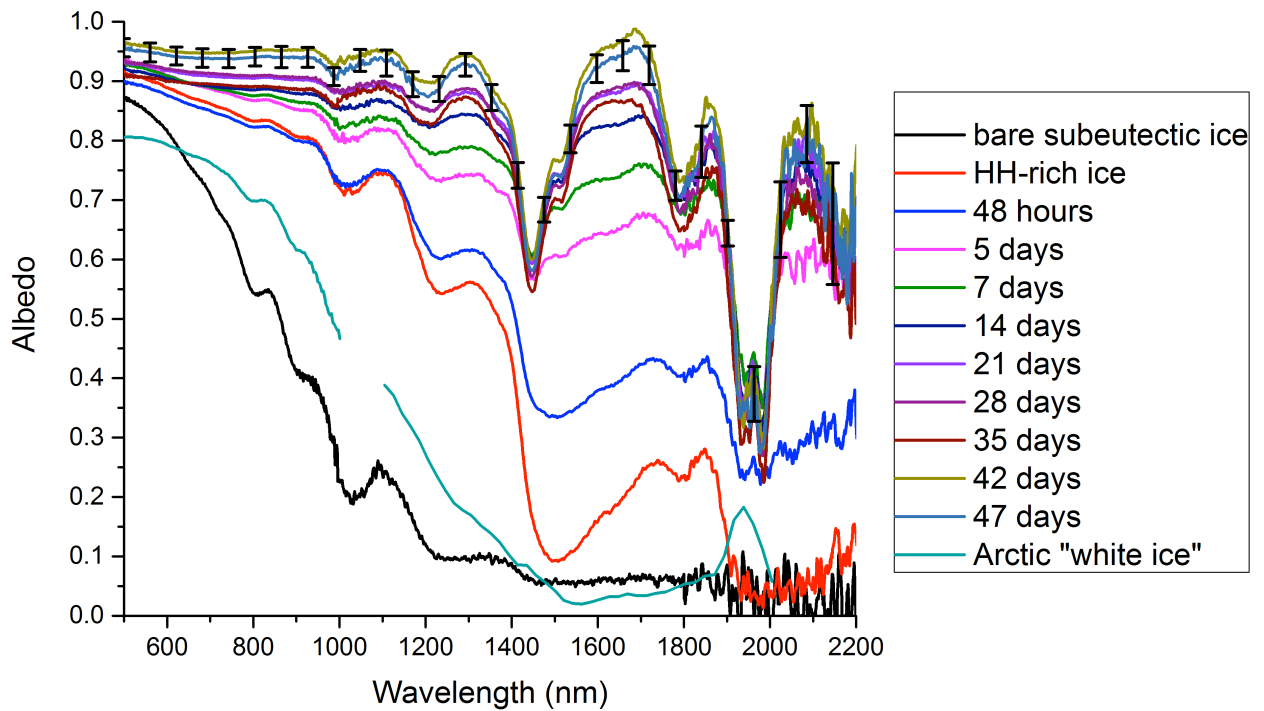


Figure 7. Spectral albedos during the development of the hydrohalite crust. Error bars shown on the 47-day albedo are calculated by taking the standard deviation of ten measurements. Error bars on other albedos would be of similar magnitude, and are omitted for clarity. A spectral albedo for snow-free, melting Arctic sea ice—called “white ice” due to the drained layer of degraded ice on its surface—is also shown for comparison (sea ice data from SHEBA archive [*Grenfell and Light, 1999*]).

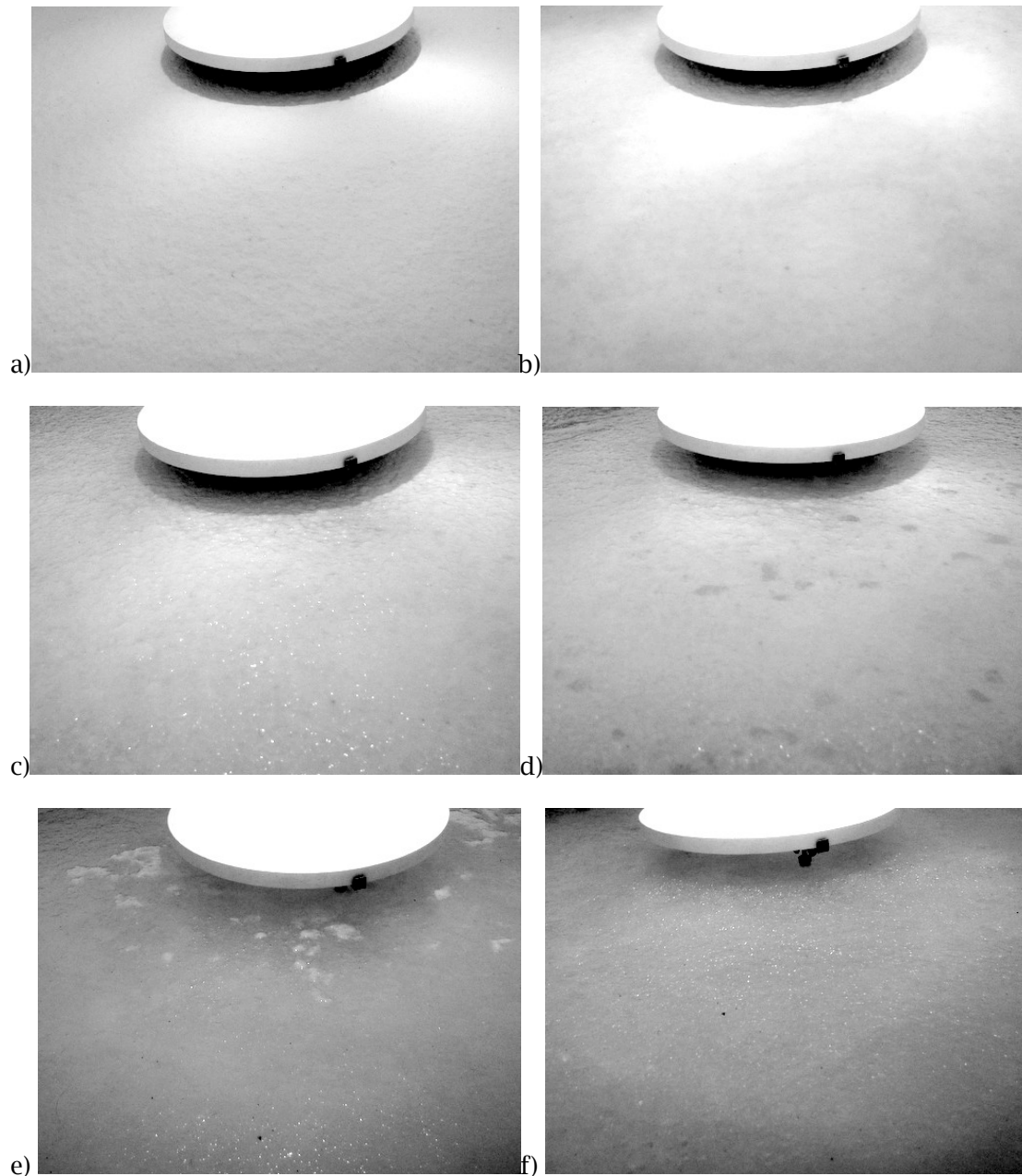


Figure 8. Progression from dry hydrohalite crust to brine-wet crust during warming of tank. These images have been processed with Picasa [<http://picasa.google.com>] to improve contrast, so they appear darker than the actual ice surface. a) initial tank surface; b) after 60 minutes; c) after two hours; d) after three hours; e) after five hours; f) after 6.5 hours.

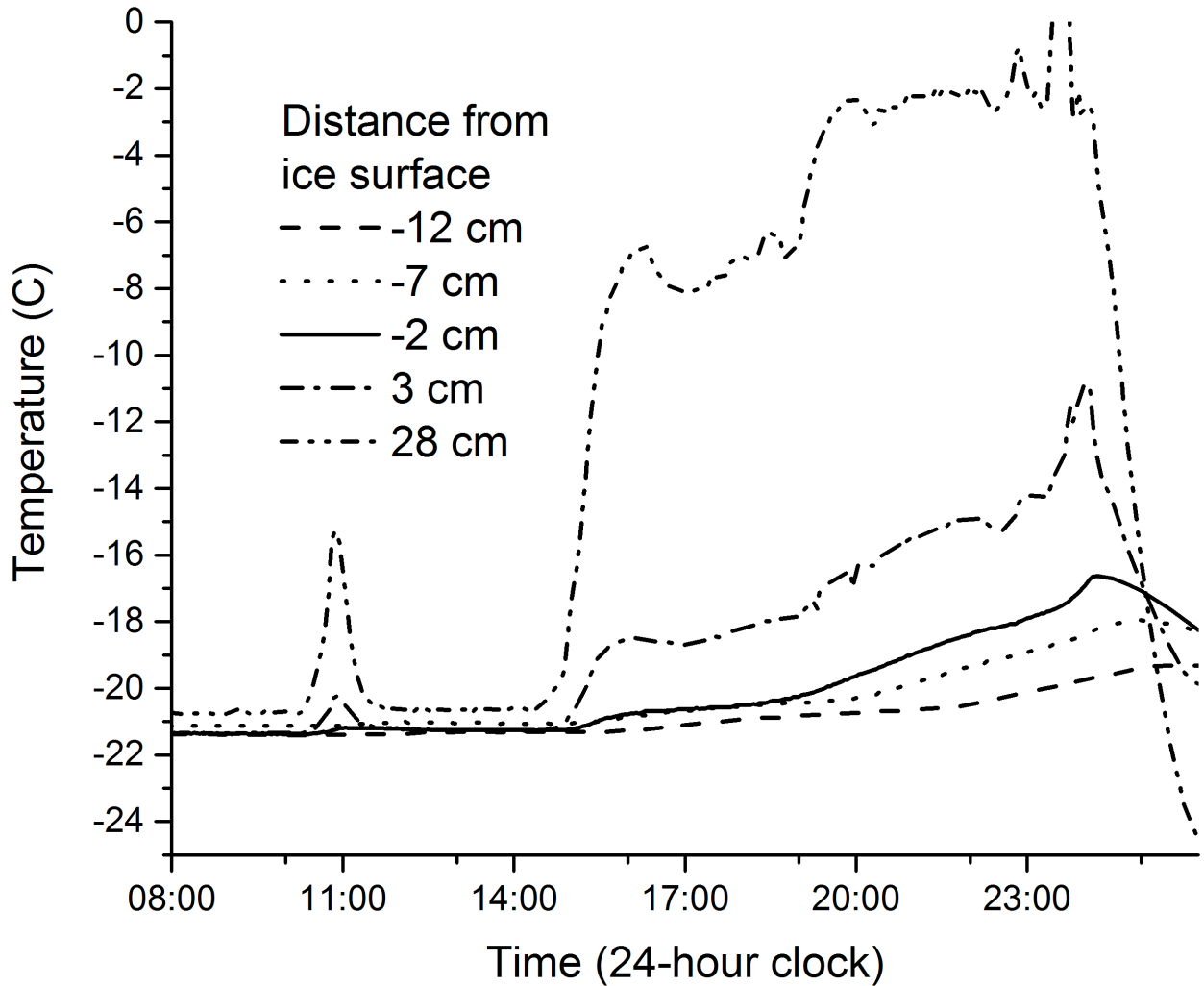


Figure 9. Temperatures during the melting phase of the experiment. The distances in the legend show approximate depth within the ice (negative) or above the ice (positive.) The spike at 11:00 is a defrost cycle. The thermistors are 30-50 centimeters away, horizontally, from the area of ice where albedo was measured, but visually the melting process appeared to progress uniformly across the entire surface of the ice.

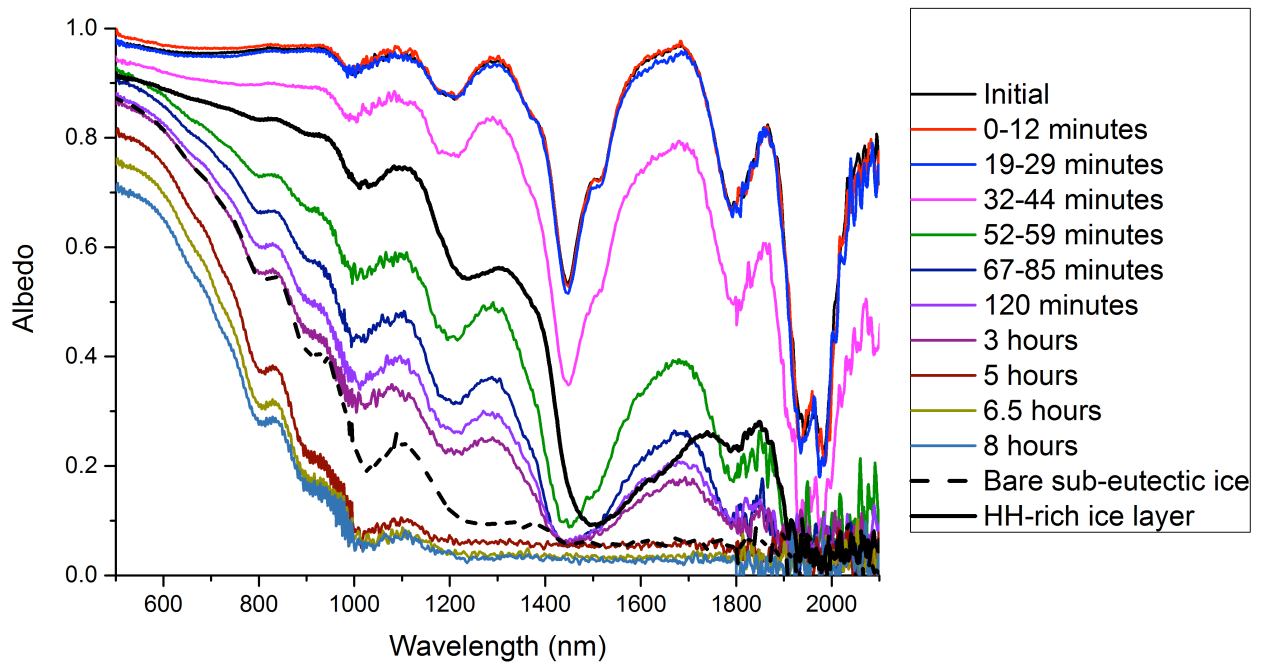


Figure 10. Spectral albedos of hydrohalite crust during melting. Albedo of bare sub-eutectic ice and albedo of the HH-rich ice layer from which the crust developed are also shown for comparison.

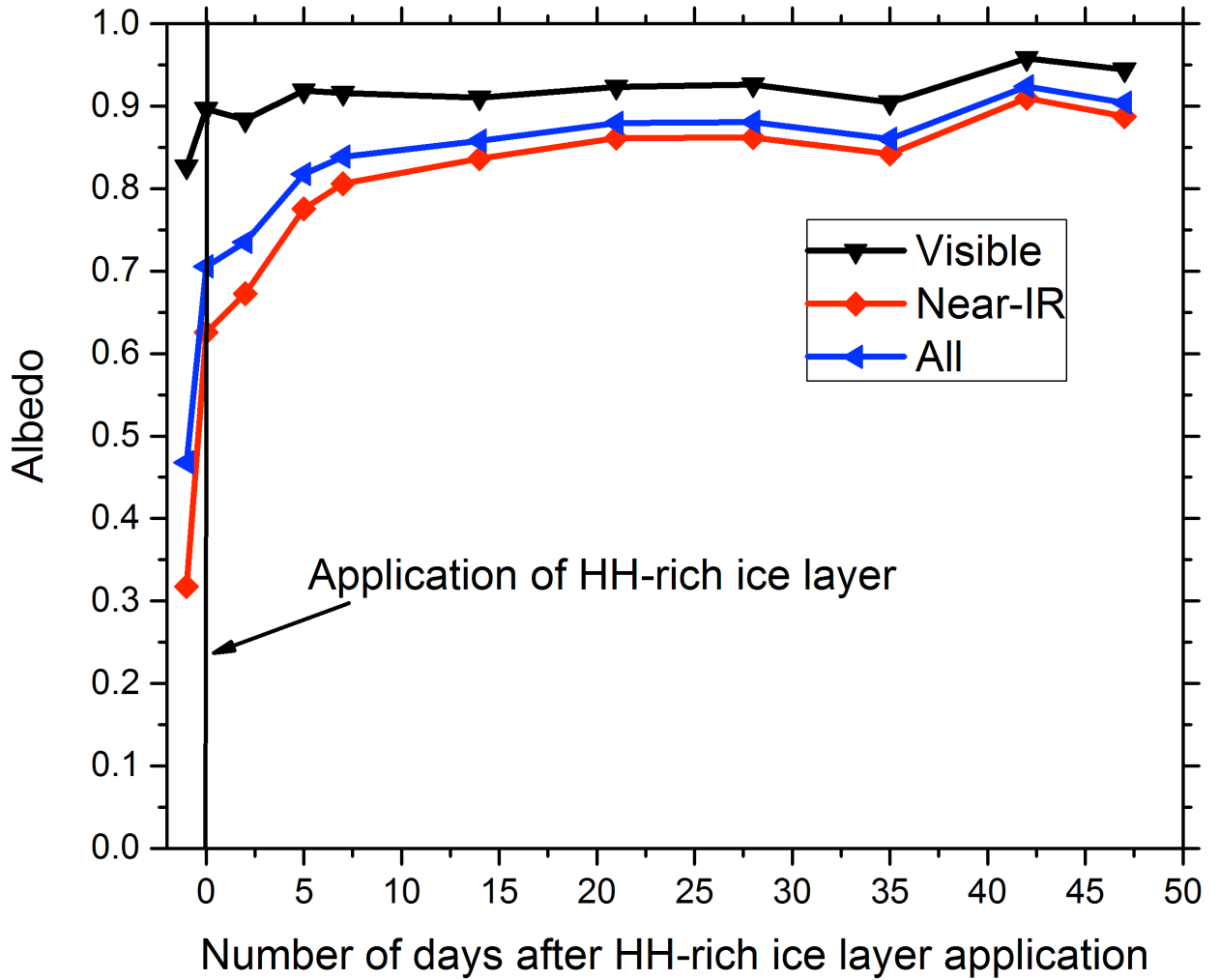


Figure 11. Broadband albedos for the growth phase of the experiment. The low albedos at the left side of the graph are the albedos for bare sub-eutectic sea ice.

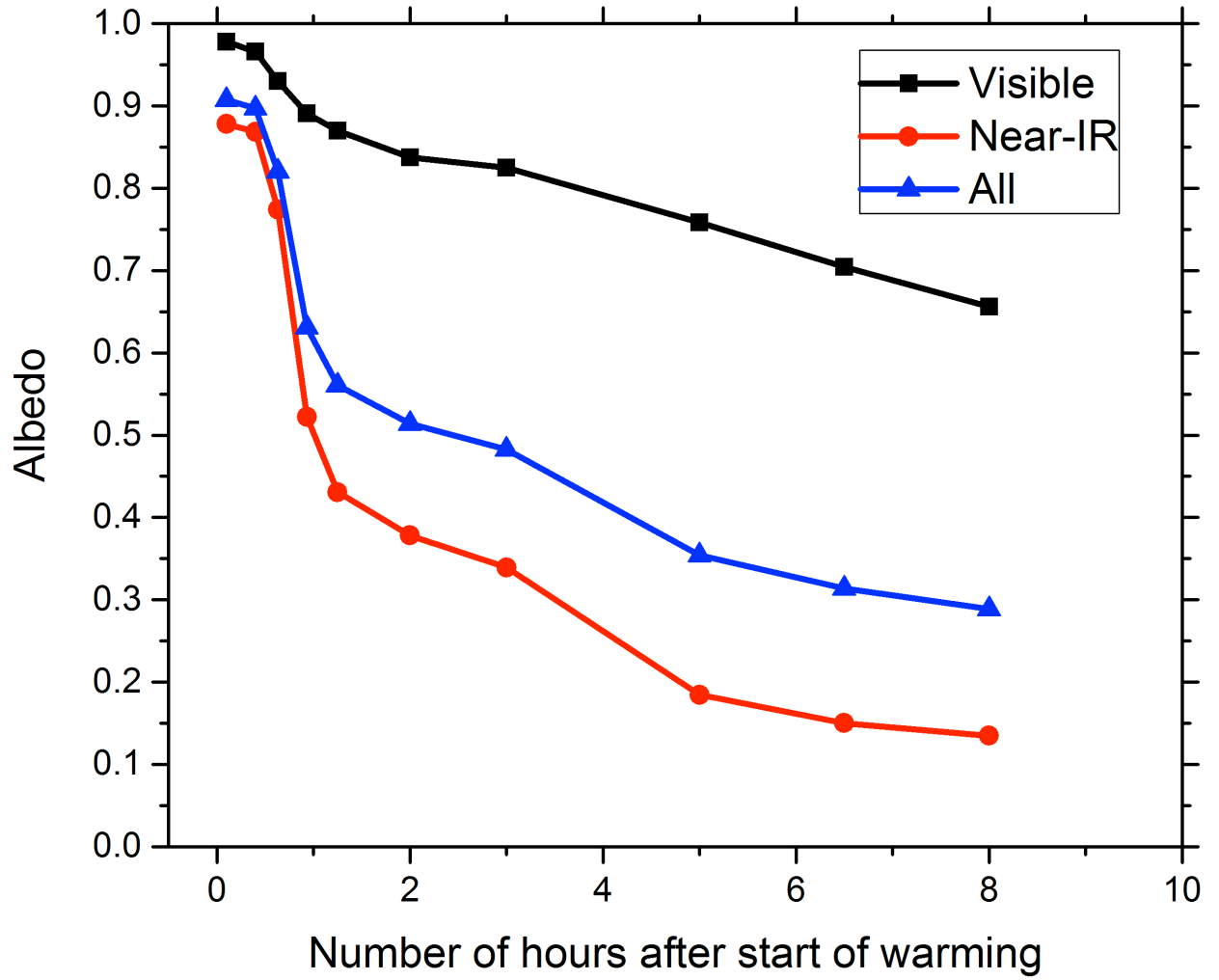


Figure 12. Broadband albedos for melting phase of the experiment.

Chapter III: An optical model of high-albedo salt crusts on Snowball Earth

The work in this chapter will be submitted to Journal of Geophysical Research - Oceans with coauthors Bonnie Light and Steve Warren. This chapter describes modeling which explains and extends the measurements made in the previous chapter. Our hydrohalite crust creation technique allowed us to take measurements quickly enough to avoid falling victim to cold room failure, but it was not directly applicable to all stages in the development of crusts on Snowball Earth, so radiative transfer modeling was necessary to develop a parameterization that would be useful to climate modelers. I used the measurements of the thickest hydrohalite crust to infer the complex refractive index of hydrohalite using a brute-force inverse-modeling-type technique.

Chapter III:

An optical model of high-albedo salt crusts on Snowball Earth

Regina C. Carns^{1,2}, Bonnie Light³, and Stephen G. Warren^{1,2}

¹Department of Earth and Space Sciences,

University of Washington, Seattle, Washington, USA

²Astrobiology Program, University of Washington, Seattle, Washington, USA

³Polar Science Center, Applied Physics Laboratory, University of Washington, Seattle,
Washington, USA

Abstract

During Snowball Earth events, tropical regions of the ocean could develop a crust of precipitated salt as a lag deposit left behind by sublimating sea ice in regions of net sublimation. The major salt would be hydrohalite, $\text{NaCl} \cdot 2\text{H}_2\text{O}$. The crystals in such a deposit can be small and highly scattering, resulting in an albedo similar to that of snow. The snow-free sea ice from which such a crust can develop has a relatively low albedo, around 0.5, so the development of a crust would substantially increase the albedo of tropical regions on Snowball Earth. Hydrohalite crystals are much less absorptive than ice in the near-infrared part of the solar spectrum, so they would alter the spectral distribution of the albedo as well as increasing it.

In this paper, we use laboratory measurements of a hydrohalite lag deposit, in combination with a radiative transfer model, to infer the inherent optical properties of hydrohalite as a function of wavelength. Using this result, we model mixtures of hydrohalite and ice representing both artificially created surfaces in the laboratory and surfaces relevant to Snowball Earth. We test the model against a sequence of laboratory measurements taken during the formation of a lag deposit of hydrohalite. We also present a parameterization for the albedo of a hydrohalite crust on cold sea ice as a function of crust thickness.

1. Introduction

Thick first-year sea ice has an albedo of 0.4-0.5, rising to 0.7 or higher if it is covered by a layer of snow [Brandt *et al.*, 2005]. Open ocean has an albedo around 0.07 [Payne, 1972; Pegau and Paulson, 2001]. This large albedo contrast between unfrozen and frozen ocean surface, and the corresponding contrast in the amount of solar heating, leads to a positive feedback called “ice-albedo feedback.” If the ice cover reaches the subtropics, it can lead to a “runaway” positive feedback that covers the entire ocean with ice [Budyko, 1969]. Earth is thought to have undergone such a transformation at least twice during the Neoproterozoic, the so-called “Snowball Earth” events [Kirschvink, 1992; Hoffman and Schrag, 2002].

As ocean water freezes, the resulting sea ice traps small inclusions of liquid brine. This brine remains in the ice until summer heating raises the ice temperature above -5°C ; around this temperature, the interconnections of brine inclusions forms a permeable network that allows the brine to drain out of the ice, leaving it with only trace amounts of salt [Golden *et al.*, 1998]. It is possible, however, that some or all of the ice on Snowball Earth could have remained cold enough to retain significant salt [Pierrehumbert *et al.*, 2011].

Surface ice on Snowball Earth could even be cold enough for the salts dissolved in the brine to precipitate into solid crystals. Several different salts are known to precipitate from seawater as it concentrates during freezing. Laboratory studies suggest that ikaite ($\text{CaCO}_3 \cdot 6\text{H}_2\text{O}$) precipitates at temperatures just below the freezing point of seawater [Hu *et al.*, 2014] and observations in modern sea ice have confirmed its presence [Dieckmann *et al.*, 2008, 2010]. Mirabilite ($\text{Na}_2\text{SO}_4 \cdot 10\text{H}_2\text{O}$) precipitates around -8°C , while the most abundant salt in seawater, sodium chloride, precipitates around -23°C as the dihydrate mineral hydrohalite ($\text{NaCl} \cdot 2\text{H}_2\text{O}$) [Marion *et al.*, 1999]. Once precipitated, hydrohalite crystals take up most of the volume of the brine inclusion and can contribute to scattering of incoming light [Light *et al.*, 2003; Carns *et al.*, 2015].

In regions of net sublimation on Earth's surface, the ice matrix around these precipitated hydrated salts would gradually sublimate away, leaving the salts behind as a lag deposit. Previous work [Light *et al.*, 2009] shows that a lag deposit of hydrohalite is highly reflective, suggesting that it could significantly influence the planetary energy balance of Snowball Earth. To quantify this effect, the albedo of an artificially created lag deposit has now been measured in the laboratory (Chapter II). In this chapter, I show our use of these data, along with radiative transfer modeling, to infer the spectral absorption coefficient of hydrohalite. Using this result along with additional known optical properties of hydrohalite and water ice allows us to predict the apparent optical properties of cold, sublimating sea ice for scenarios not tested in the laboratory.

2. Laboratory measurements

A hydrohalite (HH) lag deposit was created on a substrate of artificial sea ice in a walk-in freezer laboratory. To create the sea-ice substrate, an insulated 1000-liter tank was filled with a 24‰ solution of sodium chloride at room temperature; after filling the tank, the laboratory temperature was lowered to -20°C. The walls of the tank were insulated to ensure that the solution would freeze from the top down, so that its microstructure would be similar to that of natural sea ice. Thermistors monitored the temperature in the tank at 5-cm vertical intervals to track the progress of cooling and freezing. We measured the albedo of this surface during freezing using a novel method, described in Chapter II.

Once the tank was fully frozen and albedo measurements had been made of the ice surface at -20°C, the temperature of the cold room was lowered to -30°C to investigate the sub-eutectic behavior of the ice. Initial experiments attempted to develop a hydrohalite crust “naturally” by allowing the ice to sublimate over time. However, the freezer laboratory was unable to remain below the eutectic temperature for the several months required to develop an optically thick crust from ice with less than 10ppt salinity. We therefore developed a method to create a hydrohalite crust more quickly by creating a surface layer with a higher concentration of hydrohalite within the ice. With the surface in thermal equilibrium with the -30°C cold room, a

chilled (-20°C) solution of 23% sodium chloride by weight was sprayed onto the ice surface. The concentration and temperature of the solution were chosen to be close to the eutectic point, so that the solution would solidify into ice and hydrohalite soon after contacting the cold ice surface rather than pooling unevenly. The process was repeated several times, with the sprayed solution being allowed to freeze completely before the next application.

After 11 such treatments, the layer of ice and hydrohalite appeared optically thick, judging by its ability to obscure colored markers that had been placed on the ice before spraying. The end result was a layer consisting of 25% hydrohalite and 75% water ice by volume (assuming a density of 1.6 g cm⁻³ for hydrohalite [Adams and Gibson, 1930] and 0.92 g cm⁻³ for ice.) We estimated this irregular layer of hydrohalite-rich ice (hereafter referred to as HH-rich ice) to be a few millimeters thick.

Note that, although our primary reason for creating this layer was to reduce the amount of time required for a thick layer of hydrohalite to build up as a lag deposit, it is also analogous to a situation that might occur on Snowball Earth: a melted and refrozen pool of surface brine. Once a lag deposit of salt has built up, temperatures above the dissolution point of the hydrated salt will result in the formation of saturated brine ponds. When temperatures drop again, the ponds will freeze as a mixture of ice and hydrated salt with a composition similar to that of the layer we created in the laboratory.

After the layer of HH-rich ice was formed, the ice matrix was allowed to sublimate away, leaving behind a layer of small grains of hydrohalite with air filling the space that had previously been occupied by ice. This layer is hereafter referred to as the hydrohalite crust. We measured the albedo of the tank surface several times as the ice sublimated and the mostly ice-free layer of hydrohalite grew thicker. We expected the albedo of this ice-free hydrohalite crust to be higher than that of the HH-rich ice, due to the greater contrast in refractive index between hydrohalite and air versus that between hydrohalite and ice, and this was borne out by observations. We took measurements as the ice continued to sublimate, with initial measurements at 2, 5, and 7 days after applying the HH-rich ice layer, and measurements roughly once per week thereafter.

We continued these measurements until the albedo appeared to stabilize. Figure 2 shows a selected set of measurements from this process.

3. Modeling

The laboratory measurements include an albedo for sub-eutectic NaCl ice, an albedo for the HH-rich ice layer, and albedos taken while a hydrohalite crust of increasing thickness gradually replaced the HH-rich layer. These results give some idea of the albedos that can be expected from sea ice surfaces and hydrohalite crusts, but in order to create an accurate parameterization of hydrohalite crusts on sea ice, we need albedos for a wider range of scenarios. In order to generalize the results to the various surfaces that could exist on Snowball Earth, we can use the laboratory measurements to calibrate a radiative transfer model for mixtures of hydrohalite and ice, which will allow us to compute spectral and broadband albedos for any combination of thickness, grain size, and concentration.

Well-tested models for Mie scattering [Wiscombe, 1980] and discrete-ordinates radiative transfer [Stamnes *et al.*, 1988] already exist. The optical properties of ice are well known [Warren and Brandt, 2008]. Less work exists on the optical properties of hydrohalite. Wagner *et al.*, [2012] inferred optical constants for hydrohalite in the infrared from 1.6 to 12.5 μm , by spraying a mixture of sodium chloride and water into a chamber at 216 K and measuring the infrared extinction spectra of the resulting hydrohalite crystals. For purposes of determining albedo, however, measurements for visible and near-infrared wavelengths ($\lambda < 1.6 \mu\text{m}$) are needed.

Light *et al.* [2009] gives the real refractive index as 1.49 ± 0.02 . To completely describe the ice-hydrohalite mixture, we also require the imaginary part of the refractive index, m_{im} . We lack crystals of sufficient size to measure this property directly, but we can use our measurements of the albedo of the hydrohalite crust as the input to a simple inverse problem. For each wavelength, we can guess a value for m_{im} , then use this guess as input to the Mie scattering computation, and use the radiative transfer model to compare with the albedo measured in the laboratory.

This technique assumes that the thickest measured laboratory crust was optically thick, specifically that it was effectively semi-infinite. For each target wavelength (10-nm intervals between 500nm and 2200 nm) we ran the model for 129 possible values for the imaginary refractive index, then compared our results to the laboratory measurements and chose the value of m_{im} that allowed the model to most closely match the measured value. Figure 3 shows the albedo curve for an optically thick hydrohalite crust and the points where m_{im} was calculated, along with some example albedo curves using constant m_{im} .

Grain size is a key input value for the Mie scattering computation; this estimated grain size was the largest source of uncertainty in this calculation. The hydrohalite grains were irregularly shaped, but we estimated their “equivalent spheres” radius to be 20 μm using the prescription of *Grenfell and Warren* [1999], in which a nonspherical crystal is represented by a collection of spheres having the same total volume and same total surface area as the real crystal. We based our estimate on our photographs of crust samples and on previous measurements of hydrohalite crystals in brine inclusions of sea ice [*Light et al.*, 2009]. Figure 4 shows our sensitivity analysis for this variable, showing different model results based on assumptions of 10 μm , 20 μm , and 50 μm particle radius.

Using these results for the optical properties of hydrohalite, we modeled the initial laboratory scenario of an ice-hydrohalite mixture and followed its progression as an ice-free hydrohalite crust formed over the mixed layer and grew thicker. Figure 5 shows a schematic view of this model. The model treats the ice-hydrohalite mixture as an ice medium containing grains of hydrohalite, rather than using air as a medium for a mixture of ice and hydrohalite grains. We used the methods outlined in *Mullen and Warren* [1988] for dealing with a scatterer in an absorbing medium. The methods were originally developed using non-absorbing bubbles in lake ice as the scatterer, so we made modifications to account for the fact that our scatterer, hydrohalite, does absorb some light.

The effective complex refractive index of the hydrohalite embedded within the ice is given by m_{hh}/m_i , where m_{hh} is the complex refractive index of hydrohalite and m_i is the complex

refractive index of ice. Using this effective index as input to the Mie scattering computation gives the asymmetry factor and the scattering efficiency of the ice/hydrohalite mixture.

Following *Mullen and Warren* [1988], the absorption coefficient is approximated simply as

$$k_{mix} = f_{ice} k_{abs} + f_{hh} k_{abs} \quad (1)$$

where f_{ice} and f_{hh} are the volume fractions of ice and hydrohalite.

The single-scattering coalbedo is related to the scattering efficiency as

$$(1 - \tilde{\omega}) = \frac{k_{abs}}{k_{abs} + k_{sca}} \quad (2)$$

where k_{sca} is given by

$$k_{sca} = Q_{sca} \pi r^2 N \quad (3)$$

Here Q_{sca} is the scattering efficiency, r is the radius of the particles, and N is the number density of the particles. In this case we assume the particles to be monodisperse for simplicity. Figure 6 shows the optical properties of ice spheres, hydrohalite spheres, and hydrohalite spheres embedded in an ice matrix.

The model starts with a single layer of HH-rich ice. At the next step, the model adds a layer of hydrohalite crust; each subsequent step of the sublimation progressively increases the thickness of the hydrohalite crust layer, reducing the thickness of the HH-rich ice layer by a prescribed amount and adding the same thickness to the hydrohalite crust. Finally the HH-rich ice layer is completely replaced by hydrohalite crust, representing the complete sublimation of the ice matrix.

Note that the model does not attempt to represent processes such as sublimation over time.

The modeled crust thicknesses are chosen to match the measured albedo results (except for the 0.01 g cm^{-2} albedo, which is too high to match the 2-day measured albedo because 0.01 g cm^{-2} was the smallest increment of thickness used in modeling.)

Figure 7 shows the results of this modeling, with measured laboratory albedos plotted along with modeled albedos of HH-rich ice with a hydrohalite crust. The 47-day laboratory albedo was used to determine the optical properties of hydrohalite, so it is very close to the modeled

optically thick hydrohalite crust; there are slight differences due to smoothing of the hydrohalite optical properties. The modeled HH-rich ice layer, without a hydrohalite crust layer on top of it, matches the laboratory HH-rich ice layer closely in infrared wavelengths, but is too high in visible wavelengths.

4. Parameterization

This model allows the determination of the albedo of a hydrohalite crust of arbitrary thickness, but is too complex and computationally expensive to include as part of a global climate model (GCM). The model results shown in Figure 7 are also not directly applicable to the case of ordinary sea ice sublimating without melt, since the laboratory crust developed from a layer of ice containing 25% hydrohalite by volume, whereas ordinary first-year sea ice generally contains on the order of 10‰ of salt (before summer melt flushing.) In order to represent the natural development of a hydrohalite crust on sea ice, we model a crust of hydrohalite crystals in air over a substrate of sub-eutectic ice with something closer to normal sea ice salinity. The underlying sea ice albedo used in this modeling is the albedo measured in the laboratory for sub-eutectic ice at -30°C.

We calculated the spectral albedo for several crust thicknesses, expressed in units of grams per square centimeter, for both clear sky (at solar zenith angle 60°) and under overcast cloud (which reduces the near-infrared radiance incident on the ice). We integrated those albedos across wavelength bands commonly used in GCMs, weighting the integration using solar spectra $F(\lambda)$ for polar atmospheres from an atmospheric radiation model [Wiscombe *et al.*, 1984]. Two solar spectra are used, one for clear sky and one for cloudy sky; they are similar to the solar spectra shown in Figure 1 of Brandt and Warren [1993].

$$\bar{\alpha} = \frac{\int \alpha(\lambda) F(\lambda) d\lambda}{\int F(\lambda) d\lambda} \quad (4)$$

In this case we use 300-700 nm as the visible wavelength band, 700-2500 nm as the near-IR wavelength band, and 300-2500nm for the "broadband" albedo. Figure 8 shows the results of this modeling.

Beer's Law is a natural choice of equation for the parameterization of a substance with increasing optical depth, so decaying exponential curves (see Equation 5) are fitted to the data points. We used Origin data analysis software (v. 9.1) to fit the data. The data points at zero thickness and optically semi-infinite thickness are weighted more heavily. This helps ensure that the parameterization gives accurate results for small thicknesses (where small differences in thickness can make a large difference in albedo) and for the semi-infinite case (which all crusts will tend toward over time) at the expense of some accuracy at moderate thicknesses.

$$y = y_0 + Ae^{-x/t} \quad (5)$$

where y is the albedo, y_0 is the semi-infinite albedo, x is the crust thickness in g cm^{-2} , and t is a characteristic (e-folding) thickness. Table 1 gives the constants for Equation 5 for clear and cloudy skies in the visible, near-IR and overall.

Laboratory measurements were also made of a warming hydrohalite crust as it dissolved, but we did not model or parameterize this situation, as it is expected to be transient. Any sodium chloride brine supersaturated enough to preserve hydrohalite crystals would melt the ice underneath it until it reached equilibrium.

In the full sea-salt system, temperatures below the precipitation point of hydrohalite but above the eutectic of seawater (between -23°C and -37°C , if following the precipitation pathway described in *Marion et al.* [1999]) might result in a surface composed of hydrohalite crystals wetted by a brine containing other dissolved salts (such as magnesium chloride.) The composition of the ocean during Snowball Earth is not well constrained, but investigating the effects of other salts on the formation of lag deposits could provide a fruitful avenue for future work.

5. Discussion

In addition to its relevance to the energy balance of Snowball Earth, the modeling described here also provides a determination of the imaginary refractive index of hydrohalite in the visible region.

It is interesting to compare the albedo measurements of sodium chloride dihydrate to reflectance measurements of non-hydrated sodium chloride, as well as to other hydrated salts (Figure 9). All reflectance measurements cited here come from the ASTER spectral database [Baldridge *et al.*, 2009]. Figure 9d shows a comparison of the albedo measurements used in this study with reflectance measurements of gypsum, another dihydrate mineral. Both show absorption bands around 1400 and 2000 nm, where water absorbs very strongly; note that even the anhydrous forms of the minerals (Figures 9b, 9c) show small amounts of absorption at the same locations, presumably due to small quantities of water adsorbed onto their surface from the atmosphere. Figure 9a shows the reflectance spectrum of mirabilite, another hydrated salt known to precipitate in sea ice, and its anhydrous form thenardite. Mirabilite, with formula $\text{Na}_2\text{SO}_4 \cdot 10\text{H}_2\text{O}$, shows much stronger absorption in the infrared than gypsum or hydrohalite. Our laboratory measurements show that the albedo of a hydrohalite lag deposit is as high as that of fresh snow in the visible wavelengths, and higher in the near-IR where snow is more absorptive, making such hydrohalite crusts potentially important to the energy balance of Snowball Earth. The simplified laboratory scenario studied here included only water and sodium chloride; the full complement of salts in ocean water would be likely to change the results somewhat. Sodium chloride would still precipitate, and possibly at a similar temperature; in modern sea ice brine inclusions it begins to precipitate around -23°C (at equilibrium.) However, other salts such as magnesium chloride or calcium chloride could depress the freezing point of the remaining brine below this temperature. Laboratory experiments have also shown that sodium chloride solutions can supercool below their eutectic point. Carns *et al.* [2015] [submitted] found that brine inclusions in sea ice can supercool by as

much as 6 K below the precipitation point of hydrohalite; *Toner et al.* [2014] found supercooling of up to 8.3 K in solutions of pure sodium chloride.

Depending on the freezing pathway, modern seawater may reach its eutectic point at about -37°C, when magnesium chloride dodecahydrate ($\text{MgCl}_2 \cdot 12\text{H}_2\text{O}$) precipitates [*Marion et al.*, 1999]. Below this eutectic point, with all salts precipitated, the sea ice might develop a salt crust similar to that investigated in this study. Between -23°C and the eutectic, the presence of these other salts would result in a slush of hydrohalite crystals and concentrated brine. Measuring the albedo of such a surface, and investigating the effects of a prolonged period of desiccation, could provide a subject for future work.

Acknowledgments

The data for this paper are available at <http://dx.doi.org/10.6084/m9.figshare.1267444>.

This work was supported by NSF grant ANT-1142963.

Table 1. Constants for Equation 5.

Band	y_0	A	t
Broadband Diffuse	0.91	-0.45	0.19
Broadband Direct	0.88	-0.52	0.22
Visible Diffuse	0.95	-0.11	0.47
Visible Direct	0.94	-0.11	0.70
IR Diffuse	0.89	-0.59	0.17
IR Direct	0.86	-0.63	0.20

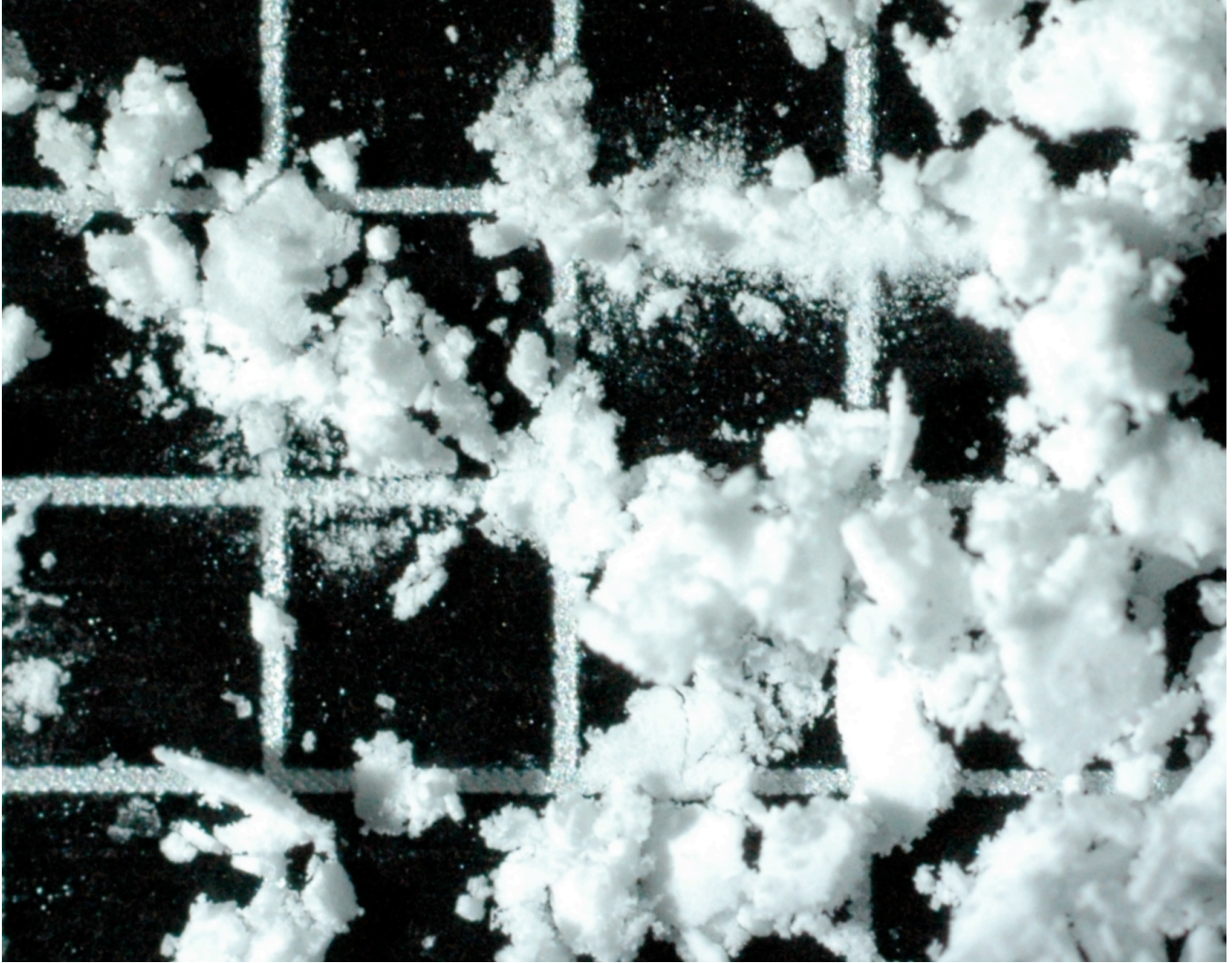


Figure 1: Grains of hydrohalite disaggregated from crust. The squares of the grid in this image are 2mm in width. The crust was fine and powdery and easy to remove from the ice surface.

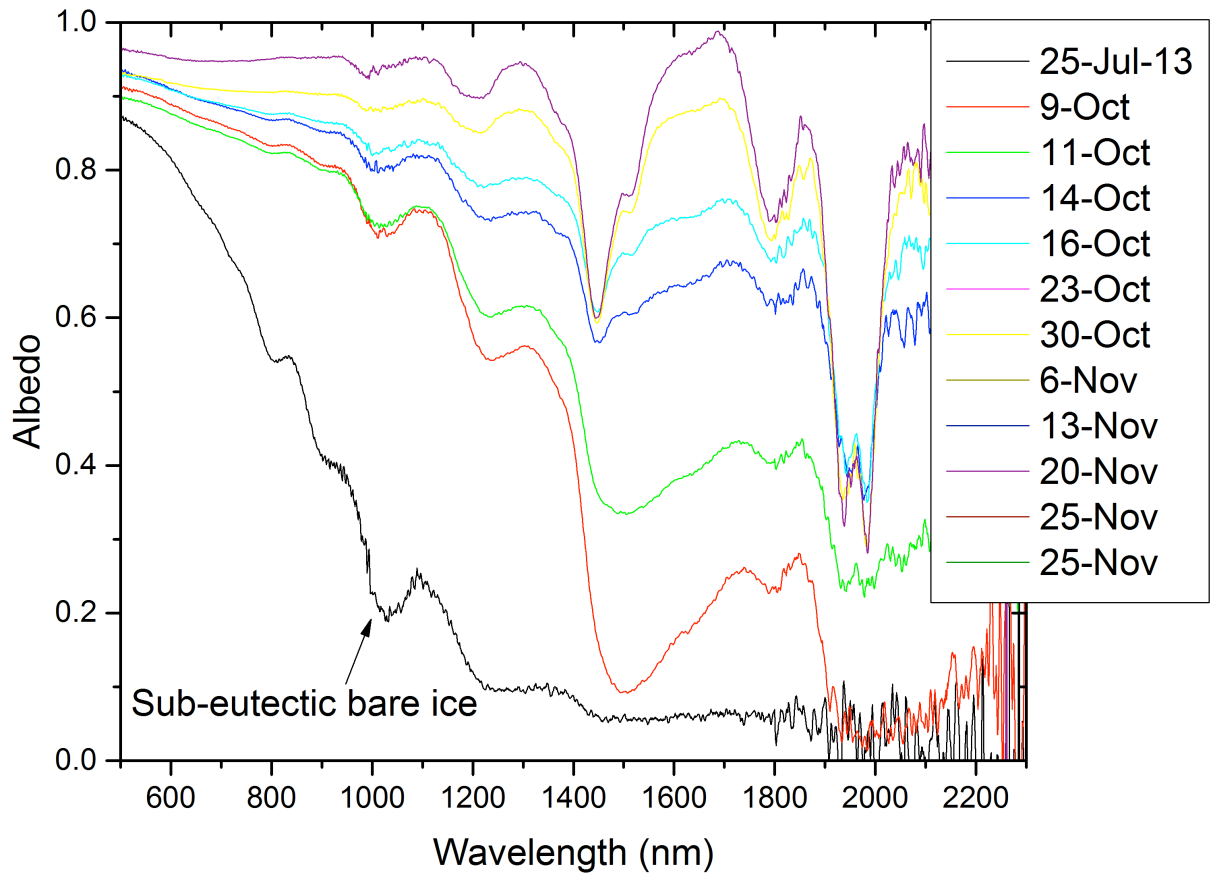


Figure 2: Selected measurements of spectral albedo from the laboratory sea-ice tank. '0 days' represents the initial state of the experiment, a layer of hydrohalite-rich ice; the subsequent progression shows the increase in albedo over time as the surface hydrohalite crust grew thicker.

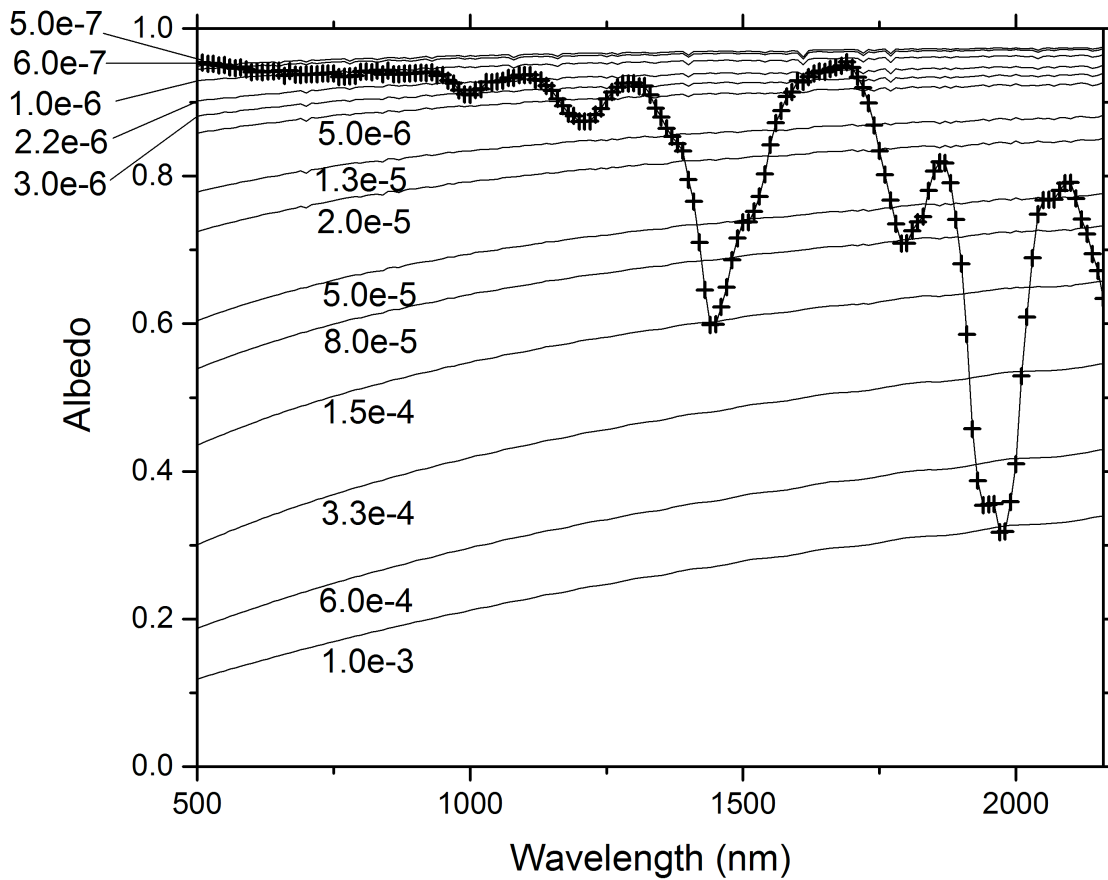


Figure 3. The measured albedo of the hydrohalite crust with selected curves superimposed, of albedo calculated using imaginary refractive index (m_{im}) independent of wavelength. The constant m_{im} curve that intersects with the albedo measurements at a given wavelength gives the inferred value of m_{im} for that wavelength. The curves are labeled with the value of m_{im} , where (for example) “6.0e-4” means 6×10^{-4} .

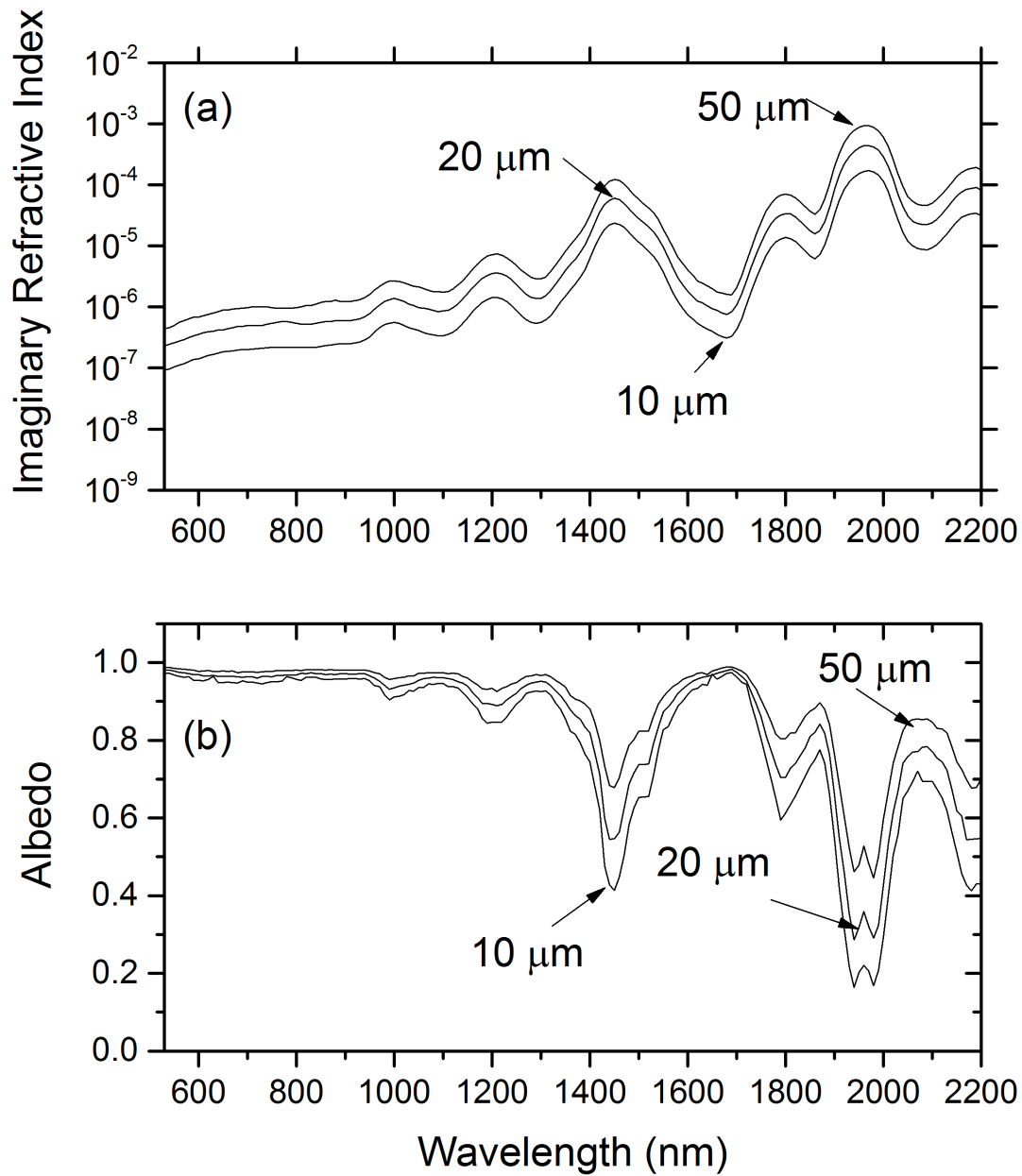


Figure 4. Sensitivity of the method to different assumptions about grain size. Shown are (a) different inferred values of m_{im} based on different grain size assumptions and (b) the results of running the albedo model using identical conditions except for the different values of m_{im} . Note that each albedo curve is calculated for a crust of 20- μm hydrohalite spheres; the labels indicate the *assumed* grain size used to determine m_{im} for hydrohalite in each case.

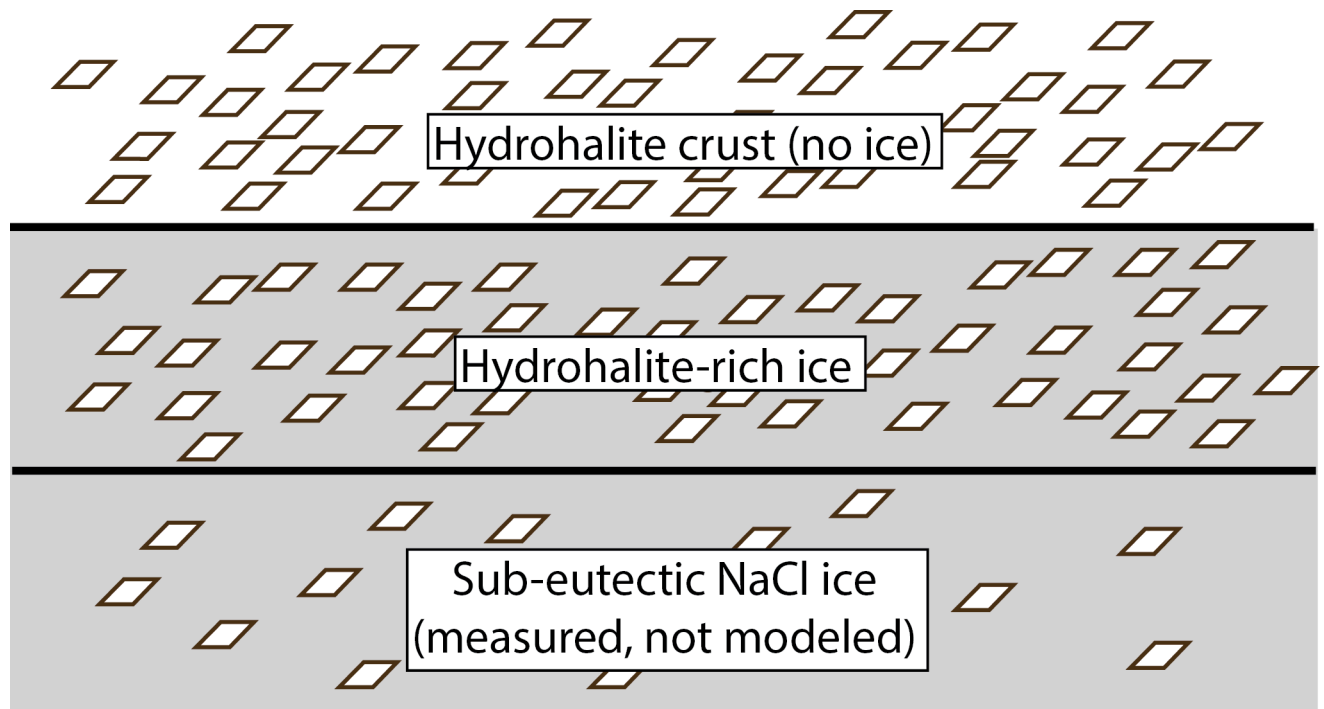


Figure 5. Schematic view of layers used to model laboratory measurements.

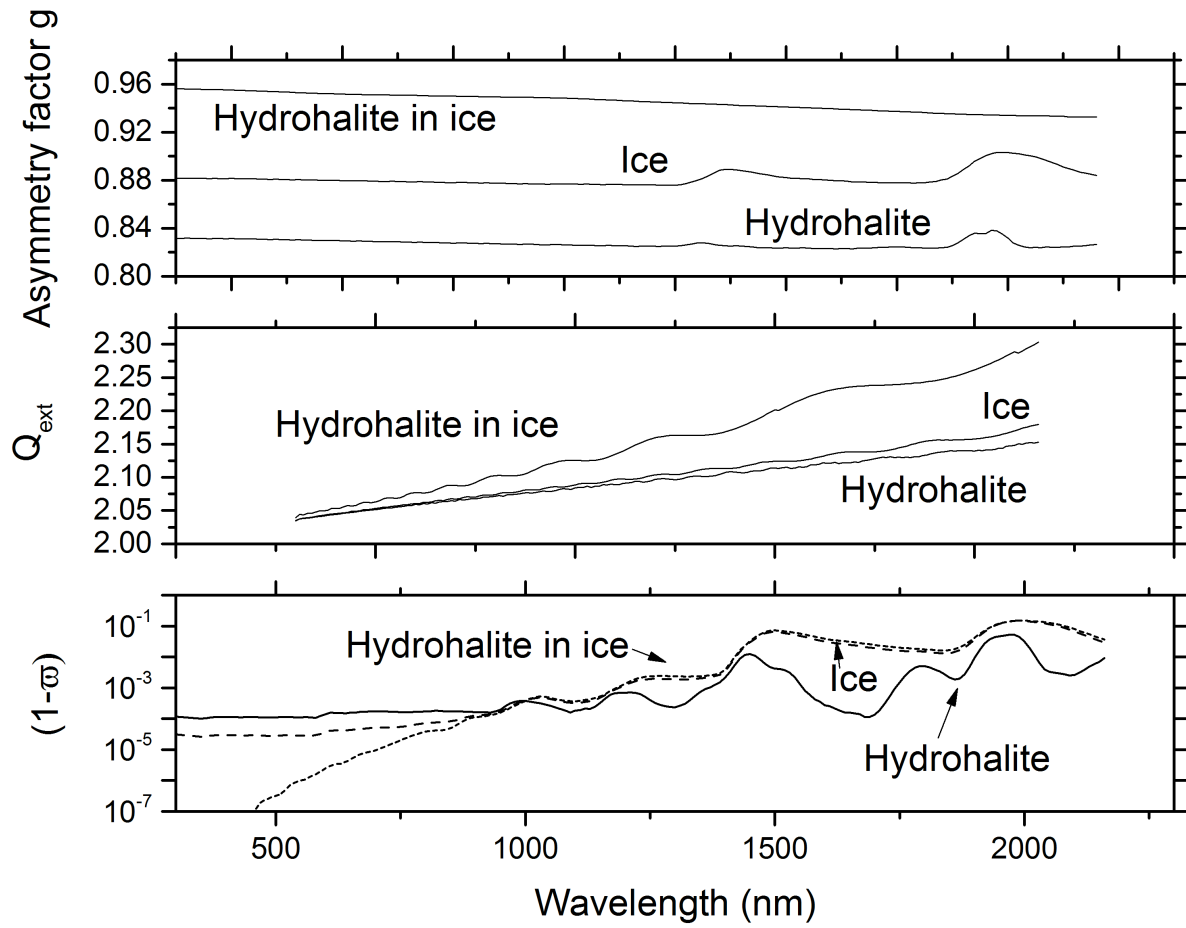


Figure 6. Asymmetry factor g , extinction efficiency Q_{ext} and single-scattering co-albedo $(1-\omega)$ for ice spheres in air, hydrohalite spheres in air, and hydrohalite spheres embedded in ice. The size of the spheres in all cases is $20 \mu\text{m}$.

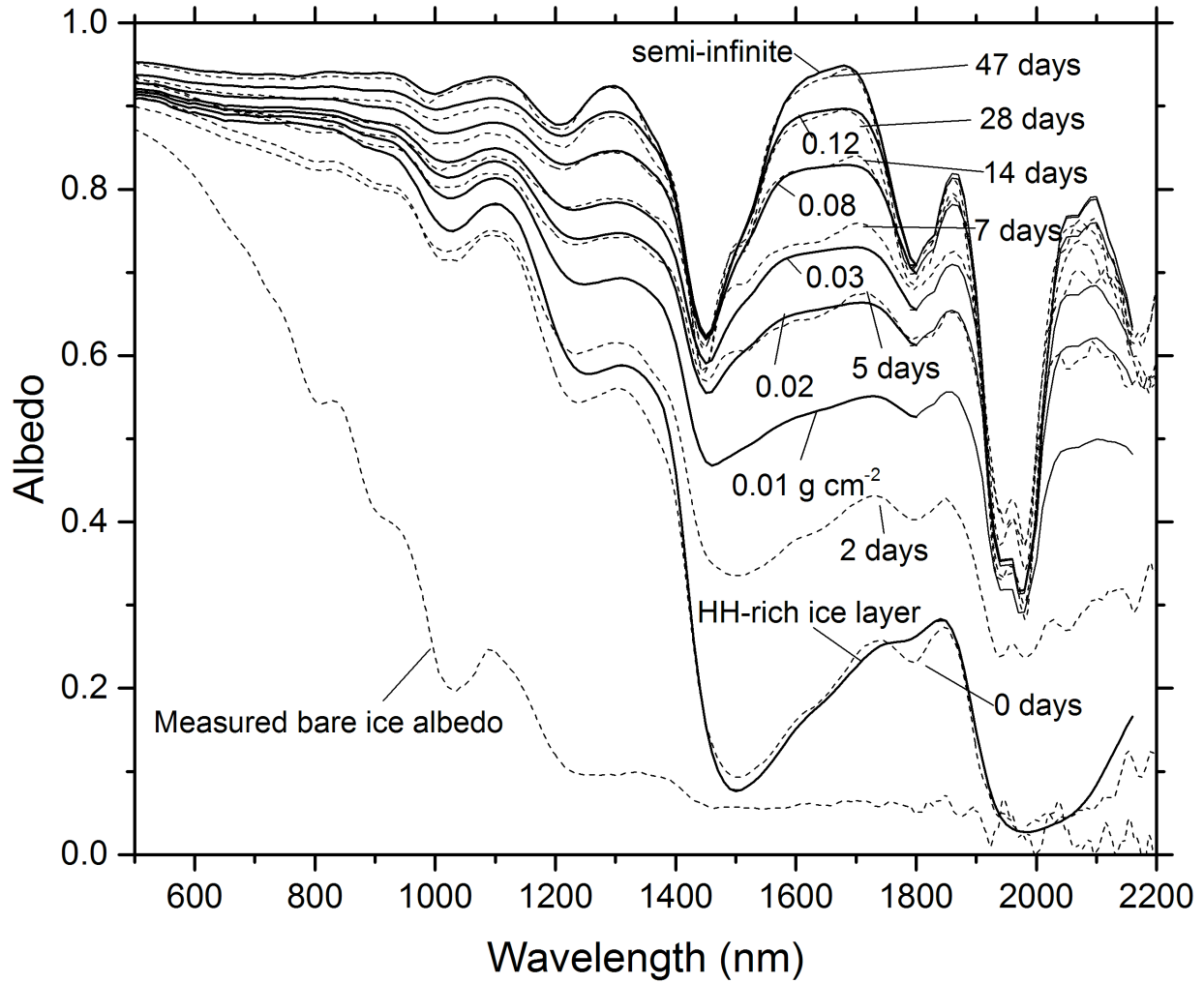


Figure 7. Comparison of modeled and measured spectral albedos for different thicknesses of hydrohalite-rich ice layer and hydrohalite crust. Dashed lines show albedos measured in the lab; solid lines show albedo output from the model (for diffuse incidence, since the light in the dome is diffuse.) Hydrohalite crust thickness for the model output is labeled in grams per square centimeter.

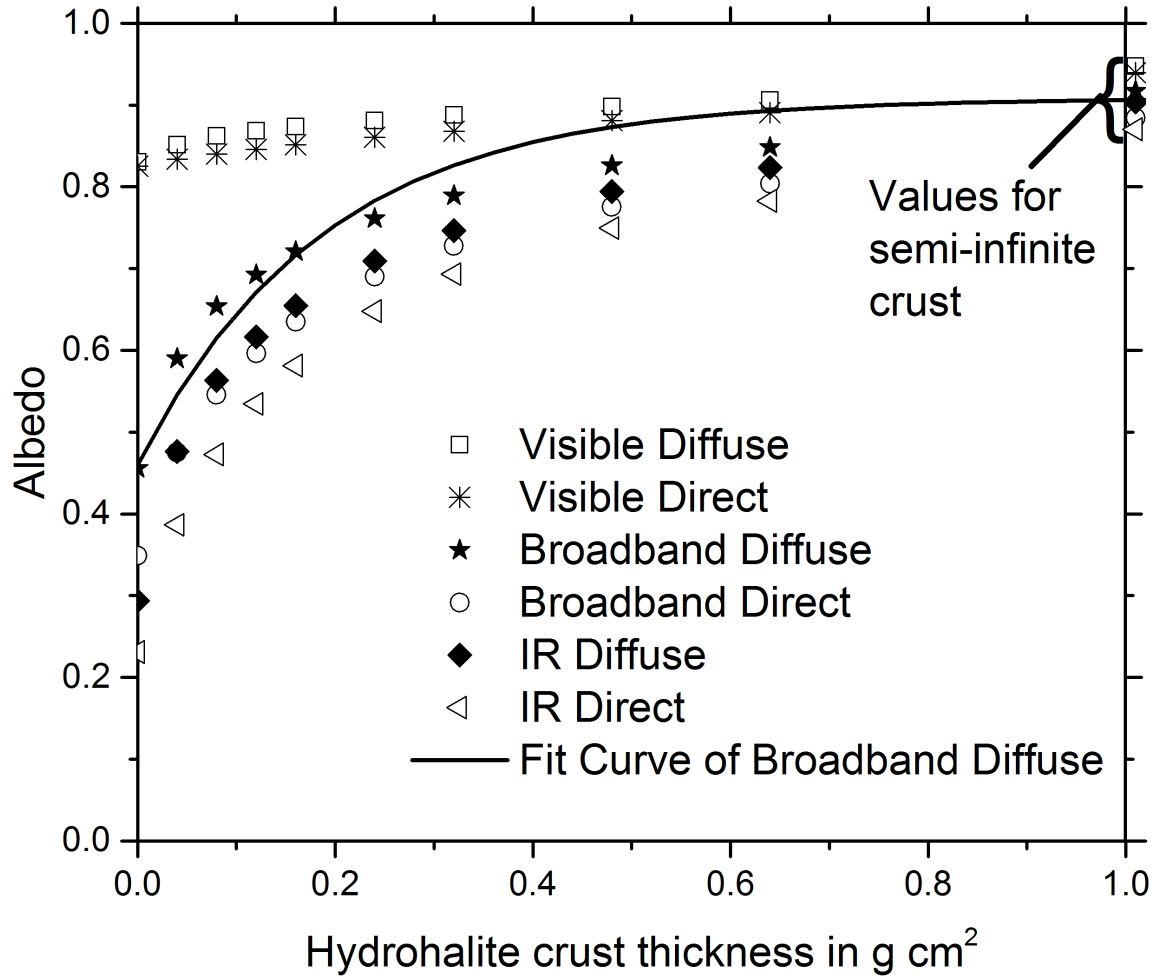


Figure 8. Calculations used for parameterization. To avoid cluttering the graph, only one line of fit is shown, the parameterization for diffuse broadband. The fit is forced to be accurate in the limits of zero thickness and semi-infinite thickness; the albedo given by the equation at moderate crust thicknesses is too high.

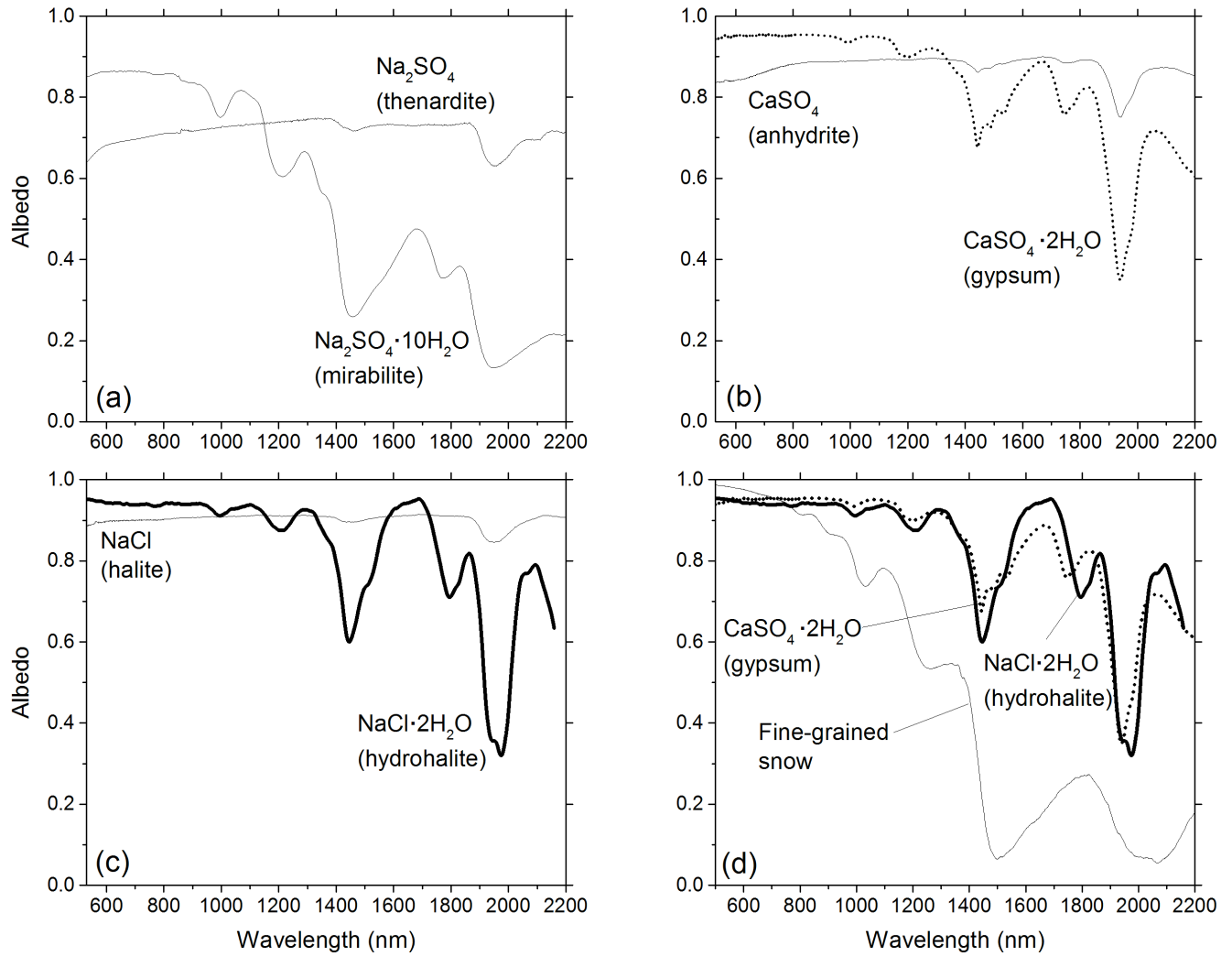


Figure 9. Comparison of reflectances of different hydrated and anhydrous minerals. Shown are (a) mirabilite, another hydrated mineral that precipitates in sea ice brine inclusions, compared to its anhydrous form thenardite; (b) gypsum, a dihydrate mineral like hydrohalite, compared to its anhydrous form anhydrite; (c) hydrohalite compared to its anhydrous form halite; and (d) hydrohalite with gypsum, demonstrating the similarity in their spectral reflectance, with snow albedo for comparison. Mineral reflectances, except for hydrohalite, are from the ASTER spectral library [Baldrige *et al.*, 2009]; snow albedo is from Hudson *et al.* [2006].

Discussion

Small changes in the albedo of ice surfaces on an Earthlike planet can alter the course of its evolution by changing planetary energy balance, or make the difference between a dark, frozen cul-de-sac and a sunlit liquid-water refuge for life. In this dissertation I have argued that the salty oceans on Earth and Earthlike planets, combined with the cold and dry conditions prevalent during the initial phases of a Snowball period, give rise to forms of ice rarely found on modern Earth. These ice types have albedos that are distinct from those usually assigned to sea ice in global climate models, and which vary based on different criteria.

1.1 Summary of accomplishments

In this work, we have

- 1) Made field measurements of the albedo of bare sea ice below the precipitation temperature of hydrohalite;
- 2) Carried out laboratory observations of natural sea ice over a range of temperatures around the precipitation point of hydrohalite to better understand its behavior;
- 3) Carried out laboratory experiments on artificially created sea ice to isolate the effects of non-NaCl ocean salts and of extracellular polysaccharides on the precipitation of hydrohalite;
- 4) Carried out laboratory experiments on artificially created sea ice to investigate the effects of freezing rate and brine pocket volume;
- 5) Developed a novel apparatus to measure albedo of ice surfaces in the laboratory and tested it against an established method for outdoor albedos;
- 6) Created a lag deposit of hydrohalite in the laboratory, and measured its albedo during both its development and its destruction by melting using the novel apparatus;
- 7) Used models to infer the complex refractive index of hydrohalite using the measurements of the albedo of the laboratory-created lag deposit;
- 8) Used the optical properties of hydrohalite and ice to develop a parameterization for the albedo of sublimating subeutectic sea ice as a function of the thickness of the salt crust.

This work, in combination with prior work on Snowball Earth ice albedos by *Dadic et al.* [2013] on the albedo of blue ice and firn (in which I also participated for the fieldwork), gives albedos for most of the ice surfaces that would occur in zones of net sublimation on the Snowball Earth oceans, under a variety of conditions.

2. Future work

Hydrohalite has proved to be more complex than expected when interacting with the other salts and substances in seawater. Some uncertainty is inevitable, since it is difficult to know the salt composition of seawater in the Neoproterozoic and currently impossible to measure the composition of seawater on Earthlike planets in other solar systems. However, other experiments and models could extend the results of chapters I and II to cover more possible circumstances.

2.1 Extending results from Chapter I

The albedo of subeutectic sea ice in the field did increase with decreasing temperature, but, as seen in Figure 1, it did not reach the albedo we observed in the laboratory for subeutectic NaCl ice. The laboratory ice was measured at a temperature of approximately -27°C , similar to the lowest temperature measured in the field. The laboratory experiments on hydrohalite precipitation in natural ice (Figure 8, Chapter I) and NaCl ice (Figure 9a, Chapter I) suggest that hydrohalite in NaCl-only ice like that used for the laboratory albedos does precipitate more quickly and completely than hydrohalite in natural sea ice, which could account for some of the difference.

However, a full parameterization of the albedo increase in natural sea ice as its temperature decreases still requires additional laboratory experiments. The thinsection method of measuring hydrohalite precipitation used in Chapter I does not seem to capture the full behavior of hydrohalite precipitation in larger volumes of sea ice, so a new experimental method might be necessary. One possible approach would be to use the albedo dome method described in Chapter II on a tank of ice frozen from water containing a full complement of sea

salts. Measuring the tank albedo, decreasing cold room temperature, and repeating the procedure until albedo reached an asymptote would provide a much more complete parameterization for the albedo of natural sea ice.

Alternatively, an optical model of sea ice that includes the effects of hydrohalite crystals within brine pockets, perhaps similar to the model described in *Light et al.* [2004] could be used to calculate albedos for arbitrarily low temperatures.

2.2 Extending results from Chapter II

Chapter II describes measurements of a tank of NaCl ice. Natural sea ice, however, contains several salts that could maintain a small quantity of liquid water within brine pockets at temperatures lower than those achieved in the laboratory. As discussed in Chapter II, such ice could still develop a lag deposit of hydrohalite crystals, but they might be surrounded by a film of highly saline brine of magnesium chloride or calcium chloride. Future experiments could create such a surface in the laboratory and measure its albedo over time as ice at the surface sublimated away and left behind hydrohalite crystals and brine. Such an experiment would also help illuminate aspects of the process that are more difficult to predict, such as whether the coating of brine would allow the hydrohalite crystals to grow larger over time due to Ostwald ripening, whether the brine would partially or fully drain through the ice, and whether the crystals would remain brine-wetted indefinitely or begin to dry out over time.

2.3 Wind tunnel tests of hydrohalite crusts

The hydrohalite crusts seen in our experiments tend to be loose and powdery. It is possible that they would be removed from the surface as soon as they developed under real Snowball conditions. A wind tunnel could be developed and mounted on the surface of a sea ice tank to determine the wind speed at which various thicknesses of hydrohalite crust would be removed from the ice. Crusts might also behave differently depending on their origins and microstructure; a crust formed from normal sea ice might behave differently than a crust that had melted, re-frozen, and re-sublimated.

2.4 Incorporation of results into climate models

The primary reason for undertaking this work was to improve models of Snowball Earth. As global climate models become faster and more powerful, they become easier and more fruitful to run, so adding the parameterization for the development of hydrohalite crust to a GCM could give interesting results comparatively easily. Given the more modest albedo increase due to the precipitation of hydrohalite within the ice, and the likelihood that a salt crust would develop rapidly under the sublimation conditions near the equator, it would be worth adding the salt crust to a GCM even before developing a complete parameterization for cold subeutectic sea ice.

Adding the full set of salt dynamics—precipitation of hydrohalite, development of hydrohalite crust, and dissolution of hydrohalite crust—to a simpler waterworld model would also help illuminate the dynamics brought into play by the additional positive feedbacks that hydrohalite creates. Colder sea ice due to hydrohalite precipitation enhances cooling, while the dissolution of a hydrohalite crust (even a relatively thin one) would lower albedo and enhance warming.

2.5 Implications for refugia

Over most of the ocean surface during Snowball conditions, sea ice with a hydrohalite crust would eventually be replaced by sea glaciers flowing in from the polar regions. However, some areas in narrow channels or in the lee of obstacles like headlands or islands would remain free of sea glaciers throughout the duration of the Snowball state. Many or all of these areas would still be below freezing, so sea ice would freeze at their surface and potentially develop a hydrohalite crust just as it would on the open ocean. Such a crust could seriously diminish the amount of light transmitted through the ice to photosynthetic organisms below, making these glacier-free areas less useful as refugia. Adding hydrohalite to models of refugia would constrain the temperatures at which they could exist.

2.6 Implications for other star systems

The albedo of a hydrohalite crust is notable because it is much higher than the albedo of the bare ice from which it develops. However, it is also notable because it reflects more strongly in the near-infrared region than either ice or snow. It is more difficult for Snowball conditions to develop around cool M-dwarf stars than it is for them to develop around Sunlike or hotter stars, but if they do develop, a hydrohalite crust would change the albedo of the ice surface even more dramatically than on Earth. Moreover, while a hydrohalite crust on Earth will eventually be displaced by sea glaciers, many planets in the habitable zone of M-dwarf stars will be tidally locked to their star, leading to very different sea ice dynamics (which might or might not facilitate the development of a perpetual hydrohalite crust.)

Figures

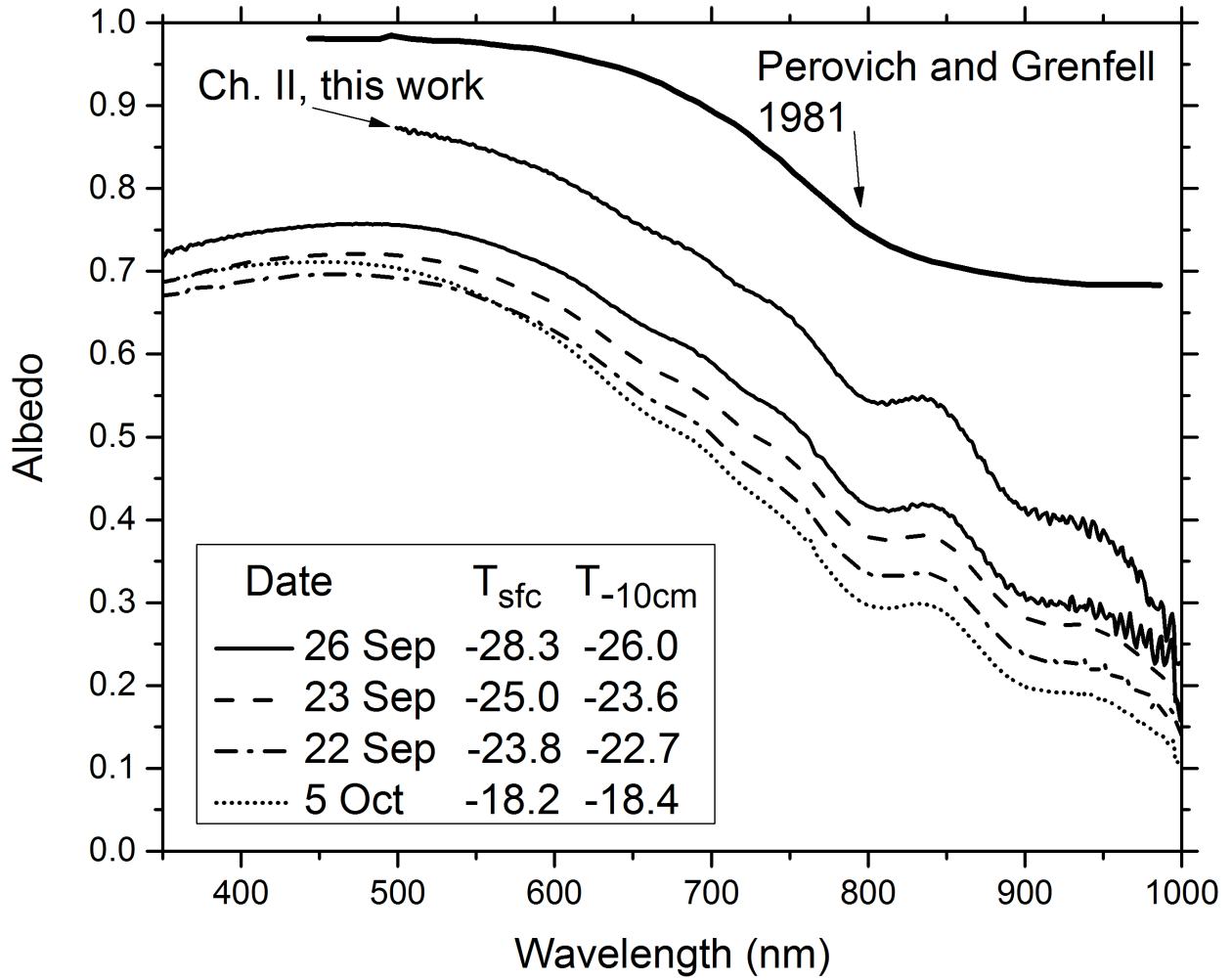


Figure 1. Comparison of results from Chapter I of this work (the lowest four albedos) with results from Chapter II and from *Perovich and Grenfell* [1981].

References

- Abbot, D. S., and R. T. Pierrehumbert (2010), Mudball: Surface dust and Snowball Earth deglaciation, *J. Geophys. Res.*, *115*(D3), D03104, doi:10.1029/2009JD012007.
- Abbot, D. S., A. Voigt, and D. Koll (2011), The Jormungand global climate state and implications for Neoproterozoic glaciations, *J. Geophys. Res.*, *116*(D18), D18103, doi:10.1029/2011JD015927.
- Abràmoff, M. D., P. J. Magalhães, and S. J. Ram (2004), Image processing with ImageJ, *Biophotonics Int.*, *11*(7), 36-43.
- Adams, L. H., and R. E. Gibson (1930), The melting curve of sodium chloride dihydrate. An experimental study of an incongruent melting at pressures up to twelve thousand atmospheres, *J. Am. Chem. Soc.*, *52*(1905), 4252-4264, doi:10.1021/ja01374a010.
- Albert, M., C. Shuman, Z. Courville, R. Bauer, M. Fahnestock, and T. Scambos (2004), Extreme firn metamorphism: impact of decades of vapor transport on near-surface firn at a low-accumulation glazed site on the East Antarctic plateau, *Ann. Glaciol.*, *39*, 73-78.
- Baldrige, A. M., S. J. Hook, C. I. Grove, and G. Rivera (2009), The ASTER spectral library version 2.0, *Remote Sens. Environ.*, *113*(4), 711-715, doi:10.1016/j.rse.2008.11.007.
- Bao, H., I. Fairchild, P. Wynn, and C. Spötl (2009), Stretching the envelope of past surface environments: Neoproterozoic glacial lakes from Svalbard, *Science*, *323*(5910), 119-122.
- Bishop, J. L., M. K. Ward, T. L. Roush, A. Davila, A. J. Brown, C. P. McKay, R. Quinn, and W. Pollard (2014), Spectral Properties of Na , Ca- , Mg- and Fe-Chlorides and Analyses of Hydrohalite-Bearing Samples from Axel Heiberg Island, poster presented at: 45th Annual Lunar and Planetary Science Conference, Universities Space Research Association, The Woodlands, Texas, doi:10.1029/2010JE003613.
- Brandt, R. E., and S. G. Warren (1993), Solar-heating rates and temperature profiles in Antarctic snow and ice, *J. Glaciol.*, *39*(131), 99-110.
- Brandt, R. E., S. G. Warren, A. P. Worby, and T. C. Grenfell (2005), Surface Albedo of the Antarctic Sea Ice Zone, *J. Clim.*, *18*(17), 3606-3622, doi:10.1175/JCLI3489.1.
- Budyko, M. I. (1969), The effect of solar radiation variations on the climate of the Earth, *Tellus*, *21*(5), 611-619, doi:10.3402/tellusa.v21i5.10109.
- Campbell, A. J., E. D. Waddington, and S. G. Warren (2011), Refugium for surface life on Snowball Earth in a nearly-enclosed sea? A first simple model for sea-glacier invasion, *Geophys. Res. Lett.*, *38*(19), L19502, doi:10.1029/2011GL048846.
- Carns, R. C., R. E. Brandt, and S. G. Warren (2015), Salt precipitation in sea ice and its effect on albedo, with application to Snowball Earth, *Submitted to J. Geophys. Res. Ocean.*

- Cox, G. F. N., and W. F. Weeks (1988), Numerical simulations of the profile properties of undeformed first-year sea ice during the growth season, *J. Geophys. Res.*, 93(C10), 12449-12460, doi:10.1029/JC093iC10p12449.
- Dadic, R., P. C. Mullen, M. Schneebeli, R. E. Brandt, and S. G. Warren (2013), Effects of bubbles, cracks, and volcanic tephra on the spectral albedo of bare ice near the Transantarctic Mountains: Implications for sea glaciers on Snowball Earth, *J. Geophys. Res. Earth Surf.*, 118(3), 1658-1676, doi:10.1002/jgrf.20098.
- Dieckmann, G. S., G. Nehrke, S. Papadimitriou, J. Göttlicher, R. Steininger, H. Kennedy, D. Wolf-Gladrow, and D. N. Thomas (2008), Calcium carbonate as ikaite crystals in Antarctic sea ice, *Geophys. Res. Lett.*, 35(8), L08501, doi:10.1029/2008GL033540.
- Dieckmann, G. S., G. Nehrke, C. Uhlig, J. Göttlicher, S. Gerland, M. a. Granskog, and D. N. Thomas (2010), Brief Communication: Ikaite (CaCO₃·6H₂O) discovered in Arctic sea ice, *Cryosphere*, 4, 227-230, doi:10.5194/tc-4-227-2010.
- Golden, K. M., S. F. Ackley, and V. I. Lytle (1998), The Percolation Phase Transition in Sea Ice, *Science*, 282(December), 2238-2241, doi:10.1126/science.282.5397.2238.
- Goodman, J. C. (2006), Through thick and thin: Marine and meteoric ice in a "Snowball Earth" climate, *Geophys. Res. Lett.*, 33(16), L16701, doi:10.1029/2006GL026840.
- Goodman, J. C., and R. T. Pierrehumbert (2003), Glacial flow of floating marine ice in "Snowball Earth," *J. Geophys. Res.*, 108(C10), 3308, doi:10.1029/2002JC001471.
- Grenfell, T., and B. Light (1999), SHEBA data archive--Spectral Albedo, Available from: http://data.eol.ucar.edu/codiac_data/sheba/data/perovich/ICEDATA/OPTICS/SPECALB/
- Grenfell, T. C., and S. G. Warren (1999), Representation of a nonspherical ice particle by a collection of independent spheres for scattering and absorption of radiation, *J. Geophys. Res.*, 104(D24), 31697-31709, doi:10.1029/1999JD900496.
- Grenfell, T. C., S. G. Warren, and P. C. Mullen (1994), Reflection of solar radiation by the Antarctic snow surface at ultraviolet, visible, and near-infrared wavelengths, *J. Geophys. Res.*, 99(D9), 18669-18684, doi:10.1029/94JD01484.
- Hadley, O. L., and T. W. Kirchstetter (2012), Black-carbon reduction of snow albedo, *Nat. Clim. Chang.*, 2(6), 437-440, doi:10.1038/nclimate1433.
- Halverson, G. P., B. P. Wade, M. T. Hurtgen, and K. M. Barovich (2010), Neoproterozoic chemostratigraphy, *Precambrian Res.*, 182(4), 337-350, doi:10.1016/j.precamres.2010.04.007.
- Han, B., and J. C. Bischof (2004), Direct cell injury associated with eutectic crystallization during freezing., *Cryobiology*, 48(1), 8-21, doi:10.1016/j.cryobiol.2003.11.002.
- Le Hir, G., Y. Donnadieu, G. Krinner, and G. Ramstein (2010), Toward the snowball earth deglaciation..., *Clim. Dyn.*, 35(2-3), 285-297, doi:10.1007/s00382-010-0748-8.

- Hoffman, P. F., and D. P. Schrag (2002), The snowball Earth hypothesis: testing the limits of global change, *Terra Nov.*, *14*(3), 129–155, doi:10.1046/j.1365-3121.2002.00408.x.
- Hoffman, P. F., A. J. Kaufman, G. P. Halverson, and D. P. Schrag (1998), A Neoproterozoic Snowball Earth, *Science*, *281*(5381), 1342–1346, doi:10.1126/science.281.5381.1342.
- Hoffman, P. F., G. P. Halverson, E. W. Domack, J. M. Husson, J. a. Higgins, and D. P. Schrag (2007), Are basal Ediacaran (635 Ma) post-glacial “cap dolostones” diachronous?, *Earth Planet. Sci. Lett.*, *258*, 114–131, doi:10.1016/j.epsl.2007.03.032.
- Hu, Y.-B., D. A. Wolf-Gladrow, G. S. Dieckmann, C. Völker, and G. Nehrke (2014), A laboratory study of ikaite (CaCO₃·6H₂O) precipitation as a function of pH, salinity, temperature and phosphate concentration, *Mar. Chem.*, *162*, 10–18, doi:10.1016/j.marchem.2014.02.003.
- Hudson, S. R., S. G. Warren, R. E. Brandt, T. C. Grenfell, and D. Six (2006), Spectral bidirectional reflectance of Antarctic snow: Measurements and parameterization, *J. Geophys. Res.*, *111*(D18), D18106, doi:10.1029/2006JD007290.
- Hyde, W. T., T. J. Crowley, S. K. Baum, and W. R. Peltier (2000), Neoproterozoic “snowball Earth” simulations with a coupled climate/ice-sheet model, *Nature*, *405*(6785), 425–429, doi:10.1038/35013005.
- Kasting, J. F., D. P. Whitmire, and R. T. Reynolds (1993), Habitable zones around main sequence stars., *Icarus*, *101*, 108–128, doi:10.1006/icar.1993.1010.
- Kindel, B. C., Z. Qu, and a F. Goetz (2001), Direct solar spectral irradiance and transmittance measurements from 350 to 2500 nm., *Appl. Opt.*, *40*(21), 3483–3494.
- Kirschvink, J. L. (1992), Late Proterozoic low-latitude global glaciation: the snowball Earth, in *The Proterozoic Biosphere*, volume 52, edited by J. W. Schopf and C. Klein, pp. 51–52, Cambridge University Press.
- Krembs, C., H. Eicken, K. Junge, and J. . Deming (2002), High concentrations of exopolymeric substances in Arctic winter sea ice: implications for the polar ocean carbon cycle and cryoprotection of diatoms, *Deep Sea Res. Part I Oceanogr. Res. Pap.*, *49*(12), 2163–2181, doi:10.1016/S0967-0637(02)00122-X.
- Krembs, C., H. Eicken, and J. W. Deming (2011), Exopolymer alteration of physical properties of sea ice and implications for ice habitability and biogeochemistry in a warmer Arctic., *Proc. Natl. Acad. Sci. U. S. A.*, *108*(9), 3653–3658, doi:10.1073/pnas.1100701108.
- Levinson, R., H. Akbari, and P. Berdahl (2010), Measuring solar reflectance—Part II: Review of practical methods, *Sol. Energy*, *84*(9), 1745–1759, doi:10.1016/j.solener.2010.04.017.
- Light, B., G. A. Maykut, and T. C. Grenfell (2003), Effects of temperature on the microstructure of first-year Arctic sea ice, *J. Geophys. Res.*, *108*(C2), 33.1–33.16, doi:10.1029/2001JC000887.
- Light, B., G. A. Maykut, and T. C. Grenfell (2004), A temperature-dependent, structural-optical model of first-year sea ice, *J. Geophys. Res.*, *109*(C6), C06013, doi:10.1029/2003JC002164.

- Light, B., R. E. Brandt, and S. G. Warren (2009), Hydrohalite in cold sea ice: Laboratory observations of single crystals, surface accumulations, and migration rates under a temperature gradient, with application to “Snowball Earth,” *J. Geophys. Res.*, 114(C7), C07018, doi:10.1029/2008JC005211.
- Light, B., R. C. Carns, and S. G. Warren (2015), “Albedo dome”: A method for measuring spectral flux-reflectance in a laboratory, *Submitted to Appl. Opt.*
- Marion, G. M., and S. A. Grant (1994), *FREZCHEM: A Chemical-Thermodynamic Model for Aqueous Solutions at Subzero Temperatures*, Report 94-18.
- Marion, G. M., R. E. Farren, and A. J. Komrowski (1999), Alternative pathways for seawater freezing, *Cold Reg. Sci. Technol.*, 29(3), 259-266, doi:10.1016/S0165-232X(99)00033-6.
- McClatchey, R. A., R. W. Fenn, J. E. A. Selby, F. E. Volz, and J. S. Garing (1972), *Optical Properties of the Atmosphere (Third Edition)*, report AFCRL-72-0497, Air Force Cambridge Research Laboratories, 108 pp.
- Micheels, A., and M. Montenari (2008), A snowball Earth versus a slushball Earth: Results from Neoproterozoic climate modeling sensitivity experiments, *Geosphere*, 4(2), 401-410, doi:10.1130/GES00098.1.
- Moczydlowska, M. (2008), The Ediacaran microbiota and the survival of Snowball Earth conditions, *Precambrian Res.*, 167, 1-15, doi:10.1016/j.precamres.2008.06.008.
- Mullen, P. C., and S. G. Warren (1988), Theory of the optical properties of lake ice, *J. Geophys. Res.*, 93(7), 8403-8414.
- Payne, R. E. (1972), Albedo of the sea surface, *J. Atmos. Sci.*, 29(5), 959-970, doi:10.1175/1520-0469(1972)029<0959:AOTSS>2.0.CO;2.
- Pegau, W. S., and C. A. Paulson (2001), The albedo of Arctic leads in summer, *Ann. Glaciol.*, 33, 221-224, doi:10.3189/172756401781818833.
- Peltier, W. R., Y. Liu, and J. W. Crowley (2007), Snowball Earth prevention by dissolved organic carbon remineralization., *Nature*, 450(7171), 813-818, doi:10.1038/nature06354.
- Perovich, D., and A. Gow (1991), A Statistical Description of the Microstructure of Young Sea Ice, *J. Geophys. Res.*, 96(C9), 16,943-16,953.
- Perovich, D., and A. Gow (1996), A quantitative description of sea ice inclusions, *J. Geophys. Res.*, 101(C8), 18,327-18,343.
- Perovich, D. K. (1979), The optical properties of young sea ice, M.S. Thesis, University of Washington, Seattle, WA, USA.
- Perovich, D. K., and T. C. Grenfell (1981), Laboratory studies of the optical properties of young sea ice, *J. Glaciol.*, 27(96), 331-346.
- Perovich, D. K., and J. A. Richter-Menge (1994), Surface characteristics of lead ice, *Engineering*, 99(C8), 16341-16350.

- Perovich, D. K., T. C. Grenfell, B. Light, and P. V. Hobbs (2002), Seasonal evolution of the albedo of multiyear Arctic sea ice, *J. Geophys. Res.*, *107*(C10), 8044, doi:10.1029/2000JC000438.
- Pierrehumbert, R. T. (2005), Climate dynamics of a hard snowball Earth, *J. Geophys. Res.*, *110*(D1), D01111, doi:10.1029/2004JD005162.
- Pierrehumbert, R. T., D. S. Abbot, A. Voigt, and D. Koll (2011), Climate of the Neoproterozoic, *Annu. Rev. Earth Planet. Sci.*, *39*(1), 417-460, doi:10.1146/annurev-earth-040809-152447.
- Pollard, D., and J. Kasting (2005), Snowball Earth: A thin-ice solution with flowing sea glaciers, *J. Geophys. Res.*, *110*, 1-16, doi:10.1029/2004JC002525.
- Pollard, D., and J. F. Kasting (2004), Climate-ice sheet simulations of Neoproterozoic glaciation before and after collapse to Snowball Earth, *Geophys. Monogr.*, *146*, 91-105.
- Pollard, D., and J. F. Kasting (2006), Reply to comment by Stephen G. Warren and Richard E. Brandt on "Snowball Earth: A thin-ice solution with flowing sea glaciers," *J. Geophys. Res.*, *111*(May), 1-7, doi:10.1029/2006JC003488.
- Pringle, D., G. Dubuis, and H. Eicken (2009), Instruments and Methods Impedance measurements of the complex dielectric permittivity of sea ice at 50 MHz : pore microstructure and potential for salinity monitoring, *J. Glaciol.*, *55*(189), 81-94.
- Purdie, C. R., P. J. Langhorne, G. H. Leonard, and T. G. Haskell (2006), Growth of first-year landfast Antarctic sea ice determined from winter temperature measurements, *Ann. Glaciol.*, *44*(1), 170-176, doi:10.3189/172756406781811853.
- Rankin, A. M., E. W. Wolff, and S. Martin (2002), Frost flowers: Implications for tropospheric chemistry and ice core interpretation, *J. Geophys. Res. Atmos.*, *107*(D23), 4683, doi:10.1029/2002JD002492.
- Shields, A. L., V. S. Meadows, C. M. Bitz, R. T. Pierrehumbert, M. M. Joshi, and T. D. Robinson (2013), The effect of host star spectral energy distribution and ice-albedo feedback on the climate of extrasolar planets, *Astrobiology*, *13*(8), 715-739, doi:10.1089/ast.2012.0961.
- Spencer, R. J., N. Møller, and J. H. Weare (1990), The prediction of mineral solubilities in natural waters: A chemical equilibrium model for the Na-K-Ca-Mg-Cl-SO₄-H₂O system at temperatures below 25°C, *Geochim. Cosmochim. Acta*, *54*(3), 575-590, doi:10.1016/0016-7037(90)90354-N.
- Stamnes, K., S. C. Tsay, W. Wiscombe, and K. Jayaweera (1988), Numerically stable algorithm for discrete-ordinate-method radiative transfer in multiple scattering and emitting layered media., *Appl. Opt.*, *27*(12), 2502-2509, doi:10.1364/AO.27.002502.
- Style, R. W., and M. G. Worster (2009), Frost flower formation on sea ice and lake ice, *Geophys. Res. Lett.*, *36*, L11501, doi:10.1029/2009GL037304.
- Toner, J. D., D. C. Catling, and B. Light (2014), The formation of supercooled brines, viscous liquids, and low-temperature perchlorate glasses in aqueous solutions relevant to Mars, *Icarus*, *233*, 36-47, doi:10.1016/j.icarus.2014.01.018.

- Tziperman, E., D. S. Abbot, Y. Ashkenazy, H. Gildor, D. Pollard, C. G. Schoof, and D. P. Schrag (2012), Continental constriction and oceanic ice-cover thickness in a Snowball-Earth scenario, *J. Geophys. Res.*, *117*(C5), C05016, doi:10.1029/2011JC007730.
- Untersteiner, N. (1968), Natural desalination and equilibrium salinity profile of perennial sea ice, *J. Geophys. Res.*, *73*(4), 1251-1257.
- Wagner, R., O. Möhler, and M. Schnaiter (2012), Infrared optical constants of crystalline sodium chloride dihydrate: application to study the crystallization of aqueous sodium chloride solution droplets at low temperatures., *J. Phys. Chem. A*, *116*(33), 8557-8571, doi:10.1021/jp306240s.
- Warren, S., and W. Wiscombe (1980), A model for the spectral albedo of snow. II: Snow containing atmospheric aerosols, *J. Atmos. Sci.*, *37*(12), 2734-2745.
- Warren, S., R. Brandt, T. C. Grenfell, and C. P. McKay (2002), Snowball Earth: ice thickness on the tropical ocean, *J. Geophys. Res. Ocean.*, *107*(C10), 31.1-31.18, doi:10.1029/2001JC001123.
- Warren, S. G. (1982), Optical properties of snow, *Rev. Geophys.*, *20*(1), 67-89, doi:10.1029/RG020i001p00067.
- Warren, S. G., and R. E. Brandt (2006), Comment on “ Snowball Earth : A thin-ice solution with flowing sea glaciers ” by David Pollard and James F. Kasting, , *111*, C09016, doi:10.1029/2005JC003411.
- Warren, S. G., and R. E. Brandt (2008), Optical constants of ice from the ultraviolet to the microwave: A revised compilation, *J. Geophys. Res.*, *113*(D14), D14220, doi:10.1029/2007JD009744.
- Weeks, W. F., and S. F. Ackley (1982), *The growth, structure, and properties of sea ice*, No. CRREL-MONO-82-1, Cold Regions Research and Engineering Laboratory, Hanover, NH.
- Wettlaufer, J. S. (1998), Introduction to crystallization phenomena in natural and artificial sea ice, in *Physics of Ice-covered Seas*, edited by M. Leppäranta, pp. 105-194, University of Helsinki Press.
- Wiscombe, W. J. (1980), Improved Mie scattering algorithms., *Appl. Opt.*, *19*(9), 1505-1509.
- Wiscombe, W. J., R. M. Welch, and W. D. Hall (1984), The Effects of Very Large Drops on Cloud Absorption. Part I: Parcel Models, *J. Atmos. Sci.*, *41*(8), 1336-1355.
- Yang, J., W. R. Peltier, and Y. Hu (2012a), The initiation of modern soft and hard Snowball Earth climates in CCSM4, *Clim. Past*, *8*(3), 907-918, doi:10.5194/cp-8-907-2012.
- Yang, J., W. R. Peltier, and Y. Hu (2012b), The Initiation of Modern “Soft Snowball” and “Hard Snowball” Climates in CCSM3. Part I: The Influences of Solar Luminosity, CO2 Concentration, and the Sea Ice/Snow Albedo Parameterization, *J. Clim.*, *25*(8), 2711-2736, doi:10.1175/JCLI-D-11-00189.1.